ISSN 0915-6348

NATIONAL INSTITUTE FOR FUSION SCIENCE

Proceeding of the 5th International Workshop on Reflectometry 5-7 march, 2001

(Ed.) K. Kawahata

(Received - Apr. 24, 2001)

NIFS-PROC-49 May 2001

RESEARCH REPORT
NIFS-PROC Series

TOKI, JAPAN

Proceeding of the 5th International Workshop on Reflectometry

5 – 7 March , 2001

Edited by K. Kawahata

National Institute for Fusion Science,
Oroshi-cho, Toki 509 – 5292, JAPAN

This is the proceedings of the 5th International Workshop on Reflectometry, which was held on 5-7 March, 2001, at the National Institute for Fusion Science. In this workshop, the latest experimental results in reflectometry (profile and fluctuations studies), new technological developments and a broad scope of the theory and simulation codes were presented.

Key Words: plasma diagnostics, electron density profile, density fluctuations, L to H transition, poloidal rotation velocity, FM-CW reflectometry, heterodyne reflectometry, pulsed radar reflectometry, O-X correlation reflectometry, Imaging Reflectometry, ultra-short pulse reflectometry, Doppler reflectometry

PREFACE

This publication contains 22 papers presented at "The 5th International Workshop on Reflectometry" held at the National Institute for Fusion Science (NIFS) on March 5 - 7, 2001. This workshop was combined with the US-Japan Workshop on "Development of Advanced Microwave Reflectometry Techniques".

The main topics of this workshop were as follows: (1) density profile and fluctuation measurements by FM-CW reflectometry and pulsed radar reflectometry, (2) X - and O – mode correlation reflectometry, (3) poloidal rotation measurements, (4) new technological developments and (5) a broad scope of theory and simulation codes. The latest trends of the MM-wave market and MM-wave applications were also discussed.

Local Organizers

Kazuo KAWAHATA (National Institute for Fusion Science)
Tokihiko TOKUZAWA (National Institute for Fusion Science)
Kenji TANAKA (National Institute for Fusion Science)
Atsushi MASE (National Institute for Fusion Science)

List of Participants

L. Bruskin	Kyushu University
Roberto Cavazzana	Consorzio RFX – Associazione Euratom
Frederic Clairet	CEA Cadarache
Garrard Conway	Max-Planck-Institut fur Plasmaphysik
Tony Donne	FOM-Instituut voor Plasmafysica 'Rijnhuizen'
Akira Ejiri	Tokyo University
Mark Gilmore	University of California, Los Angeles
Jaco van Gorkom	TEXTOR
Evgeniy Gusakov	Ioffe Institute
Kunihiko Hattori	Tohoku University
Matthias Hirsch	Max-Planck Institut fur Plasmaphysik
Hitoshi Hojo	Tsukuba University
Harukazu Iguchi	National Institute for Fusion Science
Yoshihiro Ishita	Anritsu Corporation
Akiyosi Itakura	Tsukuba University
Kazuo Kawahata	National Institute for Fusion Science
Gerrit J. Kramer	Princeton Plasma Physics Laboratory

Maria Emilia Manso	Centro Fusao Nuclear - Instituto Superior Tecnico
Atushi Mase	Kyushu University
Isamu Ogawa	Fukui University
Naoyuki Oyama	Naka Fusion Research Establishment, JAERI
Hyeon Park	Princeton Plasma Physics Laboratory
Oleg Pavlichenko	Kharkov Institute of Physics and Technology
Rostyslav Pavlichenko	Fukui University
Joaquin Sanchez	Association Euratom- CIEMAT
Kouji Shinohara	Naka Fusion Research Establishment, JAERI
Shunichi Shiraiwa	Tokyo University
Kenji Tanaka	National Institute for Fusion Science
Hiroyuki Tokuda	Toshiba Corporation
Tokihiko Tokuzawa	National Institute for Fusion Science
Paulo Varela	Centro de Fusao Nuclear - Instituto Superior Tecnico
George Vayakis	ITER
Akihide Yamamoto	Kyushu University
Takuma Yamada	Tokyo University
Akihide Yamamoto	Kyushu University

Contents

The role of reflectometry on large devices 1
J. Sanchez

Status of 3-D Microwave Imaging Systems for T_e and n_e Fluctuation and Profile Measurements on TEXTOR 2
H Park, E. Mazzucato, T. Munsat, B.H. Deng, C. Domier, J. Wang and N.C. Luhmann Jr.

Recent Experimental Results and Diagnostics on LHD 3
K. Kawahata and LHD Experimental Group

Recent Reflectometry Results from the UCLA Plasma Diagnostics Group 7
M. Gilmore, E.J. Doyle, S. Kubota, X.V. Nguyen, W..A. Peebles, T.L. Rhodes and L. Zeng

X mode heterodyne reflectometry in TORE SUPRA 18
F. Clairet, R. Sabot, Ch. Bottereau and J.M. Chareau

Measurement of the Waiting-Time Statistic of Turbulence by means of Microwave Reflectometry 22
Roberto Cavazzana.

Effects on finite density fluctuations and of the upper hybrid resonance on O-X correlation Reflectometry 26
G. J. Kramer, R. Nazikian and E. Valeo

Fluctuation and reflectometer simulation studies on ASDEX-Upgrade 30
G.D. Conway, B. Kurzan, B. Scott, H. Holzhauer, S. Klenge, W. Stuttrop
M. kaufmann , F. Jenko, F. Serra, T.T. Ribeiro, H. Zohm,
ASDEX Upgrade Team and CFN Reflectometry Group

Advances in the Density Profile Evaluation From Broadband Reflectometry on ASDEX Upgrade 35
P. Varela , M. Manso, G. Conway, ASDEX Upgrade Team

Density Measurements with Broadband FM-CW reflectometry in Advanced Scenarios on ASDEX Upgrade 39
M. Manso, S. Vergamota, I. Nunes, L. Cupido, T. Ribeiro, J. Santos, F. Serra, A. Silva
P. Varela, G. Conway, P.T. Lang, F. Ryter, R. Wolf and ASDEX Upgrade Team

Overview of reflectometer on JT-60U 43
K. Shinohara, N. Oyama, R. Nazikian and R. Yoshino

Measurement of giant ELM in JT-60U using O-mode reflectometer 47
N. Oyama, K. Shinohara, K. Kamada, Y. Miura, T. Oikawa and S. Takeji

Observation of electron density using reflectometry 51
A. Itakura, N. Goto, M. Katoh, Y. Kogi, S. Kubota, A. Mase, Y. Shima, M. Yoshikawa
H. Hojo and K. Yatsu

Pulsed Radar Reflectometer on the LHD 55
T.Tokuzawa, K. Kawahata, K. Tanaka, R.O. Pavlichenko and A. Ejiri

Pulsed radar reflectometry of broadband fluctuations 59
J.C. van Gorkom, M.J. van de Pol, A.J.H. Donne and F.C. Schuller

Two Channel Microwave Reflectometry and Interferometry Using PIN Switch 64
T. Yamada, A. Ejiri, Y. Takase, S. Shiraiwa, K. Yamagishi, M. Ushinoume N. Kasuya, Y. Nagashima,
H. Nozato, T. Mashiko, T. Akiduki, H. Kasahara, H. Yamada, H. Wada and L.M. Tozawa

Two-Dimensional Simulation for Ultrashort-Pulse Imaging Reflectometry 68
H. Hojo, K. Nakayama, G. Urata and A. Mase

Application of Ultrashort Pulse Reflectometry to a Steady State Plasma 72
A. Mase, A. Yamamoto, L.G. Bruskin, M. Ohashi and T. Deguchi

Profile Reconstruction Methods for Pulse Reflectometry 76
L.G. Bruskin, A. Yamamoto, A. Mase, M. Ohashi and T. Deguchi

Status of Doppler Reflectometry Investigations at the W7-AS Stellarator 81
M. Hirsch, E. Holzhauer, J. Baldzuhn, B. Kurzan and B. Scott

Poloidal Rotation Velocity Measurement in Toroidal Plasmas
via Microwave Reflectometry 85
O.S. Pavlichenko, A.I. Skibenko, I.P. Fomin, I.B. Pinos, V.L. Ocheretenko and V.L. Berezhniy

Homodyne Reflectometry for Density Interlock and Fluctuation Measurements
in Large Helical Device 88
Kenji Tanaka, A. Ejiri, Y. Ito, K. Kawahata. T. Tokuzawa, M. Osakabe and Y. Takeiri

The role of reflectometry on large devices

Joaquin Sanchez
JET: Task Force Leader for Diagnostics
Association Euratom - CIEMAT
28040 Madrid Spain

It would analyze the present status of reflectometry from the point of view of the contributions that the plasma physics community requires. I will also consider the ITER needs. Here, I will summarize the development of the reflectometry for last 15years.

>15 years of development

1985: first results from the "new reflectometry" (TFR, JET, Petula...).

1990: more than 15 devices planning to install reflectometers (incl JET,JT60,TFTR,...ITER).

1991: Varenna, Fast FM , PR, AM introduced.

1995: a complex system of 3 reflectometers "approved" for ITER.

1997: Varenna, discussion: lack of results from "profile reflectometry".(turbulence -though less understood- more productive!)

<2001: reaction produced, but: enough?

Status of 3-D Microwave Imaging Systems for T_e and n_e Fluctuation and Profile Measurement on TEXTOR*

H. Park, E Mazzucato and T.Munsat
Princeton Plasma Physic Laboratory

B.H. Deng, C. Domier, J. Wang, and N.C. Luhmann Jr.,
University of California at Davis

M. Pol, and A.J.H. Donné
FOM Institute

In collaboration with UC Davis and FOM, we are developing a unique combined Electron Cyclotron Emission Imaging (ECEI) and Microwave Imaging Reflectometry (MIR) system to be demonstrated on TEXTOR. During the last two years, we have successfully developed an ECEI system and determined the optimum optical system for MIR. The new MIR system is currently being tested in the run prior to the TEXTOR long shut down (March 2, 01). Based on test results at UC Davis and TEXTOR, we are confident in our ability to develop a simultaneous 3-D imaging ECE/reflectometry system based on the use of reflective optics during the down time (one year) and anticipate that this diagnostic system will provide a new level physics of fluctuation spectra and profiles on TEXTOR. The FOM diagnostic team on TEXTOR designated half of this port (20 cm [toroidal] x 45 cm [poloidal]) for the test of the imaging system with the other half of this window occupied by the Thomson system. The ECEI imaging system successfully demonstrated on the RTP tokamak has been modified to fit onto TEXTOR and the system has been used for physics study. We have tested the first Microwave Imaging System designed and fabricated based on the ECEI lens system. Qualitatively, we were able to measure focal plane in each array but multiple reflections between optical elements interfered with a more detailed analysis. We have been focused on the new system design based on reflective mirror elements. The system was installed in February and experiments on TEXTOR are currently in progress. Prior to shipping the system, we identified the characteristics of the system performance. In this paper, we will present the status of our joint undertaking including the detail design characteristics and preliminary test results.

* Work is supported by the U.S. Department of Energy, Contract No. DE-FG0395ER54295 and DE-AC02-CH0-3073.

Recent Experimental Results and Diagnostics on LHD

Kazuo Kawahata, LHD Experimental Group

National Institute for Fusion Science,
322-6 Oroshi-cho, Toki 509-5292, Japan
E-mail: kawahata@LHD.nifs.ac.jp

Abstract

LHD is a superconducting heliotron type device with l=2/m=10 continuous helical coils and three pairs of poloidal coils [1]. The major and minor radii of the plasma are 3.5-3.9 m and 0.6 m, respectively. The plasma experiment was started at the end of March 1998 with the magnetic field of 1.5 T [2]. Subsequently, the magnetic field has been gradually increased checking carefully the stability of the SC coils, and the maximum magnetic field used in the plasma experiment was 2.89 T at the magnetic axis of R_{ax} = 3.6 m. The heating power has been gradually increased, i.e., NBI up to 5.2 MW (with two beam lines), ICRF up to 2.7 MW (with two antenna system), and ECRH up to 1.0 MW (with six gyrotron tubes). The carbon tiles were installed as divertor plates to meet high power heatings, resulting in significant reduction in metal impurity concentration (Fe) and total radiation power. Upgrading of the key hardware system has led to (i) higher Te [Te(0) = 4.4 keV at <ne> = 5.3 x 10^{18} m^{-3} and P_{abs} = 1.8 MW], (ii) higher confinement [τ_E = 0.3 s, Te(0) = 1.1 keV at <ne> = 6.5 x 10^{19} m^{-3} and P_{abs} = 2.0 MW], (iii) higher stored energy W_p^{dia} = 1.0 MJ, (iv) the highest β value in helical devices [2.4% at 1.3 T, > 3.0% at 0.5 T]. In this workshop, we will report the recent experimental results on the LHD and plasma diagnostics related to mm and sub-mm wave diagnostics.

1. Characteristics of LHD Plasmas

One of the unique features of LHD plasmas is the formation of the edge pedestal. When neutral beams inject into a target plasma generated by ECH, the hot plasma region expands rapidly and eventually reaches the last closed magnetic flux surface and finally reaches divertor plates. During this rising phase, the temperature pedestal [3] forms without a rapid transition which is usually observed in the H-mode discharges on other machine. The energy confinement was systematically better than that predicted by the International Stellerator Scaling 95 [4] up to a factor of 1.6 and was comparable with ELMy H-mode confinement capability [5] in tokamaks shown in Fig.1. In order to plot tokamak confinement times in the figure of ISS95 scaling, the toroidal plasma currents are replaced by rotational transform angle with the assumption of a safety factor q profile of $q = 1 + (q_a + 1)r^4$.

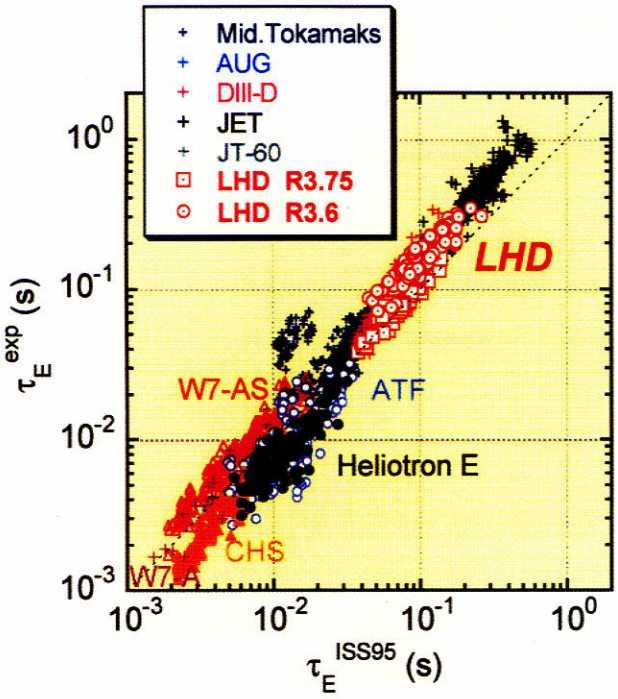

Fig. 1 Comparison of the global energy Confinement time with ISS95 scaling.

Temperature pedestal observed contributes this enhancement. ICRF power up to 1.3 MW was reliably injected into the plasma without significant impurity contamination and a plasma with stored energy of 200kJ was sustained for 5 sec by ICRF alone. Long pulse discharges over than 1 min have been successfully achieved with ICRF heating and with NBI heating [6]. With NBI heating (0.5MW), the discharge with Te = 2.0 keV and <ne> = 1.6 x 10^{19} m^{-3} lasted 80 sec. With ICRF heating(0.85 MW), a similar long pulse dis charge (duration time of 68 sec, Te(0) = 2.0 keV, <ne> = 1.0 x 10^{19} m^{-3}) was achieved. In these discharges, no increase of radiation power has been observed until the end of discharge. The pulse length is limited by the heating instrument capability and not by plasma behavior.

2. LHD Plasma diagnostics

Figure 2 show a cross-sectional view of the LHD experimental hall, including the major diagnostics. The main diagnostics are a YAG Thomson scattering syatem having 120 spatial channels with a time resolution of 20 msec, a 13-channel FIR laser interferometer for the electron density profile measurements, and charge exchange recombination spectroscopy for ion temperature profile measurement. The most challenging diagnostic on LHD is Heavy Ion Beam Probe with the beam energy of 6 MeV, just now being installed in the LHD experimental room. Among these various diagnostics, MM and Sub-MM Wave diagnostics on LHD will be described in detail. The diagnostics related to the mm and sub-mm wave technologies are summarized in table I. A lot of challenging diagnostics such as a CO2 laser polarimeter, a ultra-short reflectometer and ECE imaging have been developed under the collaborations with many universities.

For the electron density profile measurement, a multi-channel FIR laser interferometer has been developed. The optical configuration of the meter is of the Michelson interferometer type. The FIR laser is installed in the diagnostic room. The laser beam propagates about 50 m through a couple of the dielectric waveguides to reach the optical housing, which is mounted on a massive frame. The frame encircles the plasma vacuum vessel and floats on three pneumatic vibration isolation mounts in order to minimize the transmission of vibrations from

the machine. This isolation stand is 18.4 meters tall and weights about 30 tons. In this instrument, the key point for the construction of the high quality laser interferometer is how to achieve high quality and high power laser source. We have developed the laser source under the collaboration with Chubu-university from the beginning of the LHD project. So far, we have developed a powerful and stable 119 μm CH_3OH laser which has been used to measure the electron density profile of the LHD plasmas. For the future high performance operation of LHD, a powerful 57 μm CH_3OD laser pumped by a 9R(8) CO_2 laser has been developed [7] and its output power reaches to 1.18 W.

Table 1 MM/Sub-MM wave plasma diagnostics on the Large Helical Device

Interferometry	13-Channel CH_3OH Laser Interferometer 140/285 GHz MM Wave Interferometer
Polarimetry	10.6 mm CO_2 Laser Polarimeter
Electron Cyclotron Emission	14-channel Grating Polychromator Fourier Transform Spectrometer Heterodyne Radiometer (D-band and E-band) ECE Imaging
Reflectometry	Pulsed radar Reflectometry Homodyne Reflectometry for NBI Interlock

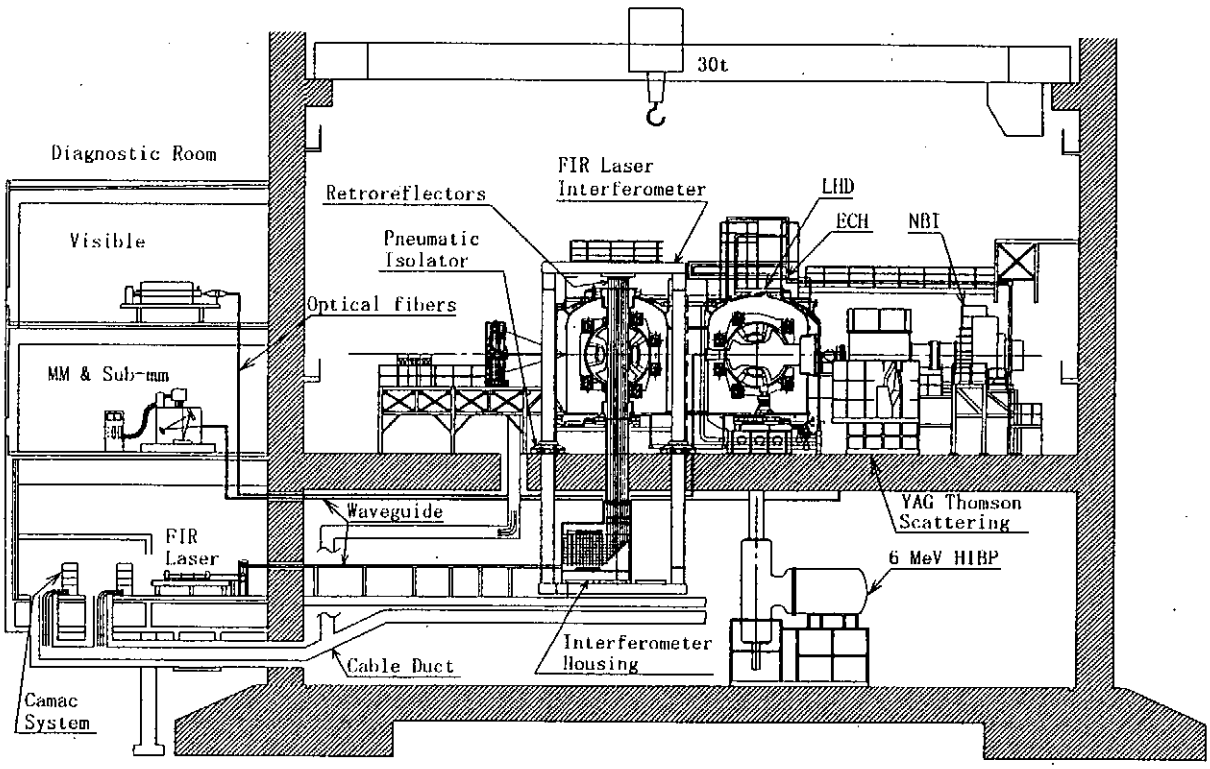

Fig. 2 Cross-sectional view of the LHD experimental hall.

In ECE and reflectometry on LHD it is important to investigate the effects of the magnetic-field shear on the polarization of the electromagnetic waves. In the ECE diagnostics, the magnetic field strength in LHD is a non-monotonous function of the radius in the sight line of the ECE diagnostic antenna and it is characterized by a large shear (see Fig. 3). The magnetic shear is defined as the ratio between the poloidal and toroidal magnetic field components, or the shear angle, θ given by $\tan\theta = B_t/B_p$. The derivative is given by $\phi = dq/dr$ (see Fig. 3). The shear in LHD is of order unity at the plasma edge. Such a large shear yields a coupled propagation of the X and O-mode polarization modes, yielding mode conversion and polarization rotation. A detailed numerical and experimental analysis of the ECE polarization has been performed [8]. It was found that if the density is sufficient high ($n_e > 0.5\ 10^{19}\ m^{-3}$) mode conversion is negligible. However, the polarization orientation rotates in the LHD laboratory frame up to the plasma edge. X-mode polarization remained perpendicular to the local magnetic field. Hence, at the edge, the X-mode polarization was observed under a specific angle in the laboratory frame, given by the local shear angle, θ (r=a) $\approx$ 34 - 30°. Numerical calculations were found to be in agreement with the experimental results. Similar situation should be appeared in the reflectometry, and the mode conversion effect on the reflectometry on LHD is under investigation by using a short-pulsed reflectometer.

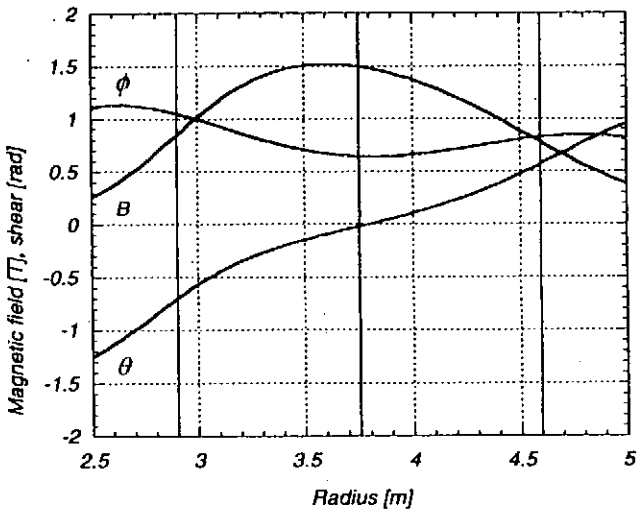

Fig. 3 The magnetic-field configuration in the line-of-sight of the diagnostic antenna. The magnetic-field amplitude, the shear angle, θ, and its derivative, ϕ, are plotted.

Acknowledgements

This work was supported in part by a Grant-in Aid for Scientific Research from the Japanese Ministry of Education, Science, Sports and Culture.

References

[1] Iiyoshi A., et. al., Nuclear Fusion **39** (1999) 1245.

[2] Fujiwara M., et. al., in the 17th IAEA Fusion Conf. (Yokohama) EX2/3.

[3] Ohyabu N., et. al., Phy. Rev. Lett. **84** (2000) 103.

[4] Strouth U., et. al., Nuclear Fusion **36** (1996) 1063.

[5] ITER Physics Expart Groups on Confinement and Transport and Confinement Modeling and Databese, ITER Physics Basis Editors, Nucl. Fusion **39** (1999) 1501.

[6] Kawahata K.,et. al., Plasma Phys. Control. Fusion **42** (2000) B51.

[7] Okajima S., et. al., Rev. Sci. Instrum. **72** (2001) 1094.

[8] deVries P.C. et. al., Phys. Plasmas **7** (2001) 3707.

Recent Reflectometry Results from the UCLA Plasma Diagnostics Group

M. Gilmore, E.J. Doyle, S. Kubota, X.V. Nguyen, W.A. Peebles, T.L. Rhodes, and L. Zeng
Electrical Engineering Department, University of California, Los Angeles, CA, USA

Presented at the Fifth Reflectometry Workshop, Toki, Gifu, Japan, 5-7 March 2001.

Abstract

The UCLA Plasma Diagnostics Group has an active ongoing reflectometry program. The program is threefold, including 1) profile and 2) fluctuation measurements on fusion devices (DIII-D, NSTX, and others), and 3) basic reflectometry studies in linear and laboratory plasmas that seek to develop new measurement capabilities and increase the physics understanding of reflectometry. Recent results on the DIII-D tokamak include progress toward the implementation of FM reflectometry as a standard density profile diagnostic, and correlation length measurements in QDB discharges that indicate a very different scaling than normally observed in L-mode plasmas. The first reflectometry measurements in a spherical torus (ST) have also been obtained on NSTX. Profiles in NSTX show good agreement with those of Thomson scattering. Finally, in a linear device, a local magnetic field strength measurement based on O-X correlation reflectometry has been demonstrated to proof of principle level, and correlation lengths measured by reflectometry are in good agreement with probes.

I. INTRODUCTION

Reflectometry can provide both electron density profiles with high spatial and temporal resolution, and density fluctuation measurements from the plasma edge to the core. One proven method for density profile measurement is the FM radar technique.[1,2] The UCLA group currently operates FM radar systems on both the DIII-D tokamak and NSTX spherical torus. In Section II, recent profile measurements from DIII-D and NSTX are shown, and progress in implementing FM relfectometry as a standard diagnostic is briefly discussed.

Section III presents correlation reflectometry measurements from DIII-D. Radial correlation lengths, Δr, are compared in DIII-D L-mode and Quiescent Double Barrier (QDB) discharges,[3,4] and are found to exhibit different scalings.

Two aspects of basic reflectometry studies are discussed in Section IV. First, the development of a magnetic field strength, $|\underline{B}|$, diagnostic based on dual mode (O-X) correlation reflectometry is presented. It is shown that, in these experiments, $|\underline{B}|$ could be determined simultaneously with the radial correlation length, Δr. Second, comparisons between radial correlation lengths measured by homodyne reflectometry and a Langmuir probe array are presented. Good agreement is found between the reflectometer and probe.

II. FM PROFILE MEASUREMENTS

Significant progress has been made toward implementing profile reflectometry as a standard diagnostic on the DIII-D tokamak. Automatic profile analysis has been demonstrated, system spatial coverage has been optimized via polarization flexibility, and upgraded data acquisition has significantly extended the time coverage.

The profile reflectometers on DIII-D are Q- (33-50 GHz) and V-band (50–75 GHz) FM radars,[5,6] that operate in either O- or X-mode.[7] The data acquisition system and analysis software have been upgraded to allow profiles to be measured every 10 ms for an entire 5 s discharge, and analyzed between shots. O-mode measurements are able to access the plasma core, while X-mode scans the edge. The O-mode system has been particularly important in measuring the steep profiles found to occur in operating modes with internal transport barriers (ITB) with good time resolution. Fig. 1 shows an example of the time evolution of the electron density at an ITB.

In order to construct X-mode profiles, the start of reflection from the right-hand cut-off must be identified. For O-mode in the core, a reliable fit to Thomson Scattering (TS) profiles at the edge must be available. Furthermore, in cases where the O-mode begins to transmit above cut-off, this point in the time record must be identified. Software is now in place and operating to automatically determine this information, and to reconstruct the profiles between shots.[7] Note that the large volume of profiles, up to 10,000 per discharge, *requires* an automated analysis system. Currently, however, operator intervention is still required to obtain profiles showing detailed agreement with those of the TS system. Development of a fully automatic system is ongoing.

An FM profile reflectometer, consisting of three O-mode systems in the bands 12-18 GHz, 20-32 GHz and 33-50 GHz, has also been installed on the National Spherical Torus Experiment (NSTX),[8] and initial results have been obtained. All three NSTX systems utilize circular horn antennas, and rotating waveguide joints so that the polarization angle can be adjusted manually. During operation, the polarization is typically aligned with the expected edge magnetic field pitch angle. Figure 2 shows a recent reflectometer profile from NSTX together with Thomson scattering measurements. As can be seen, there is good agreement between the two measurements over most of the outer half of the plasma. Note that this is the first reflectometry measurement in an ST device. These initial results are encouraging since there were concerns about problems with reflectometry in the ST's resulting from O-X mode conversion due to the large magnetic field shear.[9]

III. CORRELATION MEASUREMENTS IN DIII-D

Although some questions regarding the interpretation of fluctuation and correlation data remain,[10] correlation reflectometry is now a mature enough diagnostic to be used reliably for physics studies in magnetically confined plasmas.

Figures 3 and 4 show two recent and interesting correlation results from DIII-D.[3,11] These measurements were made with a heterodyne frequency tunable V-band (50-75 GHz) system located on the outboard midplane.[12] First, Fig. 3 plots radial correlation length, Δr, measurements in DIII-D in typical L-mode and QDB discharges. The QDB discharge is a high performance mode that exhibits both edge and core transport barriers. The core barrier, as well as sheared flow due to radial electric field, exists over a large region of the core plasma.[3,4] In the L-mode case, Δr exhibits a scaling with either the poloidal ion sound gyroradius, $\rho_{\theta s}$ (i.e. the gyroradius using T_e instead of T_i), or approximately 5-8 times the total sound gyroradius, ρ_s. In contrast, the QDB case Δr's are significantly smaller than the L-mode scaling, which is consistent with reduced turbulent transport step size and improved confinement.

Second, a comparison between reflectometer measurements and a 3D toroidal electrostatic gyrokinetic simulation[13] is shown in Fig. 4. This comparison is an early result from a program to make experiment-model comparisons in detail. The initial simulated plasmas have been circular (DIII-D plasmas are shaped), however comparisons with shaped plasmas are now under way. Measured n_e, T_i, and q profiles were used in the simulation. Two simulation results are shown, both with and without self-generated, or zonal, flows included. Without zonal flows, correlation lengths are seen to be very long – in a fact a large fraction of the total 65 cm minor radius. When zonal flows are included, Δr can be seen to reduce to values near the experimental measurements. Although the agreement is intriguing, this is a very early stage of the comparison and more work remains. Nevertheless, this seems a clear indication of the importance of zonal flow effects in gyrokinetic modeling.

IV. BASIC REFLECTOMETRY STUDIES

A. Dual mode (O-X) correlation reflectometry

Basic studies of dual mode correlation reflectometry have been conducted in the LArge Plasma Device (LAPD) at UCLA.[14,15] In addition to fluctuation/correlation length measurements, O-X reflectometry can provide a local, nonperturbing measurement of $|\underline{B}|$. If O- and X-modes are launched and received through the same pair of antennas, one might expect the cross correlation of both fluctuating signals to maximize when the two reflecting layers overlap spatially. If each signal comes from its respective cut-off layer, then the X-mode frequency corresponding to cut-off at the same spatial location as the O-mode can be written in terms of f_o and f_x,

$$f_x = \frac{1}{2}\left(f_c + \sqrt{f_c^2 + 4f_o^2} \right), \qquad (1)$$

where f_o and f_x are the O- and X-mode frequencies respectively, f_c is the electron cyclotron frequency, f_p is the electron plasma frequency, and the right-hand cutoff, f_R, has been taken for X-mode. Since f_x and f_o are known from the cross-correlation, $|\underline{B}|$ can be determined from Eq. (1).

In practice, it was found that O-X cross-correlation peaked at an X-mode frequency (for fixed O-mode) less than f_R. Fig. 5 shows the results of a typical cross-correlation of homodyne signals, $\langle I_o I_x \rangle$, where $I = A\cos\varphi$. Here $f_o = 11.0$ GHz, $B = 0.10$ T, and f_x scanned over the range shown. A Guassian fit to the data gave an X-mode frequency of peak cross-correlation, $f_{x,pk} = 12.15 \pm 0.073$ GHz, while $f_R = 12.47 \pm 0.03$ GHz. Amplitude, $\langle A_o A_x \rangle$ and phase, $\langle \varphi_o \varphi_x \rangle$, correlations yielded $f_{x,pk} = 12.17 \pm 0.082$ and 12.15 ± 0.097

GHz respectively. In all cases $f_{x,pk}$ determined from amplitude, phase, and homodyne signals were equal to within the error bars.

Figure 6 shows the X-mode frequency of peak cross-correlation vs. magnetic field for fixed $f_o = 11.0$ GHz. As can be seen, $f_{x,pk}$ lies below the right-hand cutoff in every case. Therefore, $|\underline{B}|$ cannot be determined from the simple formula, (1). However, it has been found that $f_{x,pk}$ can be accurately reproduced by a one-dimensional full wave model (code),[14] as shown in Fig. 6. In order to accurately determine $f_{x,pk}$, the code requires inputs of L_n, the density gradient scale length ($\equiv ((1/n)dn/dx)^{-1}$), and Δk_r, the radial k-spectral width of the plasma fluctuations, $S(k_r) \propto \exp\{ k_r^2 / \Delta k_r^2 \}$. Note that Δk_r is measured directly in an O-X correlation experiment, since for a Guassian k-spectrum, $\Delta k_r = 2\sqrt{2}/\Delta r$, where Δr is the 1/e radial correlation length. Experiment and model show good agreement with variation of these parameters, though the range of Δk_r studied was limited.[14,15]

A practical $|\underline{B}|$ diagnostic would use the 1D model, run iteratively, to determine B at cut-off from measured $f_{x,pk}$ and Δk_r, together with L_n from another diagnostic (e.g. a profile reflectometer). In the LAPD experiments, the accuracy of B was 5%, which was dominated by statistical error. It is likely that statistical error will dominate any measurement, and must be carefully assessed in any experiment. In a hot plasma, a knowledge of T_e might also be required for a relativistic correction to f_R.

An effect found in the O-X experiment, which is not predicted by the code, is that the maximum cross-correlation *value* decreases with magnetic field strength.[14,15] In the LAPD experiments, $\rho_{ox} \approx 0.65$ maximum at 0.05 T, decreasing to $\rho_{ox} \approx 0.4$ at 0.2 T. The reasons for this are not yet understood and may be due to 2D effects, but, practically, this may limit the diagnostic to low B-field cases (B ~ 0.1 T).

B. Reflectometer-Probe Comparisons

Detailed comparisons of turbulent radial correlation lengths measured by reflectometry and probes in the LAPD have also been made.[10] A plot comparing Δr from homodyne reflectometry to that of a probe array is shown in Fig. 7. Here Δr is taken as the 1/e length. As can be seen, there is good agreement, to within 10-15%, between reflectometer and probe in O-O, X-X, as well as O-X modes. The measured correlation lengths fell in the range $0.6 \le \Delta r/\lambda_0 \le 1.2$, or $0.7 \le \Delta r/W_{Airy} \le 1.3$, where λ_0 is the reflectometer vacuum wavelength and W_{Airy} is the Airy width.[15] Note that correlation lengths less than the vacuum wavelength were accurately measured.

Homodyne reflectometer and probe measurements also showed good agreement in power spectra and coherency in overall character, while phase signals showed agreement only in cases of low fluctuation

levels. In cases of high fluctuation levels, the phase was found to undergo a series of multi-radian phase discontinuities, or "jumps" (see ref. [16] for definitions of "low" and "high"). In these cases, the power spectra were found to approach an f^{-2} dependence, and Δr was much shorter than the corresponding probe measurements. These observations are consistent with the Random Phase Screen Model of reflectometry.[16] Finally, when a limited number of such phase jumps existed, they could be filtered out to recover power spectra and correlation lengths consistent with probe measurements.[15]

V. SUMMARY

Recent reflectometry results from the UCLA Plasma Diagnostics Group have been presented. FM density profile measurements have been presented from DIII-D and NSTX. Radial correlation measurements from DIII-D, now being used for physics studies, were also shown. Finally, basic reflectometry work on the linear LAPD on the development of a $|\underline{B}|$ measurement based on O-X correlation reflectometry, and comparisons with probes have been discussed.

ACKNOWLEDGEMENTS

The authors would like to thank the DIII-D, LAPD, and NSTX teams, particularly R.E. Bell, D. Johnson and B. LeBlanc for supplying the NSTX Thomson scattering data. Thanks also to J.-N. Leboeuf for his contributions of gyrokinetic modeling. This work was supported by the U.S. Department of Energy under grants No. DE-FG03-86ER-532225 and DE-FG03-99ER54527.

REFERENCES

[1] E.J. Doyle *et al.*, in *Diagnostics for Thermonuclear Fusion Reactors*, ed. P.E. Stott, G. Gorini and E. Sindoni, Plenum Press, New York, 117-132 (1996).

[2] C. Laviron, *et al* Plasma Phys Cont Fusion **38**, 905 (1996).

[3] E.J. Doyle, *et al* paper IAEA-CN-77/EX6/2, 18th IAEA Fusion Energy Conf, Sorrento Italy. Also accepted for publication in Nucl Fusion;

[4] C M Greenfield *et al* submitted to Phys Rev Lett

[5] K.W. Kim *et al* Rev Sci Instrum **66**, 1229 (1995);

[6] K.W. Kim *et al* Rev Sci Instrum **68**, 466 (1997).

[7] L. Zeng *et al* Rev Sci Instrum **72**, 320 (2001).

[8] S. Kubota *et al* Rev Sci Instrum **72**, 348 (2001).

[9] M. Nagatsu, T. Hayashi and T Tokishima, Jpn J Appl Phys 1 **34**, 3708 (1995).

[10] M. Gilmore, W.A. Peebles and X.V. Nguyen, Plasma Phys Cont Fusion **42**, L1 (2000).

[11] T L Rhodes *et al* 27th EPS Conf on Cont Fusion and Plasma Phys, Budapest, 12-16 June 2000, ECA Vol 24B (2000), 564.

[12] T.L. Rhodes *et al* Rev Sci Instrum **63**, 4661 (1992).

[13] J.-N. Leboeuf *et al* Phys Plasmas **7**, 1795 (2000).

[14] M. Gilmore, W.A. Peebles and X.V. Nguyen, Plasma Phys Cont Fusion **42**, 655 (2000).

[15] M. Gilmore, W.A. Peebles and X.V. Nguyen, Rev Sci Instrum **72**, 293 (2001).

[16] R. Nazikian and E. Mazzucato, Rev Sci Instrum **66**, 392 (1995).

Figure Captions

FIG. 1. Example of the time development of a steep, localized internal transport barrier (ITB) in electron density, in a DIII-D negative central shear (NCS) discharge. The portion of the profile determined by the reflectometer system is shown by open circles.

FIG. 2. Electron density profiles in NSTX vs. major radius measured by O-mode FM reflectometry (line) and Thomson scattering (triangles). Shot 104503, 97-100 ms.

FIG. 3. Radial correlation lengths in the DIII-D core as a function of plasma radius (flux coordinates) in cases of L-mode and QDB[3,4] plasmas. Lines indicate the poloidal sound gyroradius, $\rho_{\theta,s}$, in each case.

FIG. 4. Comparison of radial correlation lengths from measurements in DIII-D and Gyrokinetic simulations, with and without zonal (self-generated) flows included.

FIG. 5. Homodyne O-X cross-correlation coefficient, ρ_{ox}, vs. X-mode frequency, f_x. Error bars denote 95% confidence intervals. f_o = 11.0 GHz, B = 0.10 T. Right-hand cut-off f_R = 12.47±0.03 GHz.

FIG. 6. X-mode frequency of peak cross-correlation $f_{x,pk}$ vs. magnetic field: experiment (phase) and simulation. f_o = 11.0 GHz in each. Dashed line indicates the right-hand cut-off frequency f_R corresponding to f_p = 11.0 GHz.

FIG. 7. Homodyne reflectometer 1/e radial correlation length vs. those measured by a Langmuir probe array in the LAPD.

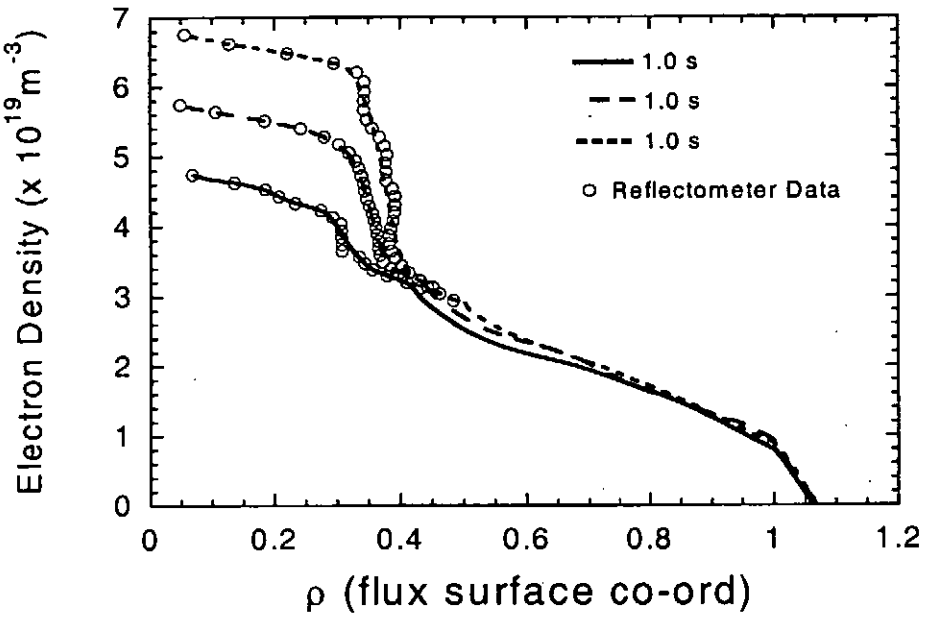

Figure 1

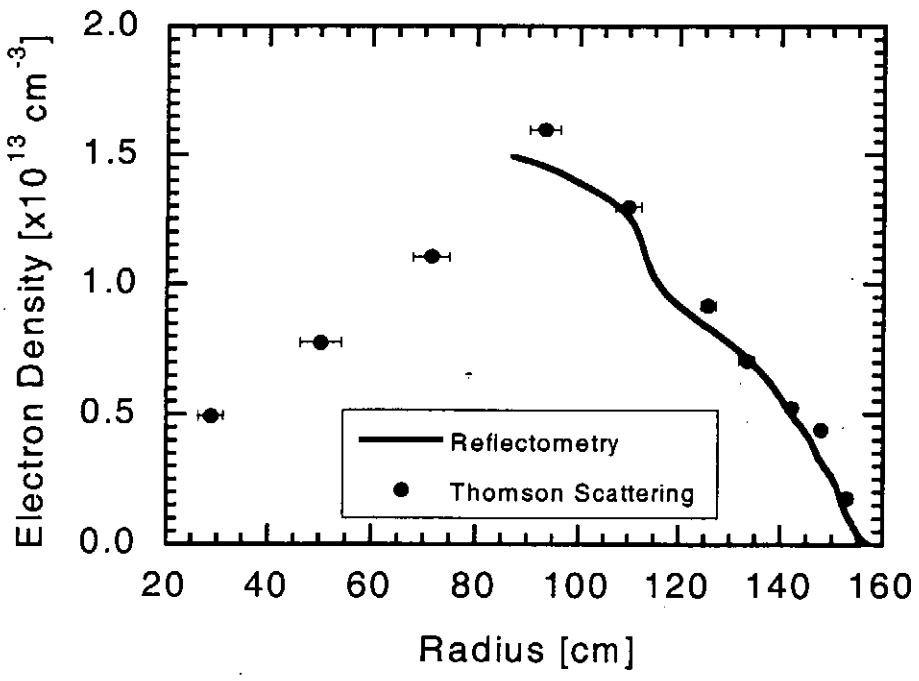

Figure 2

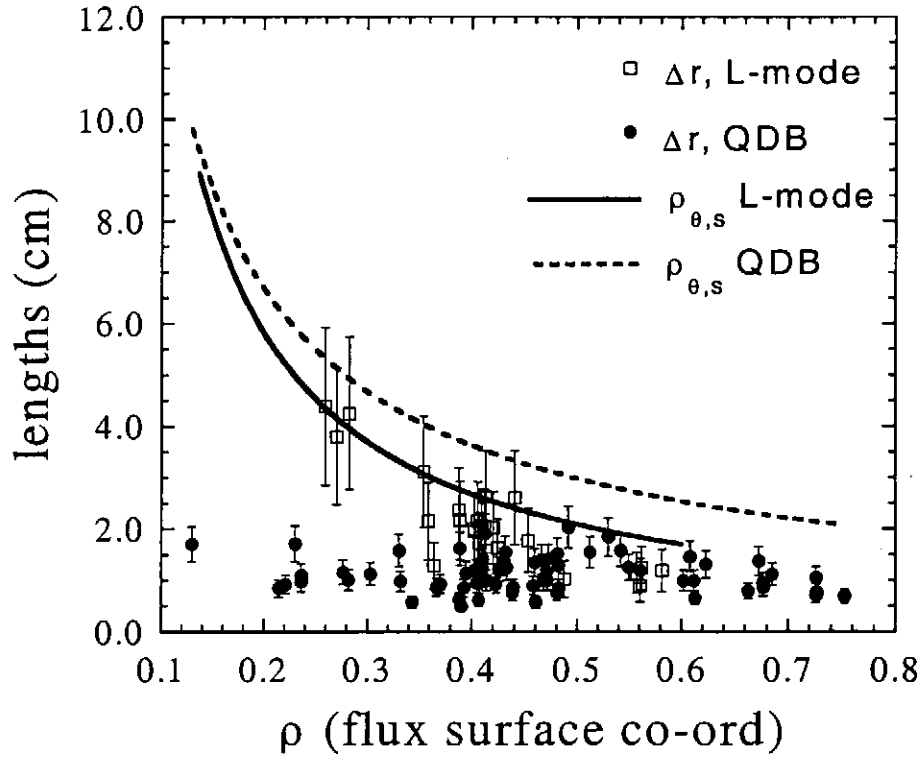

Figure 3

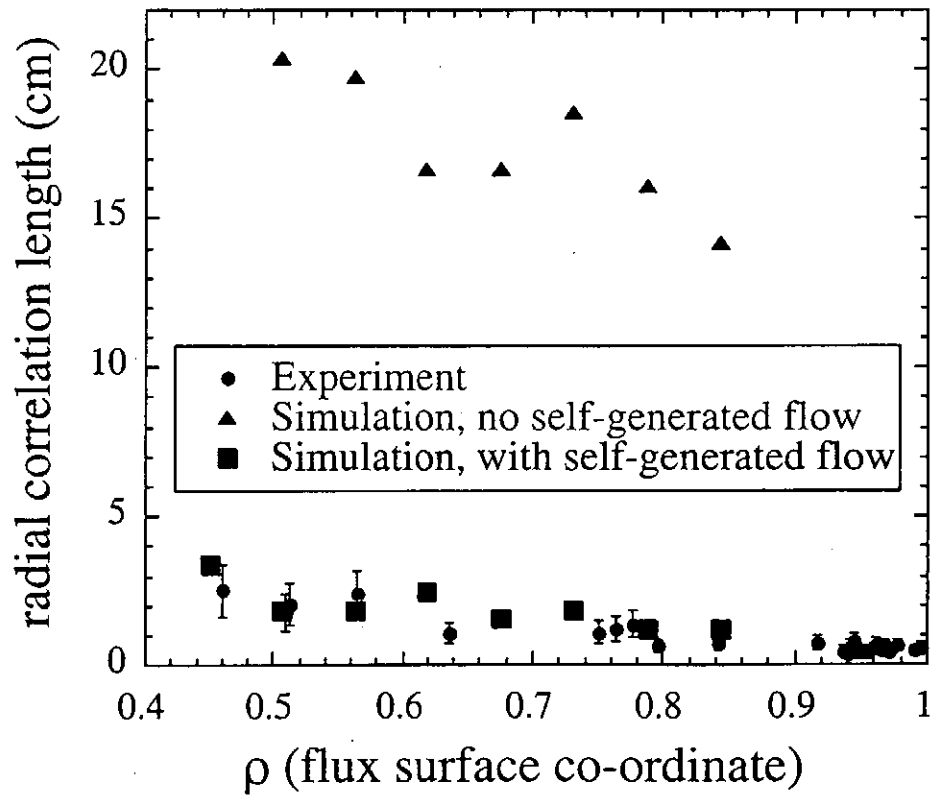

Figure 4

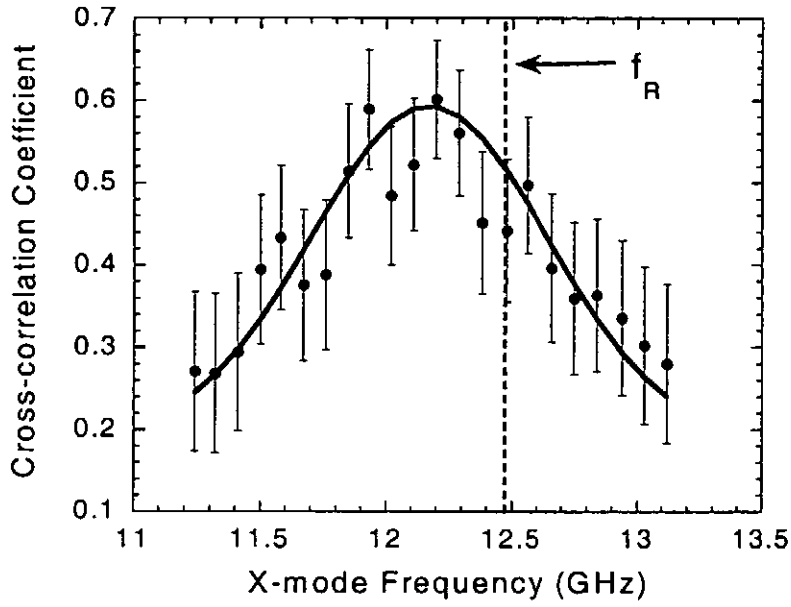

Figure 5

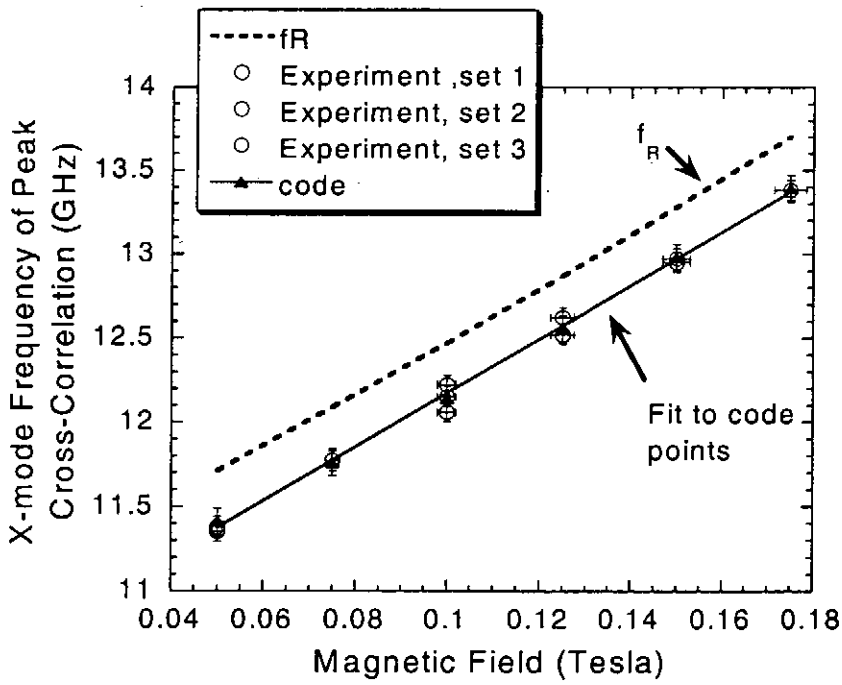

Figure 6

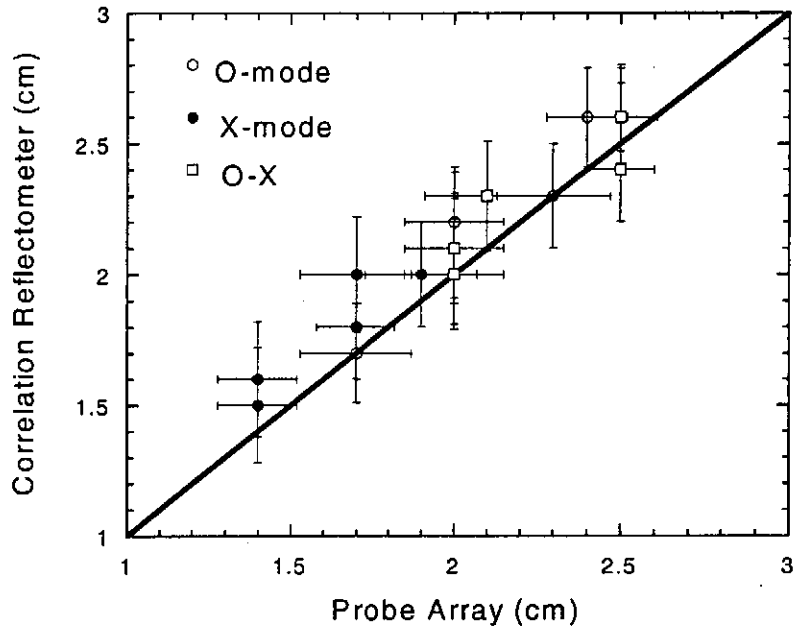
Correlation Reflectometer (cm)
Probe Array (cm)
O-mode
X-mode
O-X
1
1.5
2
2.5
3

Figure 7

X mode heterodyne reflectometry on TORE SUPRA

F. Clairet, R. Sabot, Ch. Bottereau and J.M. Chareau

Association EURATOM / CEA
Département de Recherches sur la Fusion Contrôlée
13108 Saint-Paul-Lez-Durance, FRANCE

I. Profile measurement and accuracy

The X-mode reflectometer system of TS (R=2.4m, a=0.75m, $B(0)_{max}$=4T) has been designed to measure the density profile at the plasma edge. It should cover a wide range of frequencies (from 50 to 110 GHz) according to possible variations of the toroidal magnetic field involved for plasma physic purposes. The extraordinary mode of polarisation has then been chosen as it can provide the initialisation of the profiles contrary to the ordinary mode polarisation. As a matter of fact, the first edge X-mode cut-off coincides with the cyclotron resonance, then it is possible to localise the position of this cut-off with the help of a magnetic field mapping. A former system ranging between 50 and 75 GHz (V band) has already been operated on plasma [1,2]. This set up was designed for fast frequency sweep measurements (full band in 20 μs) by using solid state sources (HTO : 13-19 GHz)) associated with frequency multipliers (active quadruplers P_{out}=10 dBm) one sweep can be repeated every 5 μs that makes this diagnostic a particularly flexible tool. An I.Q. heterodyne detection allows for high dynamic sensitivity (50 dB) and separate measurements of the amplitude and phase of the signal.

Experimentally, as the probing frequency goes beyond the edge cyclotron resonance, the amplitude of the reflected signal suddenly increases (Fig. 1). The first cut-off frequency can then be well identified to insure a precise initialisation of the density profile. the uncertainty upon the first cut-off frequency determination induce a precision of $\Delta R_{edge} \approx 1$ cm upon the profile position (Fig. 2). This uncertainty is the result of the plasma fluctuations that induce amplitude variations of the reflected signal.

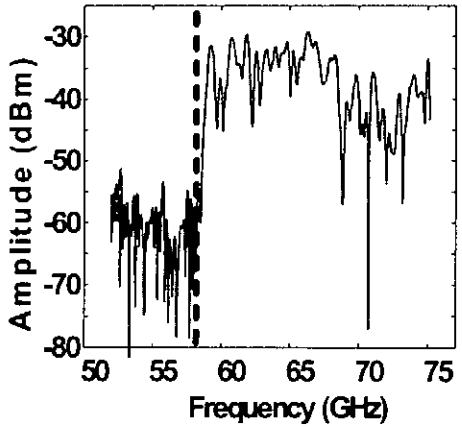

Fig. 1 : Increase of the amlpitude of the reflected signal beyond the first X mode cut-off frequency.

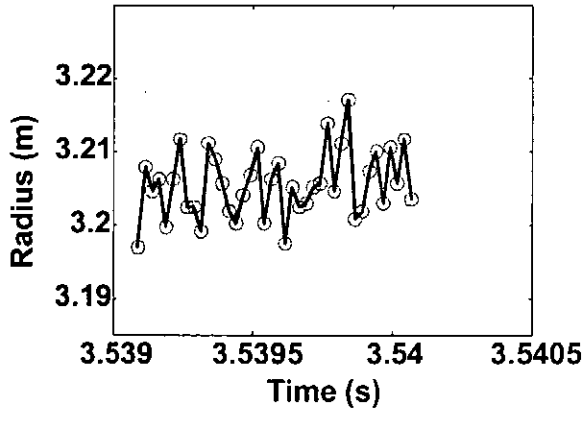

Fig 2 : Illustration of the variations on the edge plasma radius from an automatic initialisation of 40 profiles measured with sweeps of 20 μs repeated every 5 μs.

II. Experimental results

Edge plasma physic generally requires high precision measurements that can be fulfilled by the reflectometer. We give here two examples to illustrate the capabilities of the diagnostic.

1 - Density regimes

Pumping of particles and heat exhausts strongly depend on edge conditions and the density profiles is one key parameter to account for transport modellings. For a deuterium plasma whose density is continuously increased until the disruption limit is reached, three edge density regimes occur that have already been observed with fixed Langmuir probes [3]. The X-mode reflectometry accounts for the evolution of the whole edge profile (Fig. 3) and reveals that, along with the density ramp up, the edge profile is getting steeper from low to high recycling regime and exhibits clearly how a density sinking occurs from the very edge as a the plasma detachment appears.

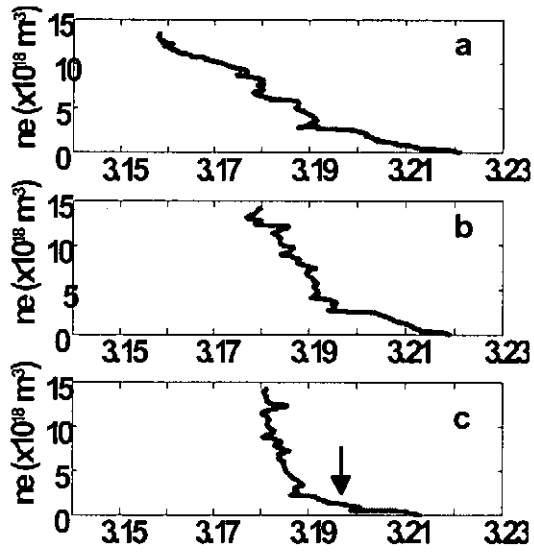

Fig. 3 : Edge profile when the plasma density increases from (a) low recycling, (b) high recycling and (c) detachment regimes. The arrow exhibit the edge density sinking.

2 - Interaction between ICRF heating and plasma edge

The properties of the boundary plasma play an important role in the power coupling of the ICRH antennas. In particular the position of the ICRF wave cut-off with respect to the antenna since this wave does not propagates in vacuum. This distance depends on the density and the density gradient in the edge. In this experiment (Fig. 4) the power is turned on and induces a rise of the plasma density (usually due to some local interaction in the scrape-off layer) then, the coupling efficiency decreases until a security turn off of the power is triggered. In this example, the plasma density increase brings on to a detachment regime condition that creates an edge density collapse (as described previously). The reflectometer measures then an increase (Fig. 5) of the distance between the ICRF antenna and its cut-off density ($ne_{ICRF} \approx 1.10^{19} m^{-3}$) that correlates with the coupling resistance efficiency.

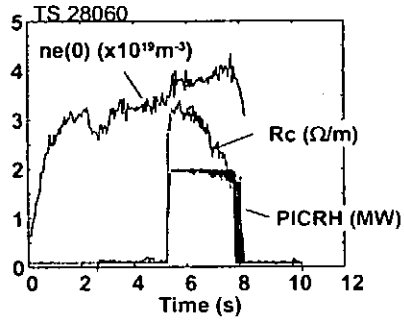

Fig. 4 : Evolution of the ICRH coupling power as the density approaches the plasma detachment.

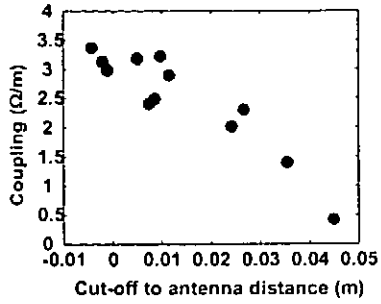

Fig. 5 : Increase of the distance between the ICRF cut-off and the antenna measured by reflectometry.

III New developments

1 - Single side band modulation

A new modulation technique using a single side band modulator (SSB) with adequate rejection properties (undesirable side bands are rejected at -20 dBc in the worst case) will now be used in the set-up. As a matter of fact, when using a conventional mixer, the signal coming out the active multiplier is spread (Fig. 6) all over numerous frequency bands (4F ± k.fm, k=0,1,2...) where only the 4F±2.fm are used for the profile measurements.

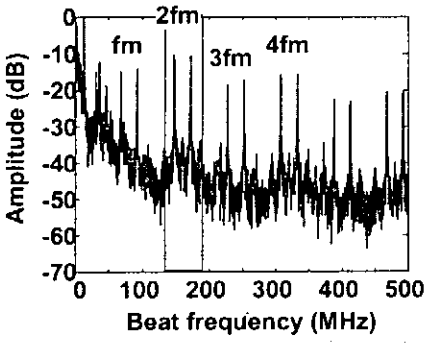

Fig. 6 : Power spectrum detected before filtering when using a standart mixer (with fm=80MHz).

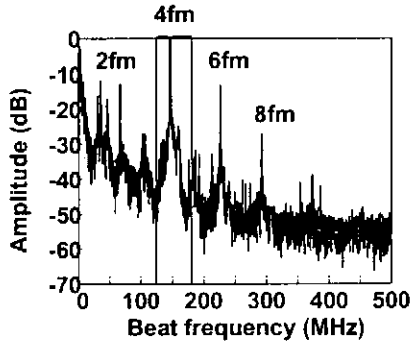

Fig. 7 : Power spectrum detected before filtering when using a single side band modulator (with fm=40 MHz).

By using a SSB the output power after the active multiplier is mainly concentrated into the 4F+4.fm only (Fig. 7). The result is a significant increase of the available power by almost 20 dB (Fig. 8) and the ability to perform fixed frequency measurements.

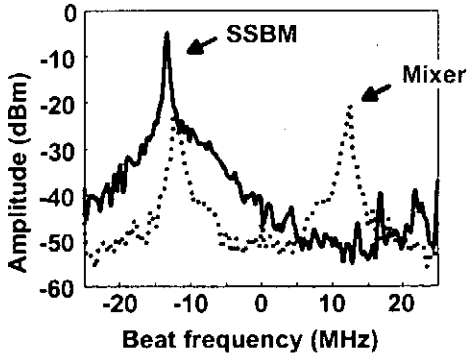

Fig. 8 : Comparison of the power spectra of a signal reflected at a mirror plate according the modulation technique (single side band modulator or mixer).

2 - W band reflectometer

An additional reflectometer working in the 75 - 110 GHz frequency domain (W band) is now under development and should be in operation for the next experimental campaign in summer 2001. Edge density measurements will be now possible for nominal magnetic field (B(0)=4T) plasma operations. The design (Fig. 9) is similar to the V band set up and use a solid state source (HTO 12 - 18 GHz) that is followed by an active sextupler (P_{out} = 0 dBm). Then both reflectometers will overlap by about 5 GHz (from 72 to 77 GHz) to insure the continuity, and will be helpful for profile initialisation and reconstruction. For both reflectometers, the detection has been set with the use of a frequency modulation of 100 MHz to account for expected beat frequencies up to 50 MHz. The IF part of the V and W band reflectometers will then be carried by 400 MHz and 600 MHz (Fig. 10) respectively.

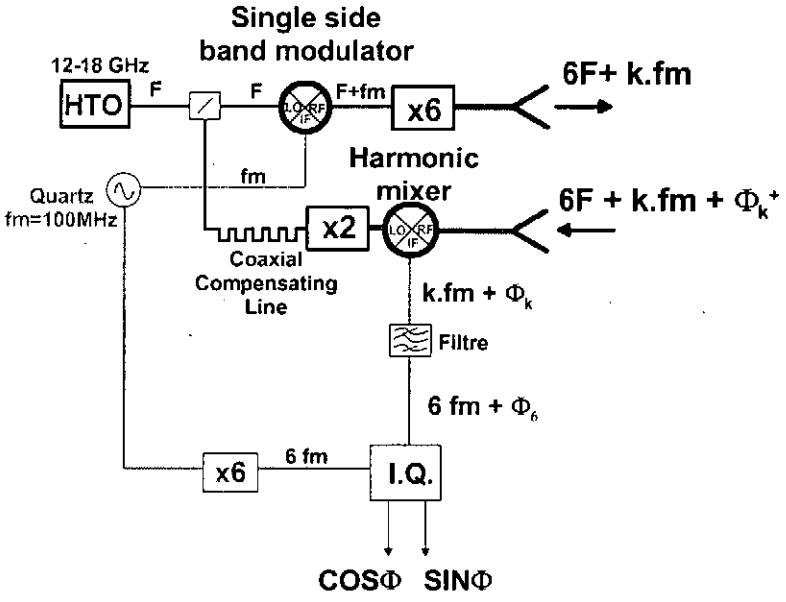

Fig. 9 : Schematic of the W band reflectometer.

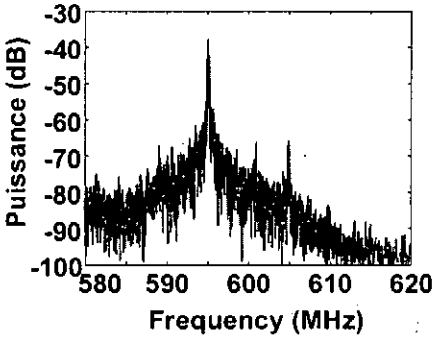

Fig. 10 : Power spectrum of a reflected signal onto mirror plate using a single side band modulator.

3 - Control and acquisition set-up

Both reflectometer can be driven independently and simultaneously. Voltage control of the HTOs is done by using two independent arbitrary waveform generators of 100 MHz max. sample frequency. They can provide fast linear frequency sweeps as well as fixed frequency operations. A GPIB connection allows for dialog with a VME bus interface. Acquisition will be performed by a four channel fast ADC module of 200 MHz max. sample frequency, 10 bits resolution (± 1.5 V max input voltage) and 32 MWords of memory per channel.

References :

[1] F. Clairet, R. Sabot *et al.* 2001 *Rev. of Sci. Instrum.* **72** 340
[2] F. Clairet, R. Sabot *et al.* 2001 *Plasma Phys. Controlled Fusion* (accepted for publication)
[3] B. Meslin, Ph. Ghendrih, A. Grosman *et al.* 1997 *Proceedings. of the 24th EPS conf., Contr. Fusion and Plasma Physics, 21A-I, 197 (Berchtesgaden, Germany)*

Measurement of the Waiting-Time Statistics of Turbulence by means of Microwave Reflectometry.

Roberto Cavazzana

Consorzio RFX – Associazione Euratom-ENEA sulla Fusione.

Corso Stati Uniti 4, I-35127 Padova - Italy

In the fusion community there is an active debate about the mechanism underlying the anomalous transport. In recent years one among the possible models candidate to explain some peculiar phenomena observed in magnetic confined plasmas is the Self-Organized Criticality (SOC) paradigm [1]. The SOC paradigm has been also invoked for astrophysical plasmas to explain the dynamics of the solar flares [2]. However in the paper of ref.[3] (B99) was pointed out that the SOC model proposed by Bak et al.[4], could not explain the probability distribution function (PDF) of the waiting times between subsequent flares. Recently the same technique has been also applied to density fluctuation measurements in RFP discharges [5].

The method proposed in B99 to analyse the PDF of waiting times is very attractive due to its simplicity. The method consists in looking for the bursts of the dissipated energy out of a more quiet background. This task can be accomplished in several ways; the simplest is, as suggested in B99, to find a threshold to discriminate the increase of the fluctuation level of a primary quantity (say density, velocity or magnetic field) and then determine the duration of quiet periods. In general the PDF of the waiting times gives a Poisson-like distribution for pure random processes; the form $p(t) \propto \exp(-t/\tau)$, implies that there is a well defined time scale τ in the system. On the other hand if the mechanism governing the system has strong internal interactions, the PDF of waiting times will display a power–law decay, which in turn means that there are no preferred time scales inside the system. This framework suggests that reflectometric measurements, due to their sensitivity to density fluctuations, can be used to identify the bursty events.

In presence of a roughness on the reflecting surface, the amplitude of the signal collected by a reflectometer is reduced; the average attenuation is roughly proportional to the fluctuation amplitude. The method of waiting time statistics has the advantage that it does not require the exact knowledge of the relation between the amplitude of the reflectometric measurements and the amplitude of the fluctuations, which relies on a proper modelling of the microwave propagation inside the plasma [6]. However the analysis is complicated by the fact that at a constant fluctuation amplitude the reflectometric signal exhibits a natural variation, which is given by the Rice distribution [7].

The question is if the property of PDF of waiting time distribution of the fluctuations survives to the mechanism of reflectometric measurement. To answer this we could make a simplification of the reflectometric measurement of the form:

$$A(t) = \left\langle \left| \sum_{p=1}^{N} \cos\left[2\left(\frac{\omega}{c}\left(d + \delta_p(t) \right) \right) \right] \right|^2 \right\rangle_{\omega}$$

where brackets denote the average over frequency ω.

The basic parameters have been chosen in order to obtain a situation that is reminiscent of the homodyne reflectometer installed at RFX [8], which has a single antenna aligned in the equatorial direction, so that the reflected radiation is in the specular direction at normal incidence. In the following the presented data have been calculated with N=40 and d = 21 cm; the amplitude has been averaged over ω in the interval 34 to 38 GHz (λ = 0.88-0.79 cm); $\delta_p(t)$ is a suitable random variable used to mimic the roughness, which remains frozen during each sweep. The thresholds used to find the waiting times has been calculated according to the method reported in B99.

Fig. 1 shows the PDFs of waiting times obtained from the signal A(t) when $\delta_p(t)$ is a pure random gaussian sequence. The two samples have been calculated with two different values for standard deviation of the phase $\sigma_\varphi = 4\pi \cdot \sigma_\delta / \langle \lambda \rangle_\omega$: their PDFs possess a clear exponential decay.

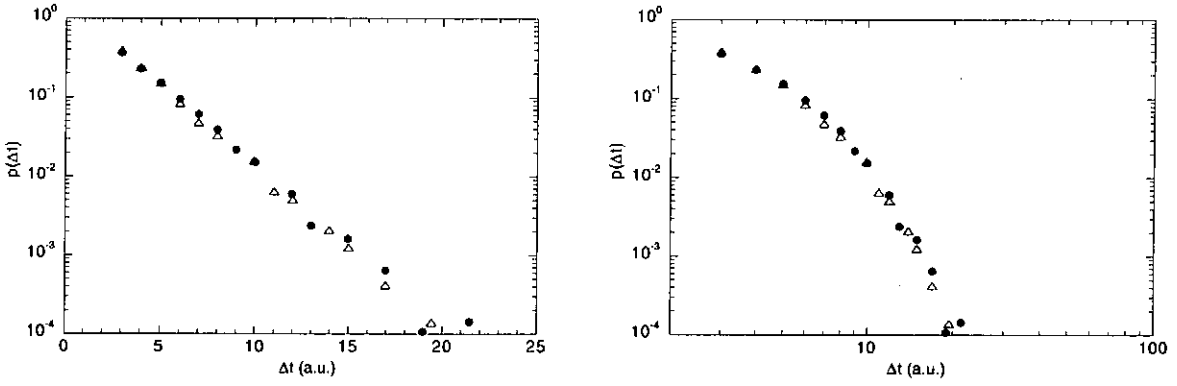

Fig. 1: PDFs of waiting times for the amplitude of reflectometric signal in the case of a random gaussian distribution for δ; black dots σ_φ = 1.4 π, triangles σ_φ = 6.4 π.

In real measurements one expects that the plasma does not change abruptly, but has some smooth evolution. This has been simulated by translating the scatterers δ at every calculation step: $\delta_p(t) = \delta_{p+q}(t - \Delta t)$ if p ≤ N-q, while new values of $\delta_p(t)$ are given if N-q < p ≤ N.

In the case (with q=4) shown in Fig. 2 the PDFs of waiting times show a power-law decay for the lower values and an exponential decay for the longer intervals. This result is not surprising, since into the system has been put a memory with a defined time, which is a possible type of interaction. Thus the PDFs are power-law distributed in the range of the memory length, while for longer times they are still exponential.

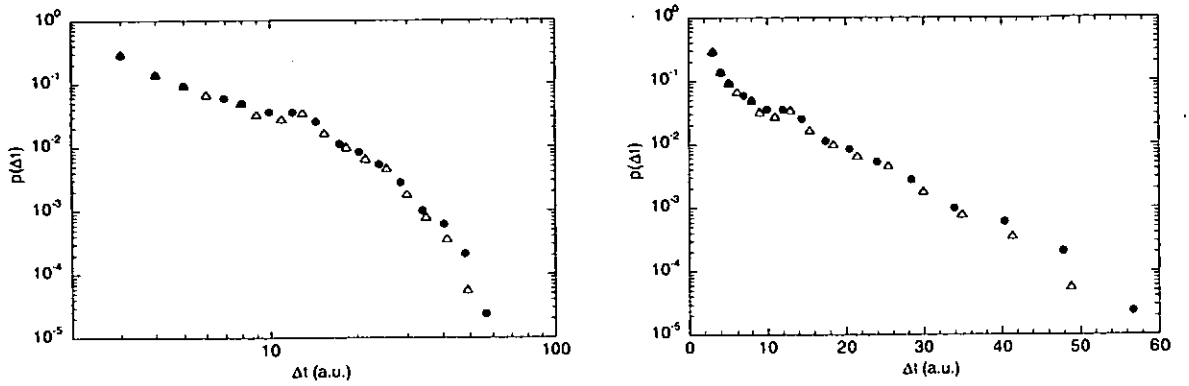

Fig. 2: PDFs of waiting times of the reflectometric signal in the case of a random gaussian distribution with memory;black dots $\sigma_\varphi = 1.4\ \pi$, triangles $\sigma_\varphi = 6.4\ \pi$.

The third case is obtained with a sequence $\delta_p(t)$ that has a PDF for waiting times which is power-law distributed (Fig. 4). In this case two different ranges with power law appear (Fig. 3). The former is due to the memory effect as in the previous case, while the latter is a property of the originating sequence.

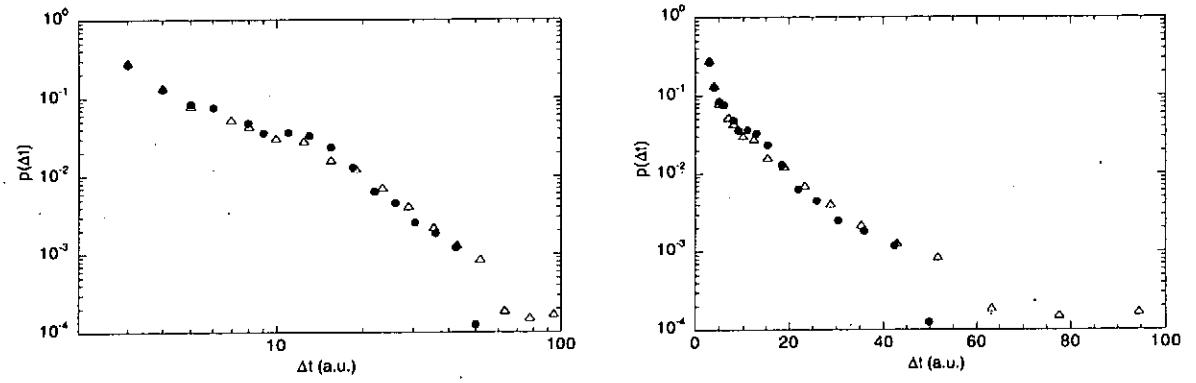

Fig. 3: PDFs of waiting times in the case of a chaotic noise δ having a power law in its PDF of waiting times;black dots $\sigma_\varphi = 1.4\ \pi$, triangles $\sigma_\varphi = 6.4\ \pi$.

It is worth to note that even if this modelling is oversimplified, there is a striking similarity between the signal obtained from the reflectometer and a sample of the simulation of the last case considered (Fig. 6).

Finally in Fig. 5 is shown the PDF for waiting times obtained in a set of RFP discharges at 300 kA are reported. The result is remarkable since the power law spans more than 2 decades; moreover the same statistical analysis, applied to the density fluctuations measured with Langmuir probes, gives a decay exponent very close to that measured by reflectometry [5].

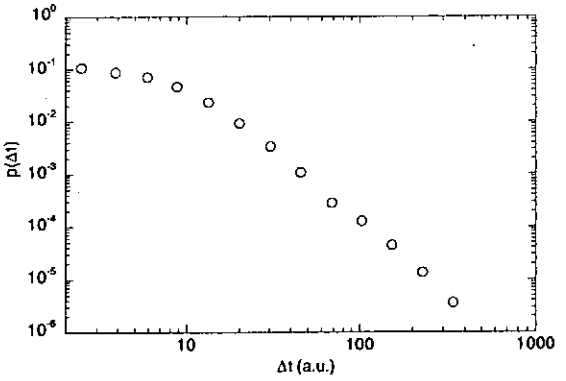

Fig. 4: PDF of waiting times for the δ(t) signal used in the simulation shown in Fig. 3.

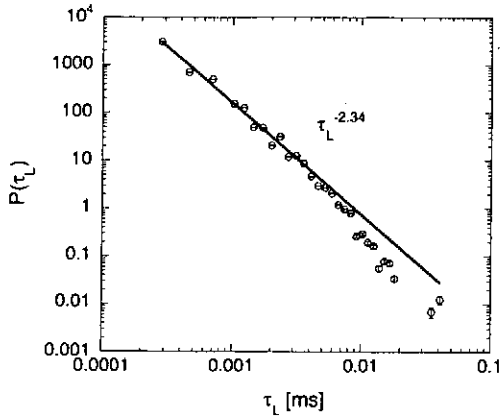

Fig. 5: PDF of waiting times of the reflectometric signal measured on RFP discharges (from ref.[5]).

The conclusion is that the waiting times measured by means of microwave reflectometry do not stem from random process, but are indeed the clear signature of plasma dynamics.

This means that, although difficult to recover, the amplitude of the reflected signal retains a non trivial amount of information about the density fluctuations. In this case, as suggested in B99, the presence of a power-law decay in the PDF makes questionable the applicability of the SOC as a paradigm for modelling the behaviour of transport in fusion plasmas.

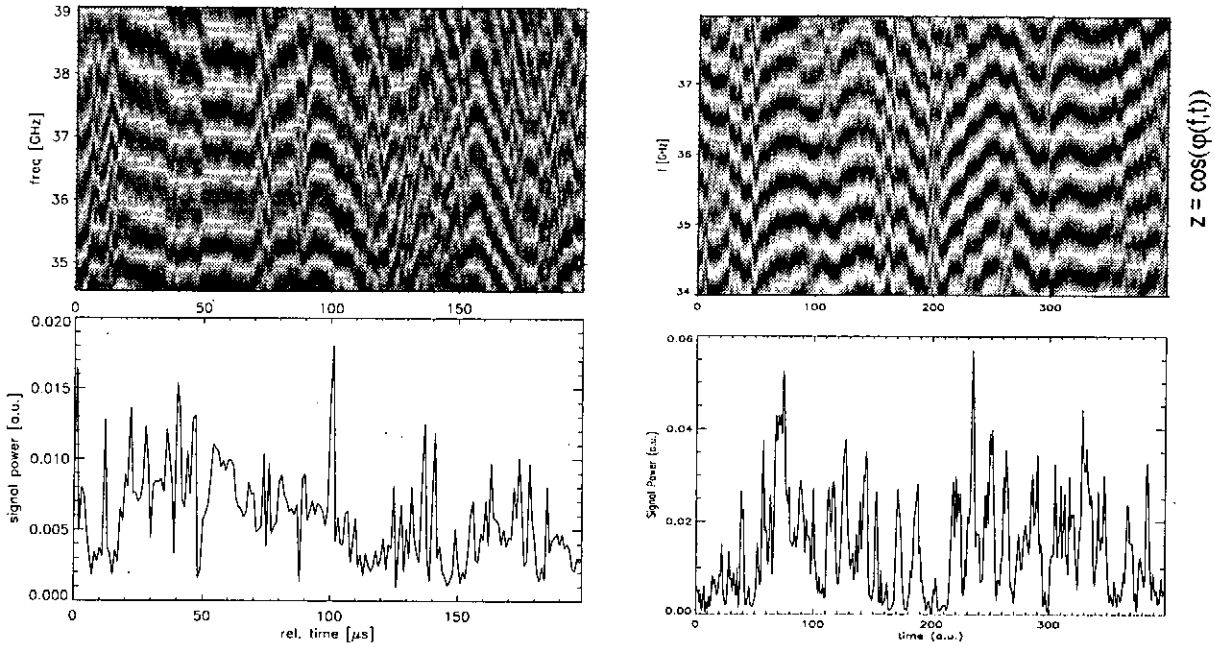

Fig. 6: comparison of zebra stripe and amplitude plot of a real reflectometric signal (left) with the simulation performed in the worst case of Fig. 3 ($\sigma_\varphi = 6.4\ \pi$).

References.

[1] D.E.Newman, B.A.Carreras, P.H.Diamond, T.S.Hahm, *Phys. Plasmas* **3**, 1858 (1996); B.A.Carreras, D.Newman, V.E.Lynch, P.H.Diamond, *Phys. Plasmas* **3**, 2903 (1996); R.O.Dendy, P.Helander, *Plasma Phys. Control. Fusion* **39**, 1947 (1997); R.Sanchez, D.E.Newman, B.A.Carreras *Nuclear Fusion*, **41**, 247 (2001).

[2] E.Lu and R. J.Hamilton, *Astrophys. J.* **380**, L89 (1991).

[3] G.Boffetta, V.Carbone, P.Giuliani, P.Veltri, A.Vulpiani, *Phys. Rev. Lett.* **83**, 4662 (1999)

[4] P.Bak, C.Tang, K.Wiesenfeld. *Phys. Rev. Lett.* **59**, 381 (1987) and *Phys. Rev. A* **38**, 364 (1989).

[5] E.Spada, V.Carbone, R.Cavazzana, L.Fattorini et al. *Phys. Rev. Lett.* in publication (2001).

[6] E.Mazzucato, *Rev.Sci.Instrum.* **69**, 1691 (1998); E.Holzhauer, M.Hirsch, T.Grossmann, B.Brañas, F.Serra, *Plasma Phys. Control. Fusion* **40** ,1869 (1998); G.D.Conway et al., *Rev.Sci.Instrum.* **67**, 407 (1996);

[7] P.Beckmann and A.Spizzichino, *The Scattering of Electromagnetic Waves from Rough Surfaces*, Pergamon Press, 1963.

[8] R.Cavazzana, M.Moresco, N.Pomaro, A.Sardella, E.Spada, *Rev. Sci. Instr.* **70**, 1056 (1999).

Effects of finite density fluctuations and of the upper hybrid resonance on O-X correlation reflectometry

G J Kramer, R Nazikian, and E Valeo
Princeton Plasma Physics Laboratory Princeton NJ 08543-0451 USA

An essential physics parameter to determine in magnetic confinement systems is the magnetic safety factor, q. In two recent articles [1, 2] a novel approach to magnetic equilibrium reconstruction has been proposed based on the reflection of microwaves of different polarizations from a magnetized plasma. The method makes use of the presence of turbulence in the plasma column by easuring the peak correlation in the reflected signal between O-mode and the X-mode waves which peaks near to where the two cut off layers coincide. From the frequency difference between the two orthogonal polarizations at the peak in their correlation the local magnetic field strength can be obtained. The reflection layer of the O-mode depends only on the plasma density whereas the reflection location of the X-mode depends both on the density and the magnetic field strength.

In the following we present results of 1D simulations incorporating the upper hybrid (UH) resonance and finite density fluctuation levels. With this code we have found two mechanisms that can lead to the degradation of the O-X correlation. The first mechanism is the effect of a significant level of density fluctuations (i.e. $\tilde{n}/n > 1\%$) and the second mechanism is the influence of the UH resonance on the X-mode scattering which is important at low magnetic fields when the UH resonance is close to the X-mode cut off. Our simulation results indicate that finite fluctuation levels can strongly influence the O-X correlation whereas the effect of the UH resonance is negligible unless the magnetic field is very low or the density scale length is very short.

The 1D simulation code is based on a tri-diagonal implicit method in which the scalar wave equation

$$\left(\frac{\partial^2}{\partial x^2} + k_0^2 \varepsilon(x)\right) E(x) = 0$$

for the electrical field, $E(x)$, is solved for a wave with a vacuum wave vector $k_0 = 2\pi/\lambda_0$ (λ_0 is the vacuum wave length). The X-mode permittivity, $\varepsilon(x)$, is given by

$$\varepsilon = 1 - \frac{(U - X)X}{(U - X)U - Y^2}$$

with $X = (\omega_{pe}/\omega)^2$, $Y = \omega_{ce}/\omega$, $U = 1 - \mathrm{i}\nu_{ei}/\omega$, $\omega_{pe} = (n_e e^2/\varepsilon_0 m_e^*)^{1/2}$ the plasma frequency, $\omega_{ce} = eB/m_e^*$ the electron cyclotron frequency and ν_{ei} the electron-ion

collision frequency. The O-mode permittivity is obtained when Y is zero. The finite electron-ion collision frequency is included to account for the pole at the UH resonance. The effective electron mass, $m_e^* = m_e(1 + 5\,T_e/511)^{1/2}$, is corrected for finite electron temperature effects (T_e the electron temperature in keV).

For the solution of the wave equation an incoming and outgoing wave are taken in the vacuum region outside the plasma as

$$E(x) = \exp(\mathrm{i}k_0 x) + \exp(-\mathrm{i}(k_0 x + \phi))$$

and integrated into the evanescent region beyond the cut-off to determine the (complex) phase, ϕ, which reflects the density fluctuations.

For the simulation of the density fluctuations we have added to the equilibrium profile a spectrum of fluctuations which gives the following density correlation function

$$\langle \tilde{n}(x_2)\,\tilde{n}(x_1)\rangle/n^2 = \left(\frac{\tilde{n}}{n}\right)^2_{x_1} \exp(-(x_2 - x_1)^2/\lambda_c^2)\cos(k_{\text{fl}}(x_2 - x_1))$$

with $(\tilde{n}/n)_{x_1}$ the fluctuation amplitude, x_1 (x_2) the fixed (variable) frequency cut off layer position, λ_c the 1/e width of the correlation and $k_{\text{fl}} = 2\pi/\lambda_{\text{fl}}$ where λ_{fl} is the characteristic fluctuation wave length.

A set of N (typically 500) random density distributions, $\tilde{n}(x)$, are generated from the correlation function. The wave equation is then solved numerically for each of these distributions to generate an ensemble of complex phases, ϕ, for the outgoing wave. This is repeated for each frequency and each mode of propagation. Finally, the normalized correlation, γ, of the complex signal of the outgoing waves, $E = \exp(\mathrm{i}\phi)$, is obtained

$$\gamma = \frac{|\langle E_O E_X\rangle|}{\sqrt{\langle |E_O|^2\rangle\langle |E_X|^2\rangle}}.$$

We have investigated the effects of finite density fluctuation levels for parameters similar to those obtained in the LAPD experiments [1]: the density scale length, $L_n = 20$ cm, the fluctuation width $\lambda_c = 1.57$ m, and $k_{\text{fl}} = 0$ m^{-1}. We have scanned fluctuation level, $\tilde{n}/n$, at two magnetic fields: $B = 0.10$ and 0.18 T. From figure 1 (a) it can be seen that the decorrelation between the X-mode and O-mode signals depends on the fluctuation level and the decorrelation is stronger at higher magnetic field strengths.

The location where the correlation peaks depends also on the fluctuation level (figure 1 (b)) and the position moves away from the equilibrium fixed channel location when $\tilde{n}/n$ increases. Even at low fluctuation levels there is a separation between the fixed channel and the peak correlation position for the full wave solution. One consequence of this analysis is the need for detailed comparison with experiment to determine if the separation of the O- and X-mode cut off layers indeed increases with fluctuation levels as the 1D simulations indicate.

The separation between the equilibrium fixed frequency O-mode reflection point and the point of maximum correlation at low density fluctuation levels can be explained successfully with the phase matching arguments as presented in reference [1]. Moreover, the excursions of the O- and X-mode reflection points at the maximum correlation

due to low fluctuation levels are very similar as can be seen in figure 2 (a) where $\tilde{n}/n = 0.01$. The distribution of the actual O-mode reflection point is distributed symmetrically around the reflection point without fluctuations, whereas the distribution for the X-mode reflection point is shifted strongly (figure 3 (b)). At high fluctuation levels these distributions broaden and shift away from the equilibrium location toward the reflectometer antennas (figure 3 (d)) for $\tilde{n}/n = 0.20$. The location of the O- and X-mode reflection points decorrelate as can be seen from the large scatter of points above the straight diagonal line in figure 3 (c), consistent with a decreased O-X correlation.

In order to investigate the possibility to use O-X correlation reflectometry as a diagnostic tool for the magnetic field strength in tokamak plasmas we have calculated the peak in the O-X correlation for an ITER like plasma as a function of the magnetic field strength for different density fluctuation levels (figure 3) with the following parameters: major radius 4.0 m, minor radius 1.5 m, parabolic density profile with central density $1.0\,10^{20}$ m^{-3} and a fixed frequency O-mode channel at 75 GHz which is reflected at 4.79 m. The correlation length, λ_c, was chosen to be 0.01 m and $k_\parallel = 0$ m^{-1}.

From figure 3 it can be seen that the O-X peak correlation is strongly affected by the level of density fluctuations. At magnetic fields above one Tesla the correlation is only significant when the density fluctuations are less than 0.5% and this number drops even further with higher field strengths. At low magnetic fields the correlation is degraded due to the presence of the UH resonance.

We have also investigated the dependence of the peak correlation as a function of the density correlation length, λ_c with the above given tokamak parameters at 3 T (figure 4). From this figure it can be seen that the frequency where the correlation peaks depends very weakly on the density correlation length and on the fluctuation level when it is below 1%. The width of the peak, however, increases with the correlation length as can be seen from the Full Width Half Maximum (FWHM) contours. Because the position of the O-X correlation peak does not depend on the density correlation length it can provide a robust measure of the local magnetic field strength.

We have shown that the decorrelation of the O-mode and X-mode signals with increasing magnetic field strength can arise from a finite level of density fluctuations. For large scale fusion plasmas the correlation between the O-mode and X-mode reflection signals may be used to determine the magnetic field strength provided that the fluctuation level is sufficiently low.

The O-X correlation measurements for determining the magnetic field strength in plasmas is promising, and should be a valuable diagnostic in fusion scale plasmas provided that the peak in the correlation can be determined with sufficient accuracy. Further work should focus on the the 2D modeling of the O-X correlations under various plasma conditions and on the degree to which the peak correlation can be measured, which will relate directly to the accuracy of the magnetic field strength measurement and its effectiveness as a constraint to determine the MHD equilibrium.

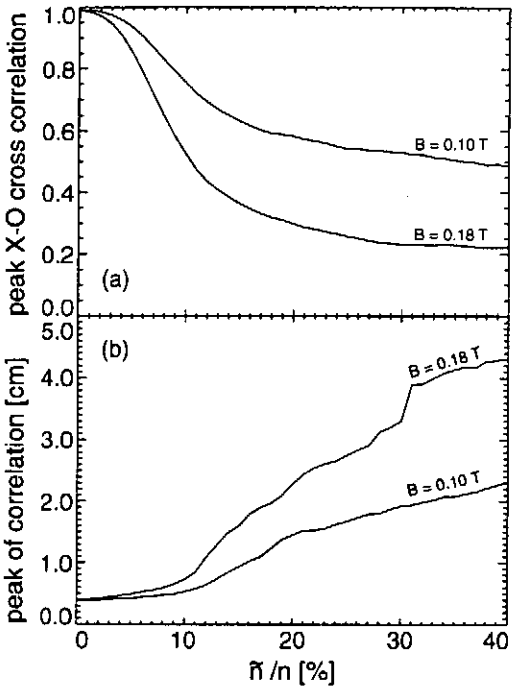

Figure 1

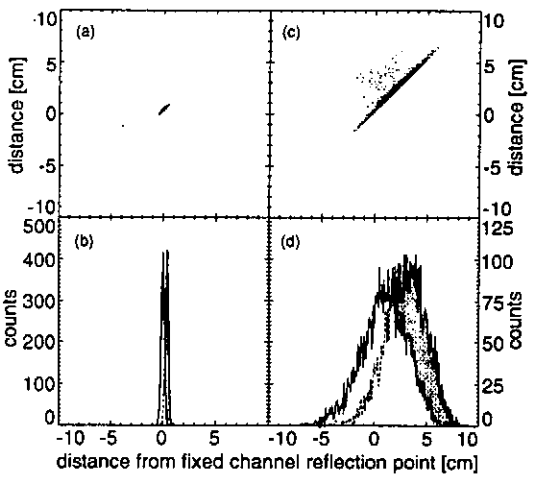

Figure 2

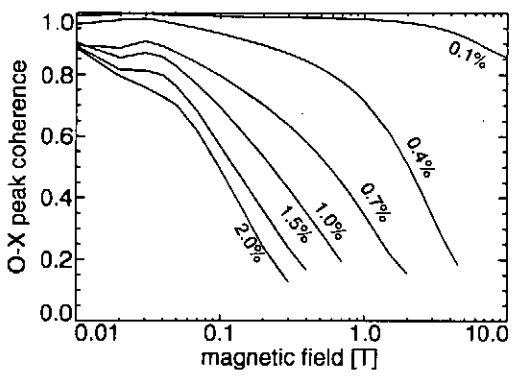

Figure 3

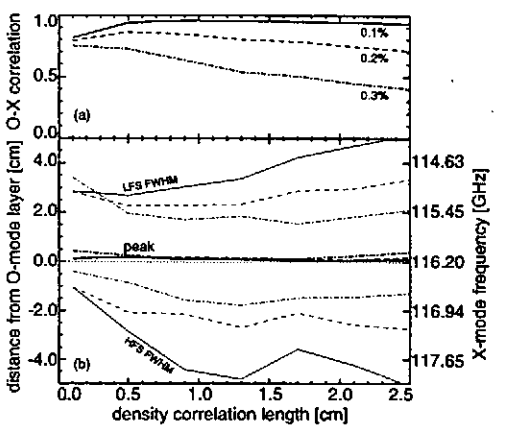

Figure 4

References

[1] Gilmore M *et al* 2000 *Plasma Phys. Control. Fusion* **42** 655

[2] Gilmore M *et al* 2000 *Rev. Sci. Instrum.* bf 72 293

Fluctuation and reflectometer simulation studies on ASDEX Upgrade

G.D.Conway, B.Kurzan, B.Scott, E.Holzhauer[1], S.Klenge[1], W.Suttrop, M.Kaufmann, F.Jenko, F.Serra[2], T.T.Ribeiro[2], H.Zohm, ASDEX Upgrade Team and CFN Reflectometry Group

Max-Planck-Institut für Plasmaphysik, Euratom-Association IPP, D-85748, Garching, Germany

[1] *IPF, Universität Stuttgart, D-70569, Stuttgart, Germany*

[2] *CFN Associação Euratom/IST, Lisboa, Portugal*

1. Introduction

Three areas of current reflectometer research on the ASDEX Upgrade tokamak are presented. First, a new Doppler reflectometer system is described together with first results on radial profiles of rotation velocities. Next is an example of fluctuation measurements using a multi-channel reflectometer, specifically the localized reduction of turbulence during internal transport barrier discharges. Finally, new results are presented from the comparison of full-wave and physical optics reflectometer simulation codes using simulated density turbulence from a Landau-fluid code. The results are also compared with real reflectometer signals with a view to validating the turbulence code.

2. Doppler reflectometry

Doppler reflectometry is a new development for measuring turbulence propagation velocities. It combines the wavenumber k selectivity of a scattering diagnostic with the radial localization of reflectometry, see ref. [1] for a description of the principles and advantages of this technique. The diagnostic on ASDEX Upgrade (AUG) consists of a single O-mode channel with a stepable (3 ms) frequency between 50 - 75 GHz. Two 12 - 18 GHz hyperabrupt varactor tuned oscillators (HTO) plus frequency quadruplers (RF & LO) are phase locked with a $\Delta f = 20$ MHz to form a heterodyne receiver with an in-phase and quadrature (IQ) detector. The output power into the oversized circular waveguide transmission lines is about 10 mW.

Bistatic hog-horn antennas with parabolic focusing reflectors are used. There are two sets of antennas on the tokamak low field side, one pair with a poloidal tilt (above mid-plane) and one pair with a toroidal tilt (below mid-plane). The actual tilt angle, typically 0 - 12°, varies with plasma shape resulting in Doppler shifts of up to 5 MHz. To measure such large shifts a 20 MHz sample rate data acquisition system is employed with a 5.125 s sample window. The reflected spectrum (from the FFT of I and Q signals) contains two components, an unshifted 0th order reflection (carrier wave) and a Doppler shifted 1st order backscatter. Due to the non-optimized antenna pattern the 0th order component tends to be broad, so a "centre of gravity" algorithm

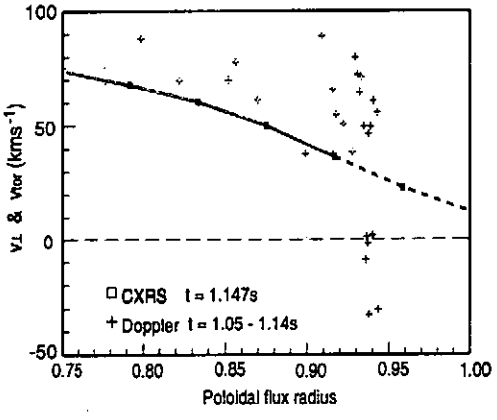

Figure 1: $v_\perp$ (Doppler) and v_{tor} (charge exchange spectroscopy) vs ρ_{pol} for shot #13443.

is used to extract the Doppler frequency f_D. A ray-tracing code is also used to calculate the precise angle of incidence θ and then the fluctuation phase velocity computed from $v_\perp = f_D/2k_o \sin\theta$. Stepping the launch frequency (and hence cutoff layer radius) during the discharge allows a $v_\perp$ radial profile to be constructed. $v_\perp$ contains both poloidal and toroidal components, although generally the toroidal component dominates. Fig. 1 shows an example during an ELM-free phase of an H-mode discharge (shot #13443). A comparison of the reflectometer $v_\perp$ with carbon impurity toroidal velocity from charge exchange spectroscopy shows good agreement in the core, where $v_\perp$ is dominated by the $E \times B$ velocity, and then a region of strong shearing close to the H-mode pedestal. Here the strong density gradient causes the diamagnetic drift velocity to dominate resulting in the observed reversal in $v_\perp$. A series of hardware upgrades are in progress, including a second channel (to permit correlation and shearing measurements), together with new X-mode antenna pairs (to probe the core plasma) and optimized antenna reflectors with side-lobe suppression (to give better k-resolution).

3. Turbulence measurements

The 9 channel O-mode (normal incidence) swept frequency system installed on AUG for high and low field side (hfs & lfs) density profile measurements [2] can also operate with fixed frequencies (Ka to V-band: 18-75 GHz) for fluctuation measurements (with a dedicated 2 channel O-mode Q & V-band homodyne system). Measurements on the reduction of turbulence around an internal transport barrier (ITB) have previously been presented [3], here we extend the analysis to demonstrate the radial behavior of the turbulence.

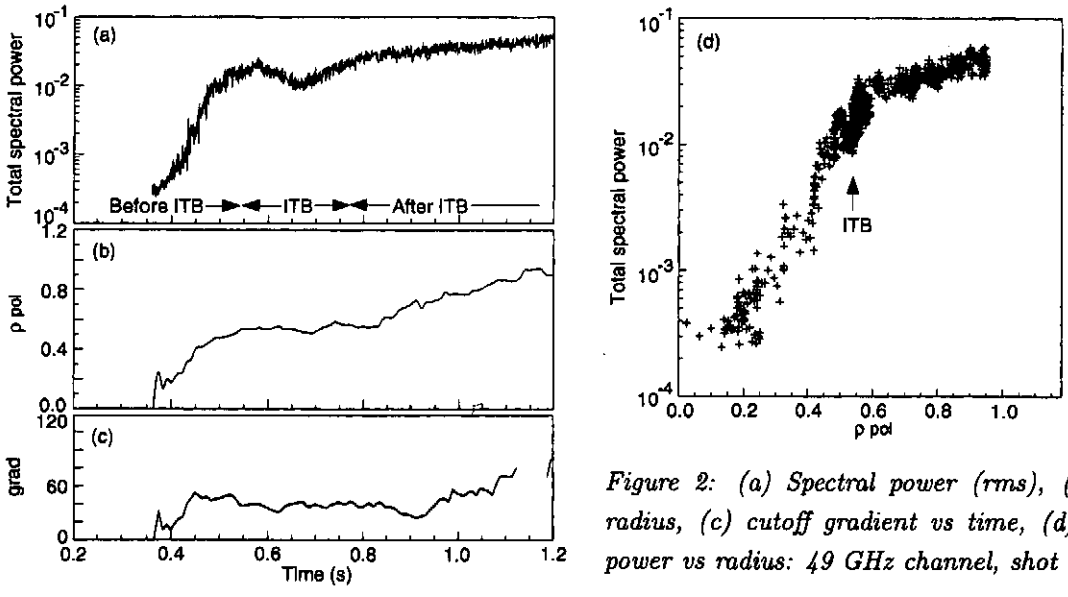

Figure 2: (a) Spectral power (rms), (b) cutoff radius, (c) cutoff gradient vs time, (d) spectral power vs radius: 49 GHz channel, shot #13553.

In fig. 2(a) the total spectral power between 1 and 250 kHz (rms fluctuation level) from a 49 GHz lfs channel is plotted as a function of time during a (2.6 T / 1 MAs^{-1} I_p ramp) L-mode edge ITB discharge (shot #13553). The signal begins after the X-point formation and the application of 5 MW neutral beam injection (NBI). The ITB forms after 0.55 s outside $\rho_{pol} \sim 0.45$ (poloidal flux radius). The triangular (peaked) density profile is maintained as the density rises with NBI fueling causing the cutoff layer to move out radially, fig. 2(b), but with a roughly constant density gradient at the cutoff,

fig. 2(c). Plotting the rms fluctuation level against the evolving cutoff layer position gives the radial profile of fig. 2(d). Each data point has an integration period of 0.512 ms, so the clustering of points shows the rapid movement of the cutoff prior to the ITB, then, stagnation during the ITB and the slow ramp out to the edge after. The fluctuation level ranges over two and a half orders of magnitude from the core to the L-mode edge, with a localized drop (factor of 5) during the ITB. The rms signal is not normalized so there is also an inherent variation in the signal level due to the changing spot size and reflected power (carrier strength) with the antenna to cutoff layer distance.

4. Simulation and modeling studies

Simulation studies are also underway with the aim of coupling turbulence and reflectometry simulation codes. The purpose of this work is two-fold: first to perform a comparison between various reflectometer simulation codes using the same input data, and secondly to validate the turbulence code by comparing with experimental reflectometer data. The turbulence code is the DALFTI Landau-fluid code [4]. This code uses values of ∇n_e, ∇T_i, ∇T_e, plus separatrix values, together with q and geometric parameters such as a, R and B from an L-mode edge AUG discharge - in this case shot #13553 (chosen for the availability of reflectometry data) - and computes the evolution of the density and temperature turbulence (using drift Alfvén and ITG models etc.). The output is a series of snap-shots in time of two dimensional (2D) density contours (radius & poloidal), which are then used as input to three different reflectometer simulation codes: a 2D explicit time dependent full wave code [5] (with a $\lambda/16$ grid and absorbing boundaries); a 2D physical optics code [6] employing a far-field Greens solution to the Helmholtz equation; and a 2D network code [7] which is an implicit stationary solution of the full wave equation. Figure 3 shows a density contour snap-shot from DALFTI together with E-field contours from the full wave code. The antenna is modeled on an AUG Q-band O-mode antenna positioned at $R = -0.03$ m with $f = 36$ GHz. The density contours show that the DALFTI code predicts large density fluctuations (several tens of percent) with density fingers/streamers reaching outwards and folding over. As a result the cutoff layers move 2 - 3 cm with several fringe jumps and cutoff layer shadowing. The output of the full-wave and physical optics codes are time series of phase ϕ and amplitude A of the reflected E-field at the antenna (normalized to a mirror reflection). Fig. 4 shows probability distribution functions (pdf) of A and ϕ fluctuations from the full-wave code (1725 time points). As expected the phase is uniformly distributed between $\pm\pi$ radians due to the multi-fringe excursion of the cutoff layer. The amplitude has the usual Rician distribution of a Radar type signal. The next step is the comparison of the simulated reflectometer signals with the input data from the DALFTI code, and with the real reflectometer data from discharge #13553.

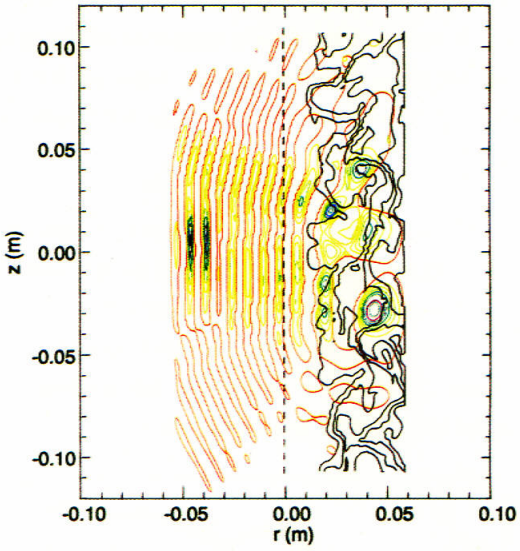

Figure 3: Snap-shot of density contours (black) from DALFTI plus E-field contours from full-wave code.

Figure 5 shows spectra for (a) the DALFTI code, (b) physical optics code (c) full-wave code, and (d) 36 GHz homodyne signal at 0.8 s (corresponding to $\rho_{pol} \sim 0.9$) for shot #13553. Unfortunately results from the 2D Network code are not available for comparison at this point. In fig. 5(a) the two DALFTI frequency spectra are for the 36 GHz cutoff layer (red) and midplane density (green) perturbations, both spectra peak around 20 kHz/0.2 cm^{-1} but decay with spectral indices of -2 and -3 respectively (discrepancy not known). For the physical optics and full-wave data spectra are shown for the phase (blue), amplitude (red) and homodyne (green) signals. Again all the spectra peak around 20 kHz and generally decay with spectral indices of $m = -2$, the exception being the full-wave amplitude and homodyne signals which decay with $m = -4$. Certainly the full-wave phase spectrum most closely replicates the cutoff layer spectrum from the DALFTI data, however it is clear that the two reflectometer codes predict different instrument response functions. This may in part be a result of the high level of cutoff layer perturbations causing a breakdown (saturation) in the physical optics solution. This will be addressed in future work. However the most promising result is drawn from the comparison with the real reflectometer spectrum in fig. 5(d). Again the homodyne signal spectrum peaks around 20 kHz and decays with $m = -2$, showing that the DALFTI code in principle correctly replicates the structure of the L-mode edge turbulence, if perhaps not the correct amplitude.

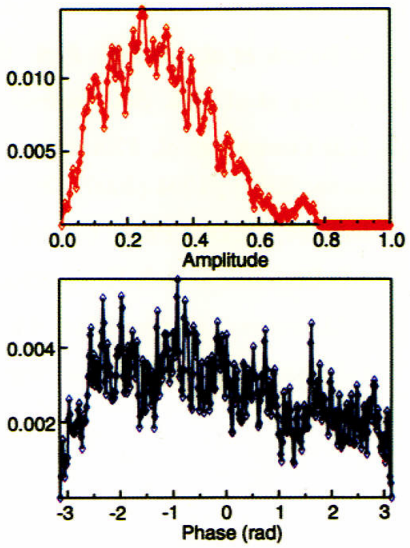

Figure 4: A and ϕ pdfs from full-wave (DALFTI shot #13553).

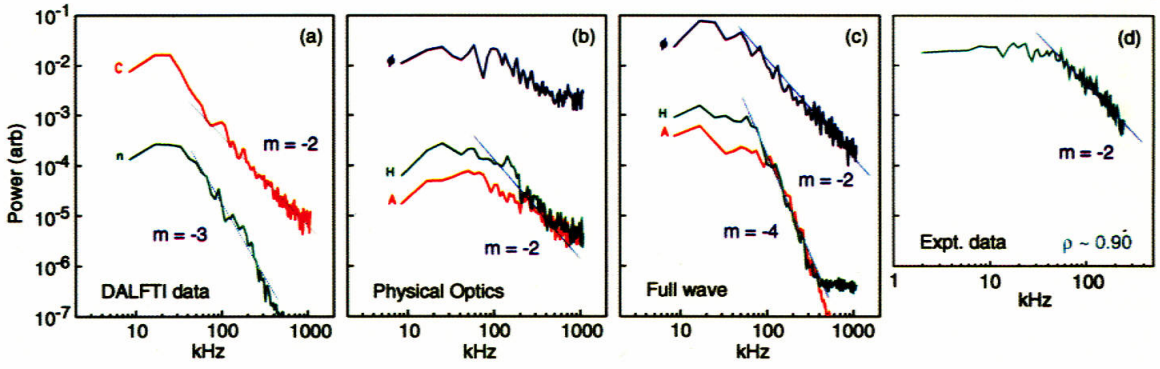

Figure 5: Spectra of: (a) DALFTI density n and cutoff C, (b) Physical optics (c) Full-wave ϕ, A and homodyne simulated signals, (d) real 36 GHz homodyne signal for #13553.

Acknowledgments

Special thanks to M.Manso, A.Silva, L.Cupido, & P.Varela for development of profile reflectometer at IPP, and S.Vergamota, I.Nunes for assistance with data collection.

References

[1] M.Hirsch *et al*, *4th Intl. Refl. Wksh. CEA report* EUR-CEA-FC-1674 (1999)

[2] A.Silva *et al*, *Rev. Sci. Instrum.* **70** 1072 (1999)

[3] G.D.Conway *et al*, *27th Eur. Conf. Control. Fusion Plasma Phys. (Budapest)* vol.24B of *ECA* (Geneva: EPS) p1004 (2000). Submitted to *Plasma Phys. Control. Fusion*

[4] B.Scott, *Plasma Phys. Control. Fusion* **39** 1635 (1997), & **40** 823 (1998)

[5] J.G.Blaschak & A.K.Kriegsmann, *J. Comput. Phys.* **77** 109 (1987)

[6] G.D.Conway, *Plasma Phys. Control. Fusion* **41** 65 (1999)

[7] E.Holzhauer *et al*, *Plasma Phys. Control. Fusion* **40** 1869 (1998)

Advances in the density profile evaluation from broadband reflectometry on ASDEX Upgrade

P. Varela[a], and M. Manso
Associação EURATOM/IST, Centro de Fusão Nuclear, Instituto Superior Técnico
1049-001 Lisboa, Portugal

G. Conway, and ASDEX Upgrade Team
Max-Planck-Institüt für Plasmaphysik, EURATOM Association
D-85748 Garching, Germany

The high temporal and spatial resolutions provided by broadband microwave reflectometry make it an attractive diagnostic technique to measure the density profile in fusion plasmas. However, great problems have been encountered due to the plasma turbulence that difficult, and sometimes prevent, the routine evaluation of density profiles. Advanced broadband systems employ ultra-fast sweeping in an attempt to perform the profile measurement in a time window smaller than the temporal scale of the main plasma fluctuations but this is not sufficient. Indeed, abrupt plasma movements and/or spatial turbulence always affect the reflectometry signals, as shown by numerical studies (with both one- and two-dimensional codes), for the case of ultra-fast sweeping and pulse radar systems. For this reason not only the system performance is important but the software tools also play a crucial role for reflectometry to become a standard density profile diagnostic. Here we present the recent advances towards automatic evaluation of density profiles from broadband reflectometry on ASDEX Upgrade. For regimes with moderate levels of plasma turbulence, density profiles are obtained from single reflectometry samples (temporal resolution of 20μs), and for higher turbulence levels average profiles are obtained from bursts of ultra-fast (20μs), closely spaced (10μs) sweeps. This method improved the accuracy and reliability of density profiles, which can now be obtained automatically from the edge to the bulk plasma – using reflectometry alone – in most plasma regimes of ASDEX Upgrade. New data processing capability has been implemented that allows the profiles to be available to the end-users 10–12 minutes after each discharge. These developments were possible due to the flexibility and high performance of the control and data acquisition systems and to the large number of measurements that can be performed with the diagnostic during each discharge (720 profiles both on the low- and high-field sides).

I. INTRODUCTION

Broadband microwave reflectometry has great potentialities to measure the electron density profile in magnetic confinement fusion devices, mainly due to the high temporal and spatial resolutions it provides, and to the relatively reduced machine access it requires. However, the automatic routine evaluation of density profiles has been hard to achieve due to the effects of plasma turbulence in the reflectometry signals. Advanced broadband reflectometry diagnostics attempt to reduce the effect of plasma turbulence by performing the profile measurement in a time window smaller than the temporal scale of typical plasma fluctuations.

The results obtained in ASDEX Upgrade with broadband ultra-fast sweeping (20μs) indicate that the perturbations exhibit by the density profile can be correlated with plasma turbulence, as well as with fast and localized movements of the density layers, such as those occurring during edge localized modes (ELMs). Numerical simulations performed with a two-dimensional full-wave code[1] that includes the relevant features of the ASDEX Upgrade broadband reflectometer, have confirmed these effects. Although some effects may be attributed in part to the finite probing time, simulation studies performed with a one-dimensional code[2] show that even in the case of the quasi-instantaneous pulse radar technique, the spatial turbulence, which cannot be avoided, still induces significant errors in the profile evaluation. This shows that not only the system performance is important but also software tools for group delay evaluation play a crucial role for reflectometry to become a standard density profile diagnostic.

Our approach in designing the ASDEX Upgrade broadband reflectometer[3,4] was to implement a flexible and high performance system complemented by advanced data analysis tools capable of estimating the group delay versus probing frequency curves in the presence of plasma turbulence. Here we present the recent advances in the data processing system that en-

[a] Electronic mail: pvarela@cfn.ist.utl.pt

abled the automatic routine evaluation of density profiles, and their availability to the users 10–12 minutes after each discharge.

The remainder of the paper is organized has follows. In Sec. II, the improvements to the profile evaluation are presented. Section III describes the automatic routine evaluation of density profiles implemented on the ASDEX Upgrade reflectometer. Finally, Sec. IV summarizes and gives some hints concerning future work.

II. IMPROVED PROFILE MEASUREMENTS

The broadband reflectometer in the ASDEX Upgrade tokamak was specifically designed to meet several measurement requirements, in particular those of density profile measurements. The system features ultra-fast sweeping and has the unique capability of probing from both magnetic field sides simultaneously. Profile measurements can be performed in several modes: (i) equally spaced covering the complete discharge, (ii) in burst-mode, with bursts of closely spaced sweeps with a larger interval between the bursts, and (iii) in a mixed mode, where parts of the discharge are covered with single measurements and others with bursts. In burst-mode, the number of sweeps per burst, the time interval between sweeps, and the spacing between bursts can be made different along the discharge. This is especially useful when it is required to cover parts of a discharge in detail, as is the case of L-H transitions.

The accuracy of profile measurements on ASDEX Upgrade depends heavily on the data processing tools. The most important piece of the data processing system is the group delay estimation code, which is based on the best-path algorithm.[5] This algorithm uses the spectrogram of the reflected signals, which shows how the reflected energy is distributed in the time-frequency domain. Fig. 1 shows two examples of spectrograms obtained during an ASDEX Upgrade H-mode discharge. The spectrogram in Fig. 1(a) corresponds to a profile measured just before (120μs) an ELM while Fig. 1(b) depicts the spectrogram corresponding to a profile measured at the onset of the same ELM as shown in the H_α trace in Fig. 1(c), where the red and blue lines mark the measurement times of the profiles corresponding to Fig. 1(a) and 1(b), respectively. The group delay curve shown in Fig. 1(a) (white line) is a good estimate due to the relative low level of turbulence when compared with the situation depicted in Fig. 1(b).

The results obtained so far in ASDEX Upgrade show that the signal-to-noise ratio (S/N) of the reflectometry signals plays an important role in the automatic evaluation of the profiles. If the S/N is high the inversion of the profile from single sweep data presents no problems, which is normally the case in plasma regimes with low levels of plasma turbulence such as in H-mode plasmas. When the level of turbulence increases the S/N ratio may become very low (in one or more probing frequency ranges) preventing the accurate inversion of the density profile. The solution to this problem usually consists in averaging over several consecutive sweeps to improve accuracy. However, care must be taken to ensure that samples are correlated so that the obtained average profile is meaningful.

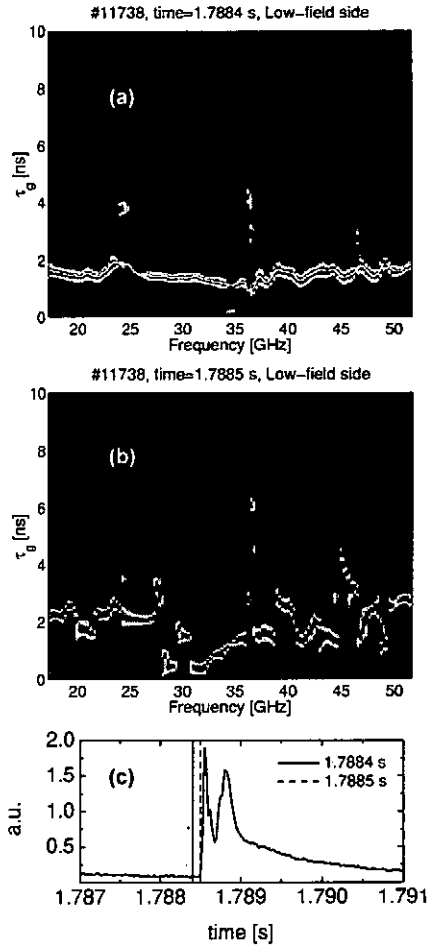

FIG. 1. Examples of spectrograms obtained from 20μs sweeps: (a) 120μs before a fast ELM occurs, (b) at the onset of the ELM, and (c) H_α emission. The vertical lines on (c) mark the measurement times of the profiles corresponding to (a) and (b), respectively.

In ASDEX Upgrade we take advantage of both the ultra-fast sweeping capability of the diagnostic and of the large number of measurements that can be performed in a single discharge to operate in burst-mode. The typical setup is to have bursts of eight closely spaced (10μs) ultra-fast sweeps (20μs) to obtain an average profile with a temporal resolution of 230μs. The interval between bursts can be tailored according to the physics needs.

The average profile cannot be obtained from simple averaging over the ensemble of group delays, as it is too sensitive to strong perturbations in the individual samples. To avoid this problem a burst-mode data analysis method has been developed. The method con-

siders all the information in the individual spectrograms to compute the burst profile. The computed burst-mode spectrogram retains the features common to the different sweeps while strongly reducing the perturbations of the individual group delays, therefore giving a more accurate and reliable burst profile. [6]

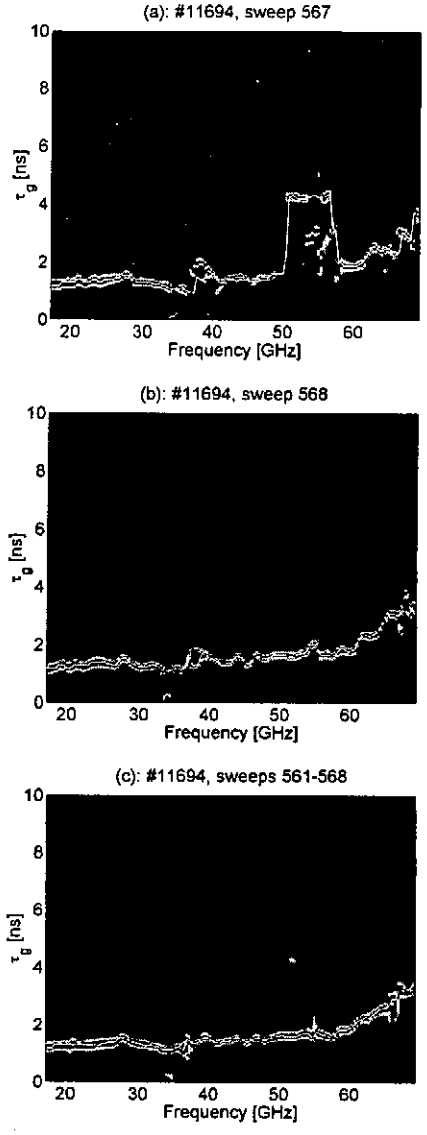

FIG. 2. Example of the application of the burst-mode data analysis method to eight (561–568) consecutive sweeps (20μs sweep time separated by 10μs) measured during an H-mode ASDEX Upgrade discharge: (a) and (b) spectrograms of two individual sweeps, 567 and 568, respectively; (c) burst spectrogram obtained with the burst-mode data analysis.

An example of the application of this analysis technique is shown in Fig. 2, which refers to the analysis of eight (561–568) consecutive sweeps spaced by 10μs. Figures 2(a) and 2(b) show two spectrograms corresponding to two individual sweeps (20μs) within the burst, where the group delays (white lines) obtained using the best-path algorithm are also displayed. In sweep 567 a strong perturbation is observed in the time-frequency distribution (and in the group delay) in the frequency range 50–58, where as in the next sweep the perturbation has disappeared. Smaller perturbations appear at different frequency locations in some of the other six spectrograms of the burst. The burst mode spectrogram (Fig. 2(c)) and the density profiles corresponding to the single and burst-mode analysis (Fig. 3) demonstrate the advantage of this multiple sweep analysis to obtain more accurate profiles. In fact, the group delay curve obtained using the burst-mode analysis is not affected by the strong deformations present in sweep 567, as it would happen if simple average were used.

Another advantage of burst-mode measurements is to improve accuracy and reliability while keeping a high temporal resolution and maintaining the profile measurement rate.

III. AUTOMATED ROUTINE EVALUATION

A crucial step for reflectometry to become a standard diagnostic is profile availability. Due to the large amounts of data acquired during a single discharge interactive data processing is not an option. The availability of the density profiles in a between-shots basis requires automatic evaluation.

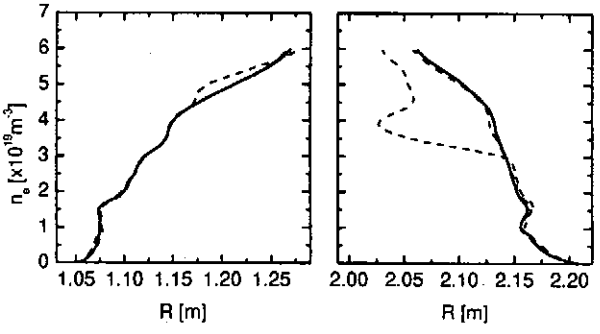

FIG. 3. Density profiles from the high-field side (left) and low-field side (right) inverted using single sweep data (dashed lines) and with the burst-mode analysis (solid lines) corresponding to the situation illustrated in Fig.2.

In ASDEX Upgrade, storage of diagnostic data is organized in shotfiles. Level-0 shotfiles contain the raw data and level-1 and subsequent shotfiles contain processed data. In the case of the reflectometry diagnostic level-1 shotfiles contain the density profiles obtained with single sweep data analysis. Level-2 shotfiles contain smoothed versions of the level-1 profiles together with median profiles, and burst-mode profiles obtained using burst-mode data analysis.

Reflectometry profiles are most useful if they are available to the end-users between discharges. With this in mind a fully automatic density profile evaluation procedure was implemented that enables to provide level-1 and level-2 profiles 10–12 minutes after each discharge. A monitoring process is launched in the background that waits for a new shot to be acquired. As soon as data is available for that shot the background process starts the level-1 and level-2

evaluation codes and waits for the next shot. The level-2 application stays idle waiting for available level-1 data. When this happens level-2 shotfile creation starts. To make the profiles available as quickly as possible the level-1 shotfile application subdivides itself into a number of smaller processes (typically eight) – a sub set of the acquired data is given to each sub process for evaluation. At the end, the results from the several sub processes are collected and the level-1 shotfile is created.

The automation of the profile evaluation faced three main problems: (1) the adjustment of the filters used to remove low amplitude modulations and high frequency noise, (2) profile initialization, and (3) the detection of the probing frequency above which the system is no longer in reflection.

As long as the S/N is high enough, the solution we adopted for the first problem was to keep the filters sufficiently open to accommodate a wide range of beat frequencies in all microwave channels. Concerning initialization, data from the X-mode channels can be used whenever available. Otherwise linear dependency on the probing frequency is assumed for the unmeasured part of the group delay. Work is going on to solve the problem of detecting the last reflecting probing frequency. An algorithm that estimates similarities between the plasma reflected signals and measurements performed while the reflectometer is in transmission mode is being developed, and it should be tested for accuracy and robustness during the next ASDEX Upgrade campaign.

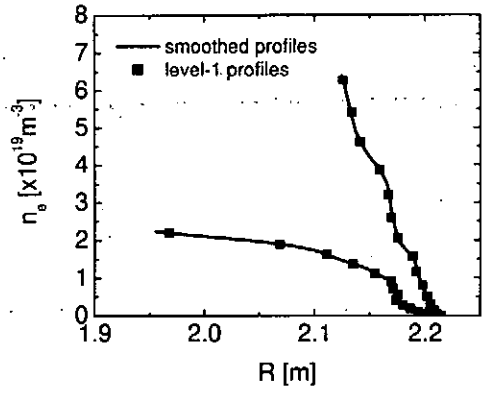

FIG. 4. Application of the smoothing algorithm to two level-1 profiles. For clarity only some points (squares) of the level-1 profiles are plotted.

Another problem is finding a suitable smoothing/fitting procedure to the group delay data that enables to obtain monotonic density profiles while retaining the essential structure of the measured profiles. An initial approach based on an iterative cubic spline approximation was implemented. The smoothing is done directly on the measured group delays (either from continuous or burst-mode measurements) to avoid the integration errors present in the inverted profiles. The iteration stops as soon as the smoothed profile is monotonic. Only profiles that become monotonic without over smoothing and with low mean-square errors are stored in level-2 shotfiles. The measured and smoothed profiles for low- and high-density examples are shown in Fig. 4. For clarity only some points of the level-1 profiles are plotted.

IV. SUMMARY AND FUTURE WORK

This paper describes the advances in the data processing system of the ASDEX Upgrade broadband reflectometer that improved the accuracy and reliability of the density profiles, which can now be obtained from the edge to the bulk plasma from reflectometry alone. The new data processing capabilities allow the density profiles to be available to the end-users 10–12 minutes after each discharge, which is a very important step for reflectometry to become a standard diagnostic. The high flexibility and performance of the reflectometer namely its capability to measure a large number of profiles during each discharge enabled the use of burst mode measurements, which are crucial to obtain accurate density profiles in the presence of high levels of plasma turbulence.

Currently, the acquisition system is based on in-house built, four channel, VME boards with 250 MHz maximum sampling rate and 720KB of memory per channel. With this setup 720 profiles can be measured on each magnetic field side, per discharge. To extend the measurement capability of the diagnostic the acquisition system is presently being upgraded to 3MB per channel, which will allow measuring 3000 profiles, per side, per shot. This will make it possible to operate in burst mode during the complete discharge.

ACKNOWLEDGMENTS

This work has been carried out within the framework of the Contract of Association between the European Atomic Energy Community and "Instituto Superior Técnico". Financial support from "Fundação para a Ciência e Tecnologia" e "Praxis XXI" was also received.

1. F. Silva, M. Manso, A. Silva, and ASDEX Upgrade Team, *Rev. Sci. Instrum.* **72**, 311, (2001).
2. S. Hacquin, *PhD* Thesis, Université Henry Poincaré, Nancy, 2000.
3. A. Silva, M. Manso, S. Vergamota, L. Cupido, L. Meneses, I. Nunes, and ASDEX Upgrade Team, *Rev. Sci. Instrum.* **72**, 307 (2001).
4. A. Silva *et al.*, *Fusion Technology*, edited by C. Ferro, M. Gasparotto, and H. Knoepfel, (North-Holland, Amsterdam, 1992), Vol. 1, p. 747.
5. P. Varela, M. Manso, I. Nunes, J. Santos, F. Nunes, A. Silva, and F. Silva, *Rev. Sci. Instrum.* **70**, 1060 (1999).
6. P. Varela, M. Manso, S. Vergamota, V. Grossmann, J. Santos, and ASDEX Upgrade Team, *Rev. Sci. Instrum.* **72**, 315 (2001).

Density Measurements with Broadband FM-CW Reflectometry in Advanced Scenarios on ASDEX Upgrade

M. Manso[1], S. Vergamota, I. Nunes, L. Cupido, T. Ribeiro, J. Santos, F. Serra, A. Silva, F. Silva, P. Varela
Associação EURATOM/IST, Centro de Fusão Nuclear, Instituto Superior Técnico
1049-001 Lisboa, Portugal

G. Conway, P. T. Lang, F. Ryter, R. Wolf, and the ASDEX Upgrade Team
Max-Planck-Institüt für Plasmaphysik, EURATOM Association
D-85748 Garching, Germany

I. INTRODUCTION

The broadband reflectometry system on ASDEX Upgrade has been primarily designed to measure density profiles with the unique capability to make measurements simultaneously at the high and low fields sides (HFS/LFS). It is equipped with nine broadband channels that simultaneously probe the plasma to obtain the complete profile in 20 ?s. A total of 1440 profiles can be obtained during each discharge. All channels can also operate in fixed frequency for fluctuation measurements. Two fixed frequency channels were added to probe selected layers routinely during the complete discharge and in particular to monitor the L to H transition. The diagnostic is now very complex and a dedicated control and data acquisition system was developed that allows great flexibility in the selection of the measuring intervals and modes of operation. The diagnostic can be remotely operated from any computer connected to the internet through in-house built client-server software with multiplatform control/monitor clients. Great progress was made since the diagnostic was built in 1991 [1], due to the optimized design and hardware improvements, and the development of novel data analysis and software tools for automatic profile evaluation [2]. Here we present recent measurements performed in different plasma regimes, namely in advanced plasma scenarios, such as improved H-mode plasmas and H-mode discharges with inboard launch pellet fuelling. The effect of plasma turbulence on profile measurements is analysed and it is shown that profile perturbations contain useful information about the plasma underlying phenomena. Finally we give examples showing the ability of the reflectometry broadband diagnostic on ASDEX Upgrade to track plasma movements.

II. DENSITY PROFILE AND FLUCTUATION MEASUREMENTS IN IMPROVED H-MODES

The improved H-mode regime in ASDEX Upgrade is generally obtained through NBI pre-heating in the current ramp up phase. The power is increased at the end of that phase causing a transition into the H-mode, and a stationary phase is obtained. Previous studies showed that the density profile peaks at lower density and exhibits a steep increase of peaking correlated with the flattening of the electron temperature. The ion stored energy increases significantly due to the density peaking while for the electrons the increase is only small [3]. Density profiles obtained with reflectometry in improved H mode regime in ASDEX Upgrade shot # 13037 are depicted in Fig.1. In this discharge neutral beam was increased from 2.5 MW to 5 MW at t = 1.040 s and the stationary phase starts at t ~1.4s. An L to dithering phase (with type III ELMs) occurs at t = 1.1 s. The further improvement of the H barrier occurs at t = 1.17 s and is stronger at t = 1.21s. An ion ITB seems to develop in the time interval 1.1s to 1.25s and collapses afterwards, back to the usual H-mode with type I ELMs (see Fig. 1a). In Fig.1 b) and c) are shown two sets of 8 profiles from O-mode reflectometry with 20 ?s temporal resolution, each set burst corresponding to 8 consecutive sweeps. The deviation between profiles in each burst is due to the plasma turbulence. These are less pronounced at t ~ 1.24s, when the level of turbulence is lower following the formation of the H barrier. Average profiles d) can be obtained from each burst, as it is depicted in Fig. 1 d) displaying the evolution of the average profiles (240 ?s) between 0.9s and 2.9s, In Fig.2 it is represented the evolution of both n_e and $?n_e/?r$ for several radial locations derived from the average profiles at radial positions, at the edge, both at HFS (R=1.20m, R=1.30m) and LFS (R=2.13m, R=2.00m), n_e and $?n_e/?r$ follow the gross evolution of both the central Ti and the stored energy, indicating

[1] emilia@cfn.ist.utl.pt

the changes in confinement. The evolution of the density gradient can be better seen at the HFS due to the lower level of plasma turbulence and more spaced flux surfaces. The gradient at the separatrix starts to peak for t ~1.1s and decreases for t ~ 2.5s, when the H to L mode back transition occurs and the confinement degrades. Interesting to note is the peaking of the profile at the inner radius between 1.1s and 1.2s (increase of both n_e and $?n_e/?r$) in the time interval where ITB develops.

A complementary analysis of the behaviour of turbulence can be obtained from fixed frequency operation. Fig.3a shows the contour plot of the power spectra reflected from a density layer $n_e \sim 3?10^{19}$ m^{-3}, in the time interval 0.6 - 2.8s. With the NBI increase at t=1.04s, the spectra of turbulence begins to change showing a gradual shift in the power to higher frequencies, which indicates the increase of the plasma rotation. A reduction of the turbulence in the range up to ~ 80 kHz is observed after 1.1s, corresponding to the L to dithering H-mode transition at the edge as well as to the formation of an ion ITB. At t = 1.21 s an abrupt suppression of the high frequency turbulence occurs (see the integrated power spectrum above 80 kHz in Fig.3b), indicating a strong development in the

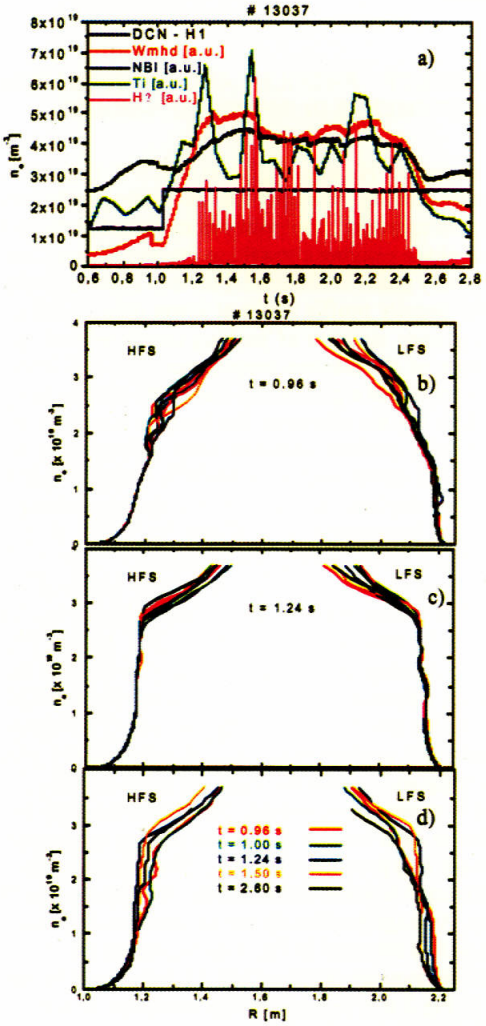

Fig. 1

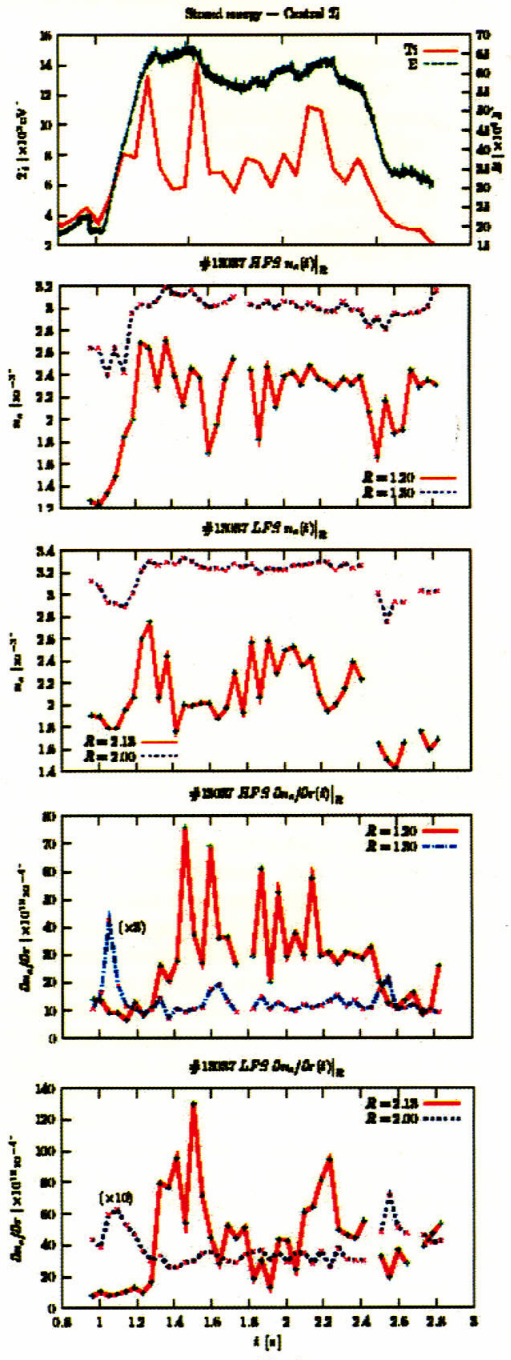

Fig. 2

H-mode barrier. The background fluctuations appearing after 1.25s correspond to type I ELMs and to the destabilization of MHD modes (seen as traces in Fig.3a), leading to the locking of a NTM at t ~ 2.5s. Above it was shown that the profile perturbations are

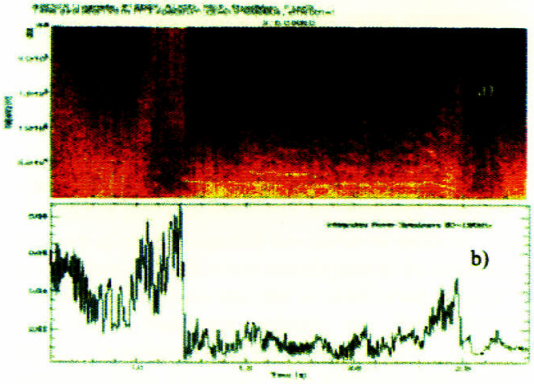

Fig. 3

strongly correlated with plasma turbulence. Another example is given in the following referring to improved H-mode discharge #13429. In Fig.4 the mapping of the level of profile perturbations in time and density (estimated with a P parameter), is shown during the ELMy H mode phase. P is defined as P = 1-?, where ? is the ratio between energy in the reflected signals that can be attributed to distance information and the total energy in the reflected waves. As the energy is concentrated in a narrow beat frequency inter-

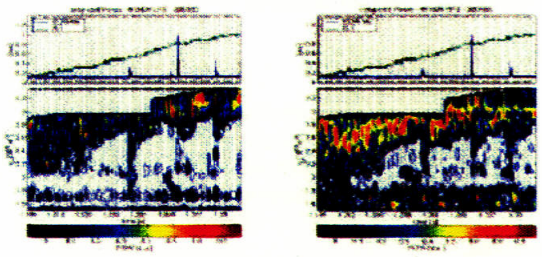

Fig. 4

val when the level of turbulence is very low, and is displaced to other beat frequencies (proportional to the group delay of probing microwaves) locations when turbulence level is high [2], the P parameter ranges from almost zero in the case of low turbulence (? ? 1), to one for strong turbulence. In Fig 4 it can be seen that the profile perturbations are low at the edge where turbulence is low due to the H mode barrier. The evolution of the edge pedestal (density) can be visualized from the evolution of the upper boundary line of the zone with reduced fluctuations. It increases following the development of the edge barrier and associated increase of the average density. After each ELM the fluctuations invade the edge region and are also seen close and inside the separatrix, corresponding to the abrupt flattening of the density profile at the onset of each ELM and slower recovery afterwards, the mapping of the profile perturbations shows, therefore, the space time evolution of ELMs. Moreover it maps the evolution of the density at the edge pedestal, which is a key indicator of confinement improvement.

III. DENSITY PROFILES DURING INBOARD PELLET LAUNCH EXPERIMENTS

A difficult situation for reflectometry is during inboard pellet experiments due to the strong plasma movements and strong ELM activity, including giant ELMs [4]. A selection of individual profiles depicted in Fig.5 shows that some profiles can be measured without significant deformations in these unfavorable

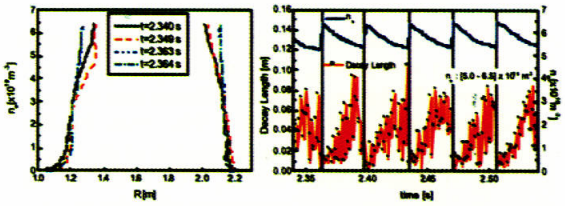

Fig. 5

circumstances. The evolution of the decay length at the plasma region n_e:5-6.5 x 10^{20} m^{-3}, reveal the peaking of the profile (decrease of decay length), after the injection of each pellet (dashed lines) followed by a flattening of the profile (increase of decay length) and a recovery before the next pellet. From the spread of the decay length points derived from individual profiles, (without any averaging procedure), it is evident that plasma turbulence induced by the pellets cause significant profile deformations. However, these do not prevent obtaining the evolution of the decay length and to evaluate the sustainment time of the peaking of the profile after each pellet. From these profile measurements a study was performed for different pellet velocities suggesting that for increased pellet injection velocity the sustainment time increases at the HFS, which may indicate an improvement of the confinement [5].

IV. TRACKING OF PLASMA MOVEMENTS

Reflectometry has been proposed as a new approach to plasma position and shape control for long pulse operation on next step machines like ITER, when magnetic systems may accumulate significant errors. This is a new application of reflectometry that should be demonstrated in present machines. The FM-CW reflectometry system on ASDEX Upgrade has unique possibilities to detect plasma movements, because it probes the plasma simultaneously at the high and low

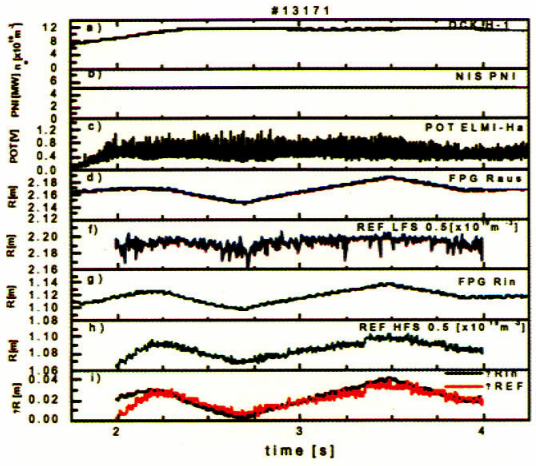

Fig. 6

field sides with identical O-mode reflectometers (not sensitive to the B-field). First experiments were performed in a discharge where the plasma was scanned radially between t = 2.2s and t = 3.8s. From Fig.6 it can be seen that the temporal evolution of the radial position of density layers with $n_e = 0.5 \times 10^{19}$ m^{-3}, at the HFS/LFS, is in good agreement with the plasma position (Rin and Raus), derived from the magnetic measurements. Due to the higher level of plasma turbulence at the LFS (ELMy H regime), the plasma movements are more clearly detected at the HFS. It should be noted that a deviation is observed for t < 2.25s (before the radial plasma position is scanned), due to density build up, as seen in the evolution of the average density (first trace at the top of Fig. 6). The

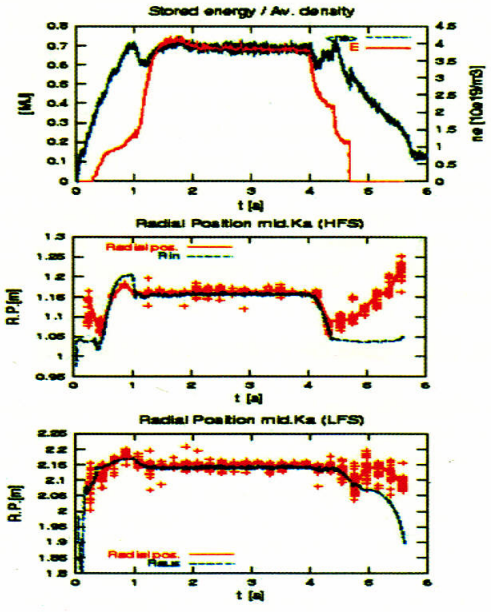

Fig. 7

next example is given in Fig.7, showing the radial movements of density layers $n_e = 0.5 \times 10^{19}$ m^{-3}, located at the HFS and LFS. Reflectometry is able to track the plasma position during both the start-up and in the stationary phases of the discharge. During the shut down phase, for t > 4.1s, reflectometry follows the movements away from the antennas of the selected density layer at both sides, indicating an asymmetric collapse of the plasma.

V. CONCLUDING REMARKS

We showed that the FM-CW microwave reflectometry on ASDEX Upgrade provides reliable and automatic density profiles in advanced plasma scenarios even in the presence of strong plasma turbulence. It was shown that profile perturbations are intrinsic to the plasma behaviour and can provide important information about the plasma phenomena. Broadband profile measurements (probing the plasma in short discrete time windows and large spatial windows) and fixed frequency probing (large time windows and narrow spatial windows) should be used in a complementary way to study plasma turbulence. HFS/LFS measurements are an important tool to the plasma diagnostic. It was shown that FM-CW reflectometry has the ability to track plasma movements, which is the first experimental demonstration where will be possible to use reflectometry for control purposes, as it is proposed for ITER. Further work is foreseen using the enhanced capabilities of the diagnostic that is presently being upgrade to improve the core measurements and to the number of profiles per discharge to 4320.

ACKNOWLEDGMENTS

This work has been carried out within the framework of the Contract of Association between the European Atomic Energy Community and "Instituto Superior Técnico". Financial support from "Fundação para a Ciência e Tecnologia" e "Praxis XXI" was also received.

1. A. Silva et al. *Rev. Sci. Instruments* **67** (12) (1996) 4138-4145
2. P. Varela, M. Manso, G. Conway and ASDEX Upgrade Team, this Workshop
3. A.G. Peeters, A. Bergmann, G.D. Conway, H. Meister, G.V. Pereverzev, G. Tardnin, O. Grüber, M. Manso, F. Serra, R. Wolf, *18th IAEA Fusion Energy Conference*, 4-10 October, Sorrento, Italy, (2000)
4. P.T. Lang and ASDEX Upgrade Team, *Nuclear Fusion*, **40**, 2, 245 (2000).
5. S. Vergamota, et al., *42nd Annual APS DPP/ICPP Meeting*, October 23-27, Quebec City, Canada, (2000)

Overview of reflectometer on JT-60U

K. Shinohara, N. Oyama, R. Nazikian*, and R. Yoshino

Naka Fusion Research Establishment, Japan Atomic Energy Research Institute, Naka-machi, Naka-gun, Ibaraki 311-0193, Japan

**Princeton Plasma Physics Laboratory, P.O. Box 451, Princeton, New Jersey 08543*

Introduction

A transport barrier is one of well-known features of high perfomace plasmas. In JT-60U, we have an edge transport barrier, ETB in H-mode plasmas and an internal transport barrier, ITB, in high-βp plasmas and reversed shear plasmas. The double barrier plasmas with the ITB and the ETB are also obtained in high-βp operations and reversed shear operations. It is important to understand what happens and what reduces the transport in the transport barrier region in order to operate such high performance plasmas in fusion reactors. It is considered the change of turbulence behavior is a key of the creation of the transport barriers. We installed a 4 channel X-mode system and a 3 channel O-mode system in order to investigate the turbulence in the ITB and the ETB region.

X-mode reflectometer system

The X-mode system is optimized for measuring the correlation length in the ITB region[1]. The block diagram is shown in Fig. 1. The reflectometer consists of four channels, two of which operate in fixed frequency and the other two channels are tunable. The frequencies of the launched waves are 115 and 130 GHz for the fixed frequency channels, and $122.5 \pm f_{bank}$ GHz, where f_{bank} = 2.73, 5.28, 6.37, 6.93 and 7.27 GHz, for the variable channels. The tunable channels can step through the five frequencies every 60 ms automatically. The correlation of fluctuations is determined from the correlation between fixed and variable frequency channels and therefore the radial profile of the correlations can be measured every 60 ms in a discharge. Quadrature phase detection is used to measure the complex amplitude, namely electric field, of the reflected wave.

By using this system, the correlation length of the reflectometer complex amplitude is measured during an ITB formation phase[2] and an ITB degradation phase[3] of reversed shear discharges. The correlation length is shorter in a steep ITB region than without ITB or in a gentle ITB region. The system is also used for investigating MHD activity like a toroidicity induced Alfvén eigenmode, TAE.

O-mode reflectometer system

The O-mode system is optimized for observing the ETB region and the relatively low density region. The O-mode system does not have an operation limit coming from the range of the toroidal field in contrast to the X-mode system. The block diagram of the O-mode system is shown in Fig. 2. Two of 3 channels are a narrow tunable ones and one channel is a widely tunable channel. Each of them is independent of the others. Thus there is a flexibility of an operation. Quadrature phase detection is used as well as the X-mode system.

By using the O-mode system, we are investigating the characteristics of fluctuations and MHD at the ETB during some different kinds of ELMy H-mode plasmas. We successfully measured the detailed dynamics of the collapse of the pedestal in a density profile by a type I ELM[4]. We also investigate the fluctuations during MARFE at the edge region. We observed a fast enhancement on the density fluctuations at the onset of a MARFE activity.

Summary

We installed the 4 channel X-mode reflectometer system and the 3 channel O-mode reflectometer system in order to investigate the transport barrier region.

By using the X-mode system, the correlation length of the reflectometer complex amplitude is measured during an ITB formation phase and an ITB degradation phase of reversed shear discharges. The correlation length is shorter in a steep ITB region than without ITB or in a gentle ITB region. The system is also used for investigating MHD activity like a toroidicity induced Alfvén eigenmode, TAE.

By using the O-mode system, we investigate the characteristics of fluctuations and MHD at the ETB during some different kinds of ELMy H-mode plasmas. We also investigate the fluctuations during MARFE at the edge region.

On the other hand, we had a problem in the maintenance of the system in the large device. We cannot access the device inside the torus hall easily and it is difficult to bring out the device quickly from the torus hall because of the radiological safety. One key is a stable high power oscillator, whose power is more than 100mW, in order to install the milliwave circuit far from the plasma as a radiation source with keeping the enough reflection power. Another key is reliable milliwave components, with a good yield rate, are available with really "catalogue specification" as it is in order to replace broken components easily.

References

[1] K. Shinohara, R. Nazikian, T. Fujita, and R. Yoshino, Rev. Sci. Instrum. **70** (1999) 4246

[2] R. Nazikian, K. Shinohara, R. Yoshino, T. Fujita, H. Shirai, G.J. Kramer and the JT-60 team, (*Proc. 17th Int. Conf. Yokohama), Post Deadline*, Vienna, 1998, IAEA

[3] K. Shinohara, R. Yoshino, R. Nazikian, T. Fujita, and Y. Kishimoto, *Proc. 26th EPS Conf. on Controlled Fusion and Plasma Physics*, Vol. 23J, (1999) 405

[4] N. Oyama, K. Shinohara, Y. Kamada, Y. Miura, T. Oikawa and S. Takeji, Submitted to Plasma Phys. Controlled Fusion

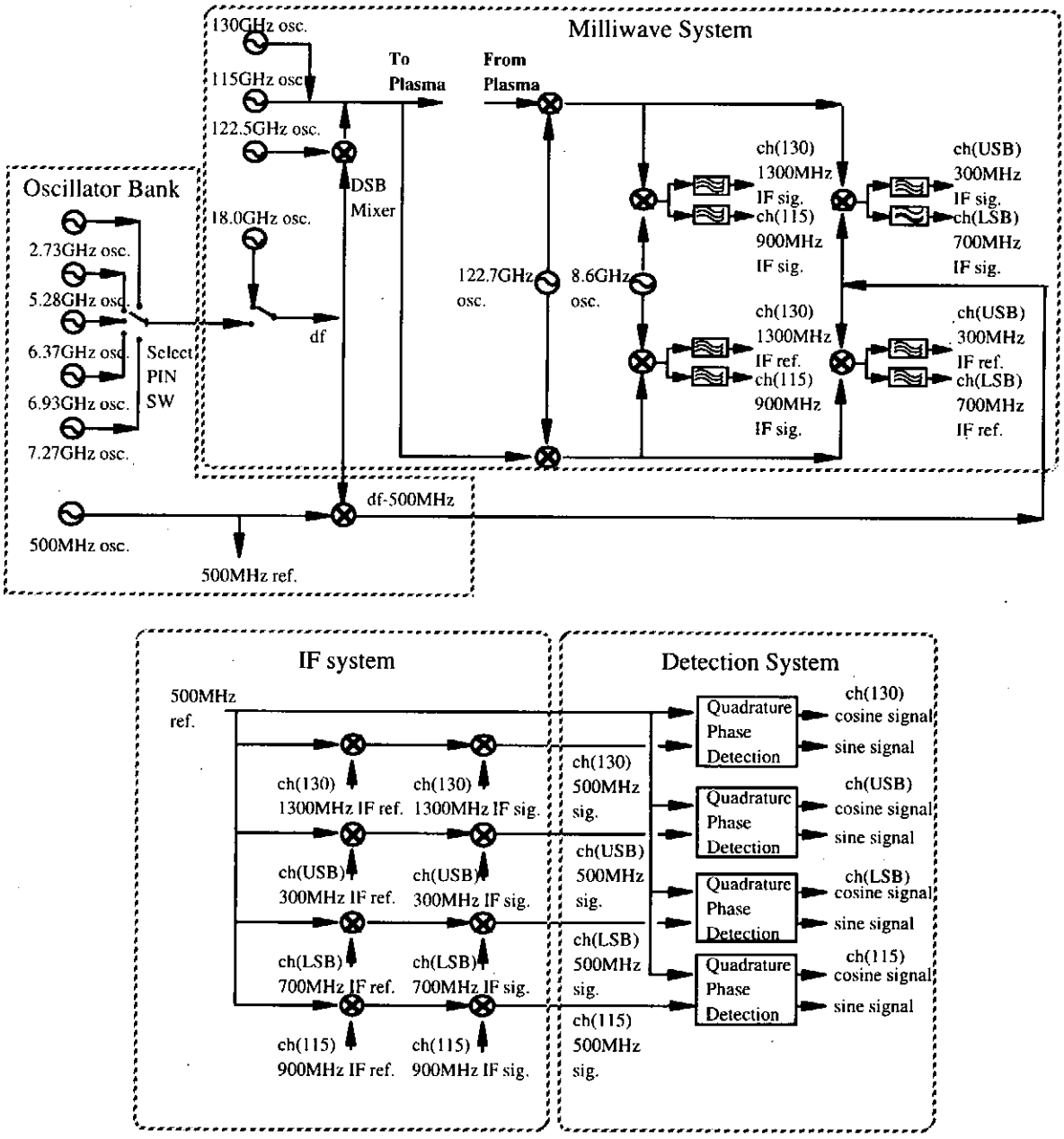

Figure1. Block diagram of 4 channel X-mode reflectometer system

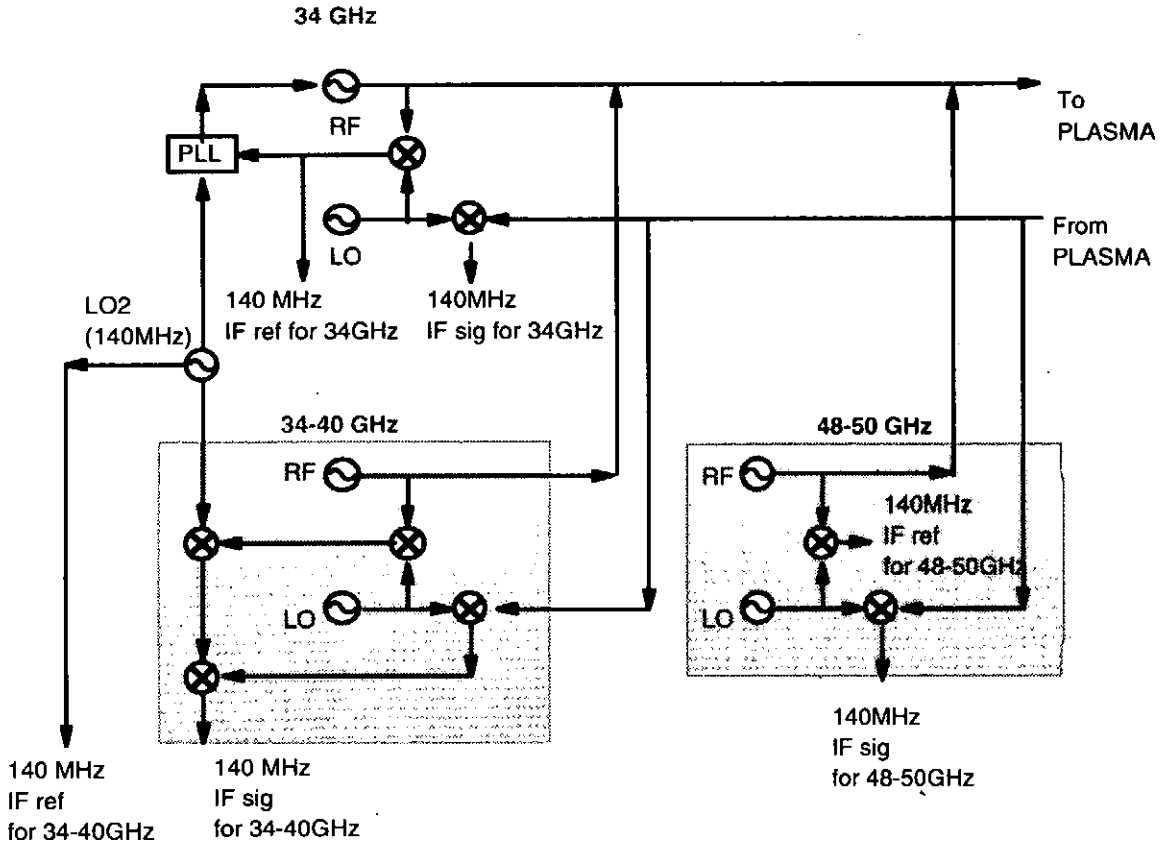

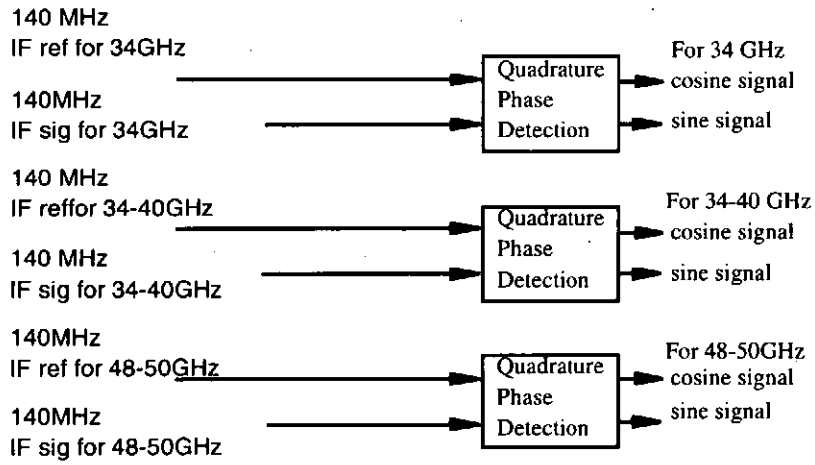

Figure2. Block diagram of 3 channel O-mode reflectometer system

Measurement of giant ELM in JT-60U using O-mode reflectometer

N Oyama, K Shinohara, Y Kamada, Y Miura, T. Oikawa and S. Takeji
Naka Fusion Research Establishment, Japan Atomic Energy Research Institute, Naka-machi, Naka-gun, Ibaraki-ken, 311-0193, Japan

1. Introduction

The study of the collapse mechanism of pedestal structure due to ELMs is important to evaluate and avoid the severity of the transient peak heat loads, which can significantly erode the target divertor plate in next step devices such as ITER. In JT-60U, extensive studies of ELMs were performed and properties of ELMs were clarified. On the other hand, the effect of the individual ELM pulses on core/edge plasma is still under investigation. Recently, three channels of the O-mode heterodyne reflectometer system have been installed at midplane on JT-60U to measure the behavior of cut-off density positions, that enable to observe such fast phenomena as ELMs in good time and spatial resolution. We present experimental results from the view point of density profile deformation together with the time scale of each ELM phase and precursor in density fluctuation.

2. Experimental conditions

Measurement of density perturbation by ELMs was performed on the high-β_p H-mode discharge with following plasma parameter, I_p = 1.5 MA, B_T = 3.65 T, $\delta \sim 0.36$, $\kappa \sim 1.55$ and $q_{95} \sim 4.8$. In JT-60U H-mode plasma, above parameters is in giant ELM onset regime. The ELM frequency, f_{ELM}, is distributed in the range of 30-100Hz. Two channels of reflectometer system have two fixed frequencies of 34.1 GHz (CH1) and 36.6 GHz (CH2), whose cut-off density is n_e = 1.44 and 1.66×10^{19} m^{-3}, respectively. The system enables to measure the movement of cut-off layer through the heterodyne signal of reflected wave. The incident wave for reflectometer is launched horizontally from low field side on the midplane through the corrugated waveguide, which is shared between O- and X-mode reflectometer. The total phase change of reflected signal, ϕ, under the WKB approximation is

$$\phi \cong \frac{2\omega}{c}\int_0^{x_c}\sqrt{1-\frac{n(x)}{n_c}}dx-\frac{\pi}{2}, \qquad (1)$$

where n_c is the cut-off density, ω is the frequency of incident wave and x_c is the distance from antenna to cut-off position. The phase delay given by equation (1) is mainly attributed to the movement of the cut-off layer and less from the density variation along the sight line.

In reflectometry, there is a common problem suffering from the scattered wave by density fluctuations, so called

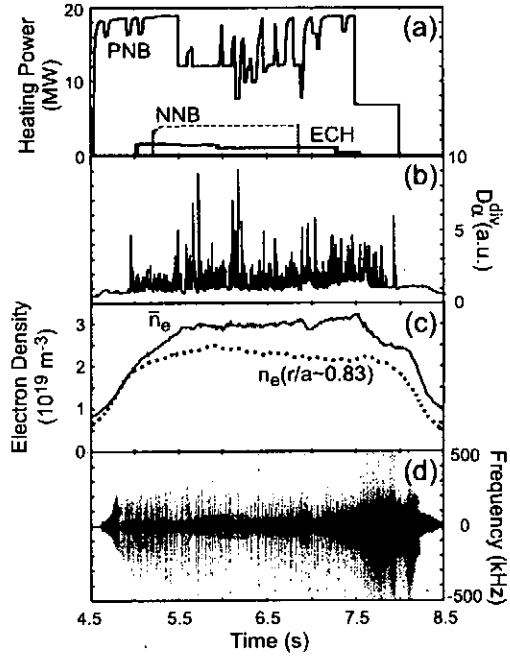

Fig. 1. Time evolution of (a) heating power, (b) sum of D_α signals in the divertor region, (c) line averaged electron density n_e and electron density n_e near the pedestal and (d) complex power spectrum of the reflectometer.

"runaway phase phenomena". In this discharge, however, the density fluctuation level at a shoulder of the pedestal as shown in Fig. 1(d) was small enough to neglect the scattering effect. Therefore, we can obtain clear phase change by ELMs without using any kind of filtering process, i.e. no phase runaway even during ELMs.

3. Detailed behavior of individual giant ELM pulse

Through the measurement of detailed behavior of giant ELMs using the reflectometer system, the characteristics of individual ELM pulse were firstly observed in JT-60U ELMy H-mode plasma. Fig. 2 shows wave forms during a typical giant ELM. The sampling times of each diagnostic are 5, 1 and 40 μs for interferometer, reflectometer and D_α signal, respectively. In reflectometer signal, Fig. 2(c), (d) and (h), (i), relative phase changes were detected clearly in both channels. Positive phase change means the movement of cut-off layer away from the antenna or the increase of electron density between cut-off layer and antenna. In the analysis of phase signal, the effect of variation in plasma equilibrium during ELMs has to be considered carefully. The drop of β_p by each ELM was < 0.05 and the variation of plasma equilibrium such as δ_{out} was < 1 cm as shown in Fig. 2(c). The gradual decrease of the baseline of phase signal plotted as a dashed line in Fig. 2(c), (d) was caused by the variation of δ_{out}.

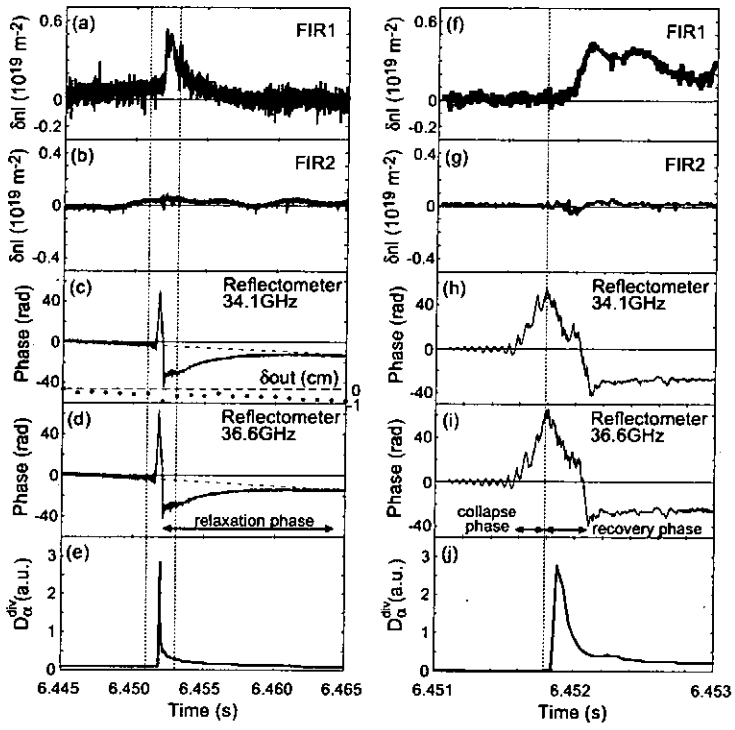

Fig. 2. Typical wave forms of (a),(b) change of line-integrated density, (c),(d) phase change of the reflectometer signal and (e) D_α signal in an ELM event. (f)-(j) show expanded wave forms between two dotted lines in (a)-(e). δ_{out} is also shown in (c). Vertical scale of δ_{out} is adjusted to equalize the migration length of the incident wave in the vacuum reconstructed from phase difference of the reflectometer signal. Definitions of collapse phase and recovery phase are shown in (i) and that of relaxation phase is shown in (d).

3.1 Collapse of pedestal structure

The phase angle change of reflectometer signal suggests the existence of three different phases in an ELM event, collapse phase, recovery phase and relaxation phase as shown in Fig. 2(d) and (i). In

collapse phase, the cut-off layer moved inward as a result of collapse in the first 100-350 μs. Then, in recovery phase, the cut-off layer moved outward beyond the initial position in 200-500 μs. Finally, it gradually returned to the similar position to the initial one taking 6-10 ms in relaxation phase. This relaxation phase was also observed in FIR1, which was a FIR interferometer with the peripheral chord as shown in figure 1, and D_α signal. Both signal had same time scale to return initial level as shown in Fig. 2(a) and 2(e).

Using equation (1), we can estimate the movement of cut-off layer from the phase change of reflected signal, under an assumption of the appropriate density profile. Basically, we assumed the linear density profile at pedestal region (inside the separatrix) and decrease exponentially at SOL region. Fig. 3 shows the reconstructed density profiles in two phases using following procedure. At first, we need initial density profile to determine the starting point as zero phase shift. The density profile measured by YAG Thomson scattering at t = 6.42 s is adopted as an initial condition. Then, the displacement of reflected position of each reflectometer channel is calculated independently using equation (1) to be consistent with each other. The maximum displacement reached 6.1 and 7.1 cm for CH1 and CH2 respectively, as shown in Fig. 3(a). In this case, reflected position reached 10 cm inside the separatrix, which corresponded to twice the pedestal width of ~5 cm.

In Fig. 3(b), the density profile and reflected positions measured when the next laser pulse was fired, at t = 6.453 s, are shown. The cut-off position measured with reflectometer was consistent with the density profile by the YAG Thomson scattering. One interesting point is that, in relaxation phase, the density in the SOL region seems to be much larger than collapse phase, and that is why the line-density of FIR1 increased in this phase as mentioned above. The timing of increasing the D_α signal was significantly faster than that of the line-density in FIR1 as shown in Fig. 2(f), (j). Therefore, the increase of SOL density is not due to the particle directly provided by collapse of density pedestal into the SOL region but as a result of enhancement of recycling at the divertor region due to the ELM heat load.

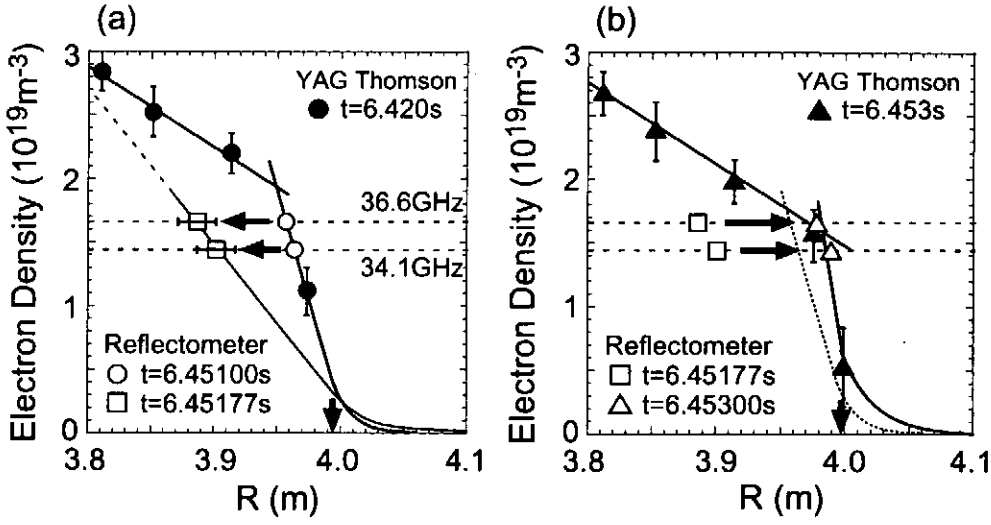

Fig. 3. Reconstruction of the movement of cutoff layer in two phases, (a) a collapse phase and (b) a relaxation phase. Open symbols show the measured positions of the reflectometer and closed one show the electron density measured with YAG Thomson scattering. Dotted line in (b) shows the initial position as shown in (a). Arrows on the horizontal axis show the radial position of outer separatrix.

3.2 Precursor in the density fluctuation

In reflectometer signal, we can see the clear density fluctuation (precursor) before the collapse phase of ELM as shown in Fig. 4(a), (b). A coherent oscillation in two reflectometer channels developed at $t = 6.1396$ s, about 320 μs before the collapse phase. Radial displacement of the precursor is estimated to be ±1.1 cm just before collapse phase, using same density profile model to reconstruct phase signal in figure 3.

The precursor was observed in the most of ELMs. The time scale of precursor phase was 200-500 μs. Precursor frequencies was almost constant in the precursor phase of an ELM and that was in the range of 10-25 kHz in this discharge. The obvious plasma parameter correlated with the frequency of precursor such as toroidal plasma rotation has not been understood.

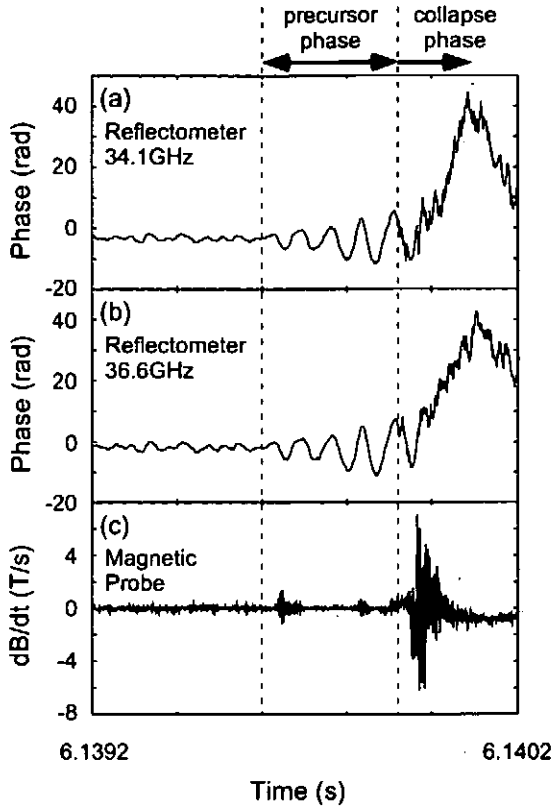

Fig. 6. (a),(b) phase change of the reflectometer signal and (c) magnetic fluctuation measured with magnetic probe (Mirnov coil). A precursor oscillation develops at t = 6.1396 s, around 320 μs before the collapse phase of ELM in the reflectometer signal.

Although the density fluctuation as a precursor clearly observed in reflectometer signal, there was no clear magnetic precursor in magnetic fluctuation as shown in Fig. 4(c) as well as other devices. On the other hand, the precursor oscillation was also observed in temperature fluctuations at pedestal measured with heterodyne radiometer. This may suggests the mode which causes precursor in density fluctuation has a well localized eigenfunction or higher mode number.

4. Summary

The reflectometer system successfully measures the movement of cut-off layer during an ELM activity without any kind of filtering correction of the reflected signal, because the scattering effect on the system can be neglected at the pedestal in high performance ELMy H-mode plasma in JT-60U. An ELM event can be classified into precursor phase, collapse phase, recovery phase and relaxation phase. The typical time scale of each phase is 200-500 μs, 100-350 μs, 200-500 μs and 6-10 ms, respectively. Due to a collapse of pedestal structure in a density profile by one ELM, a certain density layer, located near the shoulder of the pedestal, moved about 7 cm inside the plasma in collapse phase. The cut-off layer reached the 10 cm inside the separatrix, which corresponded to twice the pedestal width of ~5 cm. In relaxation phase, the increase of SOL density was observed in both reflectometer and interferometer as a result of enhancement of recycling at the divertor region due to the ELM heat load. A precursor that has the displacement gradually growing up to ~ ±1 cm in a density profile is clearly observed in the reflectometer signal, though there is no clear precursor in magnetic fluctuation.

Observation of Electron Density Using Reflectometry

A.Itakura, N.Goto[1], M.Katoh[2], Y.Kogi, S.Kubota[3], A.Mase[4], Y.Shima, M.Yoshikawa, H.Hojo and K.Yatsu

Plasma Research Center, University of Tsukuba, Tsukuba 305-8577, Japan

Abstract

Two types of microwave reflectometer are installed in the GAMMA 10 device for electron density measurement. One is an ultrashort-pulse reflectometer in an ordinary wave mode. An impulse generator, 65 ps full-width at half maximum is used as its microwave source. The five-channel receiver system measures the time-of-flight. Their center frequencies are 7, 8, 9, 10 and 11 GHz. Location of reflected point is calculated from the time-of-flight. An electron density profile is reconstructed.

The other is a fast frequency-sweep reflectometer in an extraordinary wave mode. A hyperabrupt varactor-tuned oscillator is used and is swept from 11.5 GHz to 18 GHz. Beat frequency between the injected wave and the reflected wave depends on the path length and the sweep frequency. It is adjusted not to match the ICRF heating frequency. A density profile is also reconstructed from the phase difference. This system has a rather simple receiving system.

I. Introduction

Recently, microwave reflectometry has been intensively developed[1]. It utilizes cutoff effect of the plasma for the incident electromagnetic wave. This system has an advantage of good spatial resolution in radial direction though it requires a single viewing port.

Two types of reflectometries are installed in the central cell of GAMMA 10 device [2]. One is an ultrashort-pulse reflectometer and the other is a fast frequency-sweep reflectometer. In this paper observation of radial electron density distribution is described. The tandem mirror GAMMA 10 is described in ref.3.

Present address:

1) Keyence Corporation

2) Toshiba Electronics Engineering Corporation

3) Department of Physics, University of California, Los Angels, USA

4) Advanced Science and Technology Center for Cooperative Research, Kyushu University

II. Ultrashort-Pulse Reflectometry

Figure 1 shows a schematic diagram of the ultrashort-pulse reflectometer[4]. Detailed description of the system is described by Kubota et al.[5] for four-channel system. The microwave source is an impulse generator and pulse width is 65 ps full width at half maximum. The impulse is fed into the amplifier through a waveguide for waveform shaping. It is launched from pyramidal horn in the ordinary wave mode (O-mode). The signal reflected by the plasma cutoff layer is received by the horn of the same type and is amplified by a preamplifier. It is divided into 5 channels and selected by band-pass filters, whose center frequencies are 7, 8, 9, 10, 11 GHz having band width of 3% of center frequency. Then they are detected by Schottky barrier diodes, amplified and fed into measurement system for time-of-flight. The time-of-flight is measured by a time to amplitude converter. The converter starts by trigger output of the impulse generator, which is synchronized with the clock of analog to digital converter. The time to amplitude converter stops conversion by the discriminator output signal of each received channel. The amplitude of output is proportional to the time of flight and is converted again to digital signal, which transferred to data acquisition system. These data are processed using computer software MATLAB after the shot. The location of horn system of the reflectometer is 0.6m from the midplane in the central cell.

Plasma is initiated by plasma guns located at both ends of the device at 50.5 ms. Then it is produced and sustained by ion cyclotron range of frequency (ICRF) applied in the central cell. Electron cyclotron resonance heating (ECRH) for formation of plug potential is applied during 125 ms and 225 ms by two sets of gyrotrons in the plug regions.

An interferometer having movable horn system is located at 0.6 m from the midplane of another side of the central cell. It is expressed that the time-of-flight measured by the reflectometer is coincide with the calculated one from density distribution derived from the interferometer by Kubota et al.[5]. Electron density is derived with the assumption that the density at radial location r=-0.18 m is 0, because the radius of central cell limiter is 0.18 m. Data of the time-of-flight are approximated as a polynomial expression to integrate to the density which corresponds to the receiving frequency channel. Though the analog to digital converter takes data at every 8 μ s, data of the time-of-flight are averaged for 1ms to avoid noise. Reconstructed radial density profile at t=100 ms is shown in Fig.2. In this system maximum receiving frequency is 11 GHz, so that density higher than $1.5 \times 10^{18}\ m^{-3}$ cannot be obtained.

This system has an ambiguity for the absolute value of the radial position, because the radial density distribution is not known. The solid line of Fig.3 is a radial density profile derived from the interferometer for the other shot. The radial location derived from the time-of-flight, i.e., the reflectometer, approximately 20 % larger than that derived from the interferometer.

III. Fast Frequency-Sweep Reflectometry

A schematic diagram of the fast frequency-sweep reflectometer[6] is shown in Fig.4. The microwave generator is a hyperabrupt varactor tuned oscillator (HTO). It generates 11.5 – 18 GHz with tuning voltage of 0 – 15 V, which is swept by sawtooth generator. The wave is transmitted to the plasma through a hog-horn antenna in the extraordinary wave mode (X-mode). Magnetic flux density in the central cell is 0.4 T, i.e., electron cyclotron frequency is 11.2 GHz. So, measured density is $4x10^{16} - 1.4x10^{18}$ m^{-3}. Reflected wave is received by the standard horn antenna and is mixed with the reference signal, which is divided from the transmitting wave. This signal causes a beat signal. It is amplified and stored by a high speed digitizer or digital storage scope. Frequency of the beat signal is a function of sweep rate and path difference. The path difference varies depending on the incident frequency. The beat frequency must be selected so as to distinguish it from the frequency of heating systems, i.e. 6.36 MHz, 9.9 MHz and 10.3 MHz. It is already known that low frequency fluctuations are existed in the central cell region. The repetition rate must be higher than the characteristic frequency of the fluctuations. Here, the repetition rate is 50 kHz and sampling rate of digitizer is 40 MHz. This system has good temporal resolution. Figure 5(a) shows a line integral of electron density measured by a microwave interferometer as a function of time. At 153 ms sharp peak is shown. This is caused by the injection of hydrogen ice pellet to increase density. A radial density distribution is reconstructed by the phase difference extracted from the mixer output signal. Figure 5(b) shows a reconstructed density profile as a function of time. It clearly displays the density increase caused by the injection of pellet.

IV. Summary

Microwave reflectometries are installed in the central cell of the GAMMA 10 device. Radial density distributions are observed. They have good spatial and temporal resolutions. The ultrashort-pulse reflectometry has an ambiguity for the absolute value of the radial location. This will be solved by expanding the receiving frequency range to the lower frequency.

Acknowledgements

The authors acknowledge the members of the GAMMA 10 group for their collaboration.

References

[1] Mase,A., Tokuzawa,T., Bruskin,L.G., Kogi,Y., et al., J. Plasma Fusion Res., 74 (1998) 1189.

[2] Itakura,A., Goto,N., Katoh,M., Kogi,Y., et al., Trans.Fusion Tech. 39 (2001) 265

[3] Yatsu, K., Bruskin, L.G., Cho,T., Hamada,M., et al., Nuclear Fusion, 39 (1999) 1707.

[4] Itakura,A., Katoh,M., Kubota,S., Mase, A., et al., J. Plasma Fusion Res., 76 (2000) 1198.

[5] Kubota,S., Onuma,T., Kato,M., Mase, A., et al., Jpn. J.Appl.Phys., 38 (1999) L202.

[6] Tokuzawa,T., Mase,A., Oyama,N., Itakura,A., Tamano,T., Rev.Sci.Instr., 68 (1997) 443.

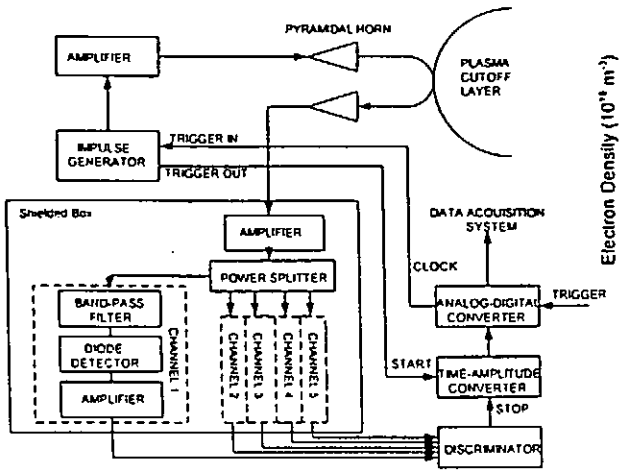

Fig.1 Ultrashort-pulse reflectometer

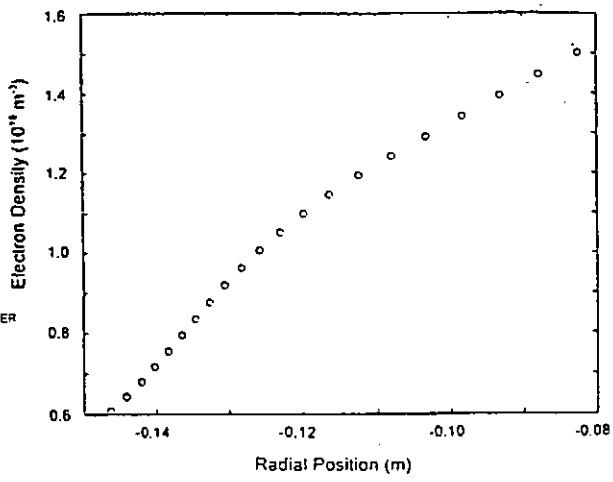

Fig.2 Derived density distribution

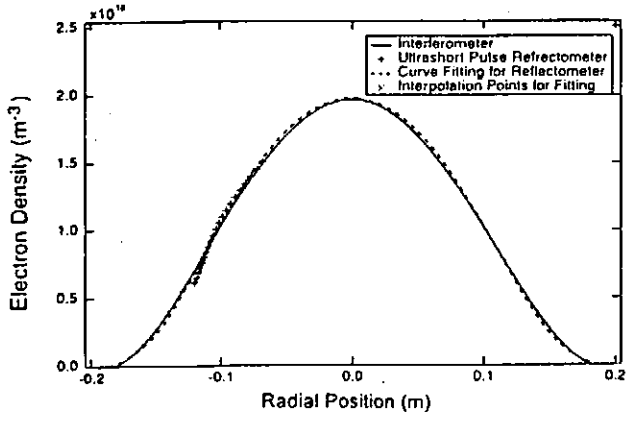

Fig.3 Calibration by interferometer

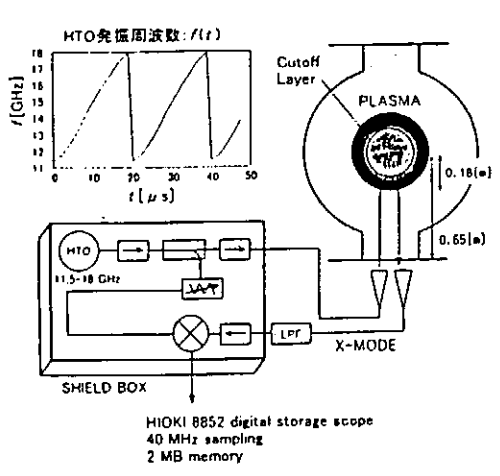

Fig.4 Fast frequency-sweep reflectometer

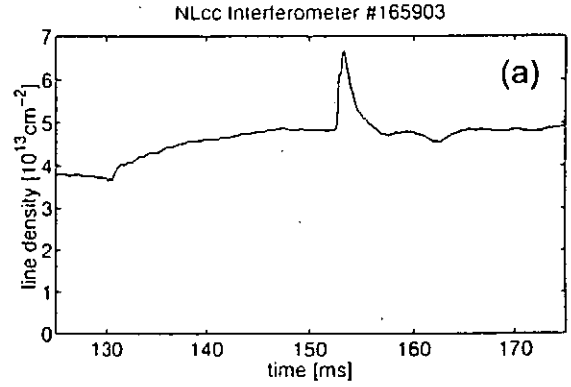

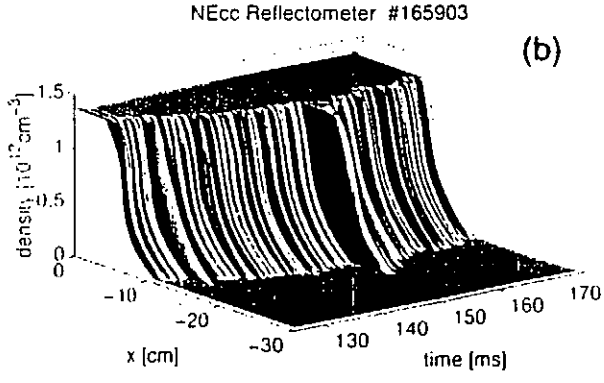

Fig.5(a) Line integrated density measured by interferometer

(b) Density profile derived by reflectometer

Pulsed Radar Reflectometer on the LHD.

T. Tokuzawa, K. Kawahata, K. Tanaka, R. O. Pavlichenko[1], A. Ejiri[2]

National Institute for Fusion Science, Toki 509-5292, Japan,
[1]Research Center for Development of Far-Infrared Region, Fukui University, Fukui 910-8507, Japan
[2]Graduate School of Frontier Sciences, Univ. Tokyo, 113-0033, Japan

Abstract

Large Helical Device (LHD) has a complicated structure to make a helical magnetic field and it causes that the polarization direction of the electromagnetic wave is not definite for the direction of the magnetic axis. Pulsed radar reflectometry is a suitable reflectometric technique, in order to study the effect of the strong magnetic shear for the polarization of the microwave. Because pulsed radar reflectometry is measured the delay time of the reflected wave directly, X-mode and O-mode polarized waves can be distinguished. We have constructed three channel pulsed radar reflectometer system for the present. The pulse width and the repetition rate are usually about 2ns and 100kHz, respectively. It is found the LHD plasma is initiated near the magnetic axis and then expanded. The delay time is almost agreement with the calculated delay time using the density profile measured by the far infrared laser interferometer in the edge region.

1. Introduction

It is very important to know the edge density profile and fluctuation information for the magnetic confined plasma experiments. In order to measure these plasma parameters with high temporal and spatial resolution, we try to apply microwave reflectometer on LHD (the major radius is 3.6 - 3.75 m, the averaged minor radius is 0.6 m, and the magnetic field strength on the plasma axis is up to 2.91 T).[1, 2] Reflectometer is a compact system, needs a small access to the device, and also has a higher resolution than conventional diagnostic methods. For these benefits, several types of reflectometer have been used in world fusion devices.[3-12] Since LHD has a complex magnetic field configuration and also has a large magnetic shear, the launched and the reflected microwave may have a complicated behavior such as the mode conversion or the polarization rotation.[13, 14] To study the effect of the strong magnetic shear, the pulsed radar reflectometer is a suitable reflectometric technique.

Because pulsed radar reflectometry measures the delay time of the reflected wave, it can be distinguished between X-mode and O-mode polarized waves even if unexpected pulses are returned. Additionally, the pulsed radar reflectometer does not affect by spurious reflections from vacuum windows, waveguides, and also by the electron cyclotron emission.

2. Pulsed radar reflectometer system

A concept of the pulsed radar reflectometry is described as follows. A wavepacket at a given frequency with short time duration propagates into a plasma and then propagates back out from the critical cutoff layer in a plasma. By performing such double-pass time-of-flight (TOF) measurements on the reflected wave, the distance to the reflecting layer can be computed. The advantages of pulsed radar reflectometry are the following. 1) Density profiles and density fluctuations can be measured using several fixed frequency sources, simultaneously. 2) Density profile measurements via TOF are fast and direct.

We construct V-band and R-band pulsed radar reflectometers. The schematic of V-band 2 ch pulsed radar reflectometer system is shown in Fig. 1. 60GHz and 65GHz Gunn oscillators are used as sources. The output powers of both sources are 100 mW. A PIN switches are used as a pulse modulator using the tuned signal of the generated impulse output. The microwave pulses pass through the oversized waveguide in order to avoid the deformation. The separate, transmitter and receiver horns are used in order to avoid the mixture of spurious reflecting components in the waveguides, vacuum window, etc. The antenna is a conical horn with a Teflon lens for focusing the microwave beam and can be moved horizontally and rotated using a remote controller. The reflected wave picked up by the receiver horn is mixed with the local microwave, which the frequency of the local oscillator is 78 GHz, in a mixer. The intermediate frequency signal is divided and each signals are filtered by band-pass-filter with the bandwidth of ±1.0 GHz then detected and converted from the envelope of the reflected wave to the pulse. The reference pulse for the TOF measurement is measured using V-band detector, which is located at just after the PIN switch to avoid the jitter of the pulse generator and the PIN switch. Figure 2 shows these three detected pulses which are amplified by each inverse amplifiers. The pulse width is around 2 ns and the repetition rate is 100 kHz in the standard operations. The detected pulses are fed to a diagnostics room using the electro-optical converters and the optical cables. Then TOF measurement is carried. A constant fraction discriminator (CFD) is used to obtain the start and the stop pulse for the time-to-amplitude converter (TAC), because the

pulse amplitude is changed during the plasma discharge. The obtained data is acquired by CAMAC (Aurora 14 with 12 bits 1 Mword memory) and stored by a windows-NT based personal computer.

3. Experimental results

LHD plasma is usually initiated by ECH and then neutral beam is injected. Launching an X-mode microwave pulse the initial critical layer of the right-hand cutoff frequency of 60 GHz is located at R=4.3m and that of 65GHz is located at R=4.2m, where R is the major radius. Figure 3 shows the time evolution of the delay time. 65GHz reflected pulse appears at 0.415s and then 60GHz reflected pulse appears with 20ms delay. It is clearly found that the plasma is initiated in the core region and then plasma is expanded.

When two O-mode microwave pulses made by R-band reflectometer system are launched, two pulses are reflected from corresponding positions of each plasma frequency. The time evolution of the delay time is shown in Fig. 4(b). In this figure, the dotted lines are the delay time measured by pulsed reflectometer and the solid lines are the calculated delay time using the density profile measured by FIR interferometer. The reflected pulses seem to be appeared when the electron density reaches to be the corresponding cutoff densities. But the value of the delay time is not agreement with the calculated value except the edge region. This disagreement is probably caused by the ambiguity of density profile reconstruction and/or by the error of estimation for the polarization. We need to study the detailed effect of the magnetic shear to the wave propagation using the simulation analysis.

Acknowledgements

This work was supported in part by a Grand-in-Aid for Scientific Research from JSPS.

References

1 M. Fujiwara *et al.*, Nuclear Fusion, **39**, 1659 (1999).

2 O. Motojima *et al.*, Physics of Plasmas, **6**, 1843 (1999).

3 B. Brañas *et al.*, Rev. Sci. Instrum. **70**, 1025 (1999).

4 C. AJ.Hugenholt *et al.*, Rev. Sci. Instrum. **70**, 1034 (1999).

5 C. W. Domier *et al.*, Rev. Sci. Instrum. **70**, 1038 (1999).

6 S. Kubota *et al.*, Rev. Sci. Instrum. **70**, 1042 (1999).

7 R. Cavazzana *et al.*, Rev. Sci. Instrum. **70**, 1056 (1999).

8 E. J. Doyle *et al.*, Rev. Sci. Instrum. **70**, 1064 (1999).

9 A. Silva *et al.*, Rev. Sci. Instrum. **70**, 1072 (1999).

10 Y. Lin *et al.*, Rev. Sci. Instrum. **70**, 1078 (1999).

11 M. Gilmore *et al.*, Rev. Sci. Instrum. **70**, 1085 (1999).

12 T. Tokuzawa *et al.*, Rev. Sci. Instrum. **68**, 443 (1997).

13 I. Fidone and G. Granata, Nucl. Fusion **11**, 133 (1971).

14 K. Nagasaki *et al.*, Phys. Plasmas, **6**, 556 (1999).

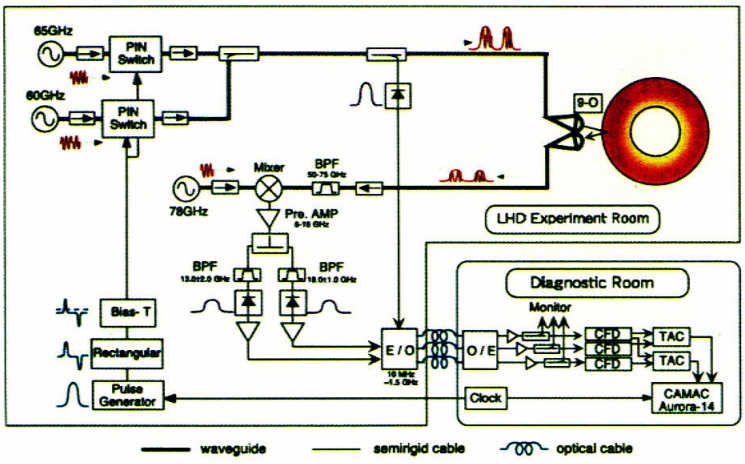

Fig. 1. Schematic of 2ch U-band pulsed radar reflectometer system. The R-band system is similar; the probe frequencies are 33 and 39GHz, and the local frequency is 51GHz.

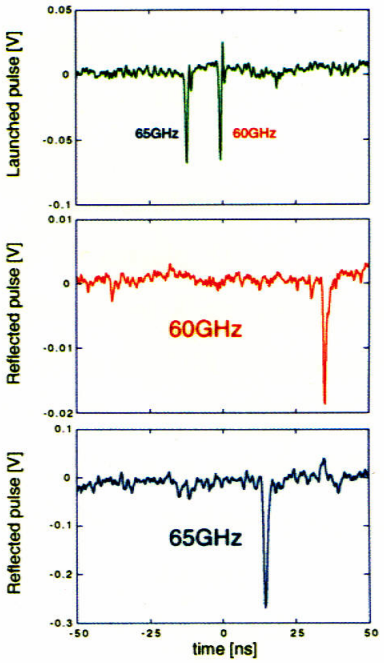

Fig. 2. The launched pulse and the reflected pulses.

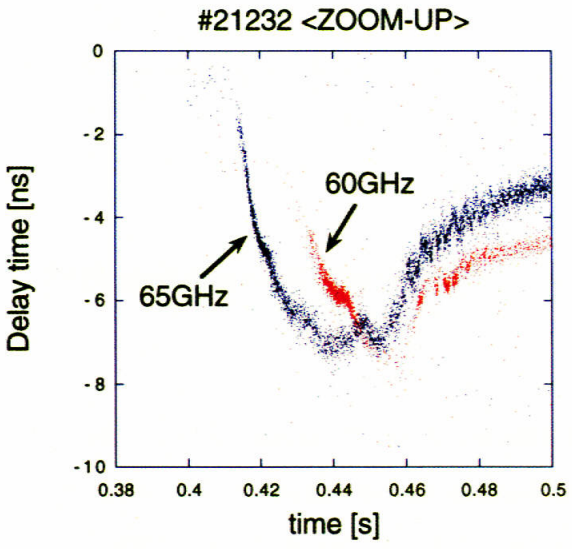

Fig. 3. Time evolution of the delay time of reflected pulses.

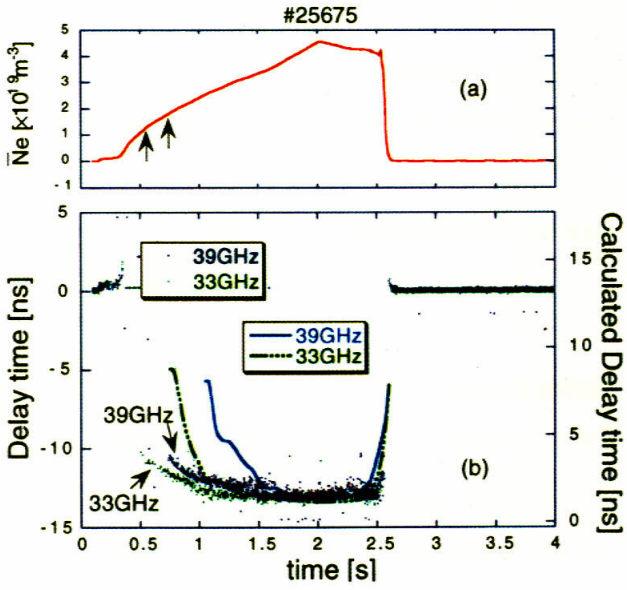

Fig. 4. (a) Time evolution of the averaged density and (b) the delay time of reflected pulses with involving the calculated delay time using density profile.

Pulsed radar reflectometry of broadband fluctuations

J.C. van Gorkom, M.J. van de Pol, A.J.H. Donné, and F.C. Schüller
FOM-Instituut voor Plasmafysica 'Rijnhuizen', Association EURATOM-FOM, partner in the Trilateral Euregio Cluster (TEC). Postbus 1207, NL-3430 BE Nieuwegein, The Netherlands

The possibility to use pulsed radar reflectometry for turbulence studies is investigated. Good qualitative agreement is found between the power spectrum of variations in time-of-flight and the quadrature spectrum of a continuous-wave fluctuation reflectometer. Standard Fourier analysis is hampered considerably by missing samples in part of the experimental data. Using the Lomb-Scargle normalised periodogram for power spectrum estimation, reliable spectra are obtained even for signals in which as much as 60% of the samples is missing.

Introduction

TEXTOR-94 is equipped with a ten-channel pulsed radar reflectometer, measuring the time-of-flight in reflection of short (approx. 1 ns) microwave pulses. The system currently installed is a ten-frequency O-mode system running at a 20 MHz total pulse repetition rate [1,2]. This translates to ten-channel measurements at 2 MHz, or four or two channels at a maximum rate of 5 or 10 MHz, respectively. The accuracy in the time-of-flight determination for a single pulse equals 74 ps. Several subsequent pulses can be averaged to further lower this figure. The goal of the diagnostic is three-fold: to study density profile developments, coherent macroscopic fluctuations, and broadband microscopic fluctuations.

The system differs from previous pulsed radar reflectometers mainly in two ways: in the higher number of channels (ten versus four) and in the very high pulse repetition rate (2–10 MHz versus 500 kHz). The number of channels will allow for reconstruction of the full (LFS) density profile, while the high pulse repetition rate makes the study of broadband density fluctuations possible.

Pulsed radar techniques have, to our knowledge, not yet been employed for the study of broadband density fluctuations in tokamaks. The time-of-flight of pulses can be expected to be sensitive not only to the precise location of the reflecting layer, but also to fluctuations in the local gradient just before reflection. Some degree of robustness against 2D interference effects might be expected, since each pulse contains a range of frequencies.

Earlier work has shown the presence of non-coherent fluctuations on time-of-flight signals: on RTP, a spread in the plasma reflection time-of-flight of about 300 ps was observed, compared to a spread of only 30 ps without plasma [3]. Also on T11-M an increased time delay scatter during plasma was reported and attributed to plasma inhomogeneities [4]. Investigations on the RTP system ruled out instrumental effects as cause of the increased scatter. Two possible causes remained, each of which could fully account for the observed scatter: a possibly decreased signal-to-noise ratio due to strong background emission from the plasma combined with a low power level of the reflected pulses, or, alternatively, density fluctuations in the plasma. The distribution of the scattered time-of-

flight signal remained near-gaussian. Data taken from the present TEXTOR-94 system is expected to contain more information because of the much higher sampling rates that can be reached.

The rest of this contribution will focus on a method for the analysis of high sampling rate pulsed radar data. In order to distinguish between plasma fluctuations and noise as cause for signal broadening, the statistical properties of the signal should be studied. Here we will concentrate on the power spectrum, also of high interest for studying the plasma fluctuations themselves.

Power spectrum estimation

Conventional FFT analysis for power spectrum estimation does not work well for part of the pulsed radar data. The analysis is hampered by the fact that sometimes many samples in the time series are missing: launched pulses for which the detected reflection was not high enough to trigger the time-of-flight measurement.

These 'lost pulses' occur because the reflected pulses generally show a large variation in amplitudes. Constant Fraction Discriminator modules ensure that this variation in itself does not lead to a significant walk in the measurement of the pulse flight times. To prevent false triggering on noise, however, these discriminators only trigger on pulses higher than an adjustable threshold amplitude. If the average pulse amplitude is low, then part of the pulses will not exceed this threshold amplitude. The cause for the large amplitude scatter in the reflected pulses is probably related to plasma density fluctuations. Note, however, that the important factor for losing pulses is the average reflected amplitude, which depends mainly on probing oscillator strength and on the distance from the antennae to the reflecting layer. Depending on these factors and on the setting of the threshold amplitude, the fraction of lost pulses can be anything between 100% (very low oscillator power, reflecting layer in the very centre) to 0% (oscillator power at or above design value, reflecting layer in gradient region).

For profile measurements one can use an average value for the time-of-flight, which is well defined even for the case of a large fraction of lost pulses. For power spectrum estimation, however, one needs to find a way to treat the resulting missing samples in the time series. Three cases are distinguished:

Case I: No pulses are lost. In this case the power spectrum can be easily calculated by conventional Fourier transformation, applied in a sliding Hamming or other

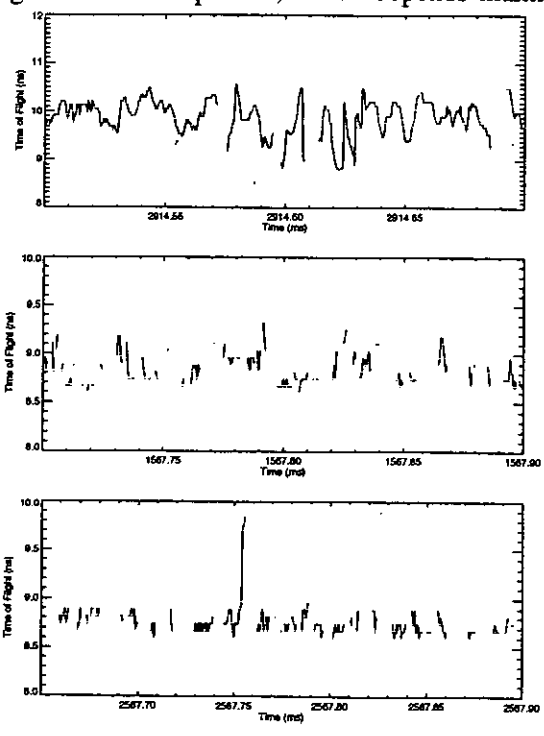

Fig. 1: Details of some time-of-flight time traces. The top trace corresponds to case II; the two lower traces stem from discharge #91082 and are case III.

suitable data window to obtain a spectrogram.

Case II: A small fraction (<10%) of pulses is lost, distributed more or less evenly over time. See for an example the top trace of figure 1. In this case we might expect the spectrum to be reasonably unaffected by the missing samples, provided we assign some reasonable values to them. Several options are possible: we choose to substitute the missing samples by linear interpolation from neighbouring points. After this we proceed as in case I with Fourier analysis.

Case III: A large fraction (>10%) of pulses is lost, or the missing pulses adjoin in time to form large gaps in the data. In this case we cannot expect valid data from standard Fourier analysis anymore. The assumption we make to fill in the missing points, whatever it is, is going to have a significant impact on the resulting spectrum. For this case therefore, we use a different analysis method: the Lomb-Scargle normalised periodogram. This method was designed to detect periodic signals in irregularly sampled data sets, in a way that is mathematically equivalent to the least-squares fitting of sines of different frequencies to the data [5,6, our implementation: 7,8]. We have applied the method in a short, sliding Hamming window and, like in the Fourier analysis, averaged over several windows.

Even though a large portion of the data falls into cases I and II it has been important to develop a standard analysis algorithm for case III, since this then covers all data. We want to successfully recover spectrograms from all discharges and channels, even from those with extremely bad signal quality, to have a fluctuation measurement in each and every discharge.

Results

The capabilities of the different methods for spectrum estimation will be demonstrated on an extremely 'low-quality' signal of only 40% detected pulses. Some zoomed-in portions of the signal are shown in the two lower traces of fig. 1. An overview of the different phases of the discharge is depicted in fig. 2. The top two graphs in this figure show the evolution of line integrated electron density and the total diamagnetic energy content of the plasma. In this particular discharge the effect of strong D_2 puffing on confinement in the Radiative Improved (RI) mode was investigated. The increase in energy confinement following the neon injection at t = 1.1 s is completely undone by a strong D_2 puff, starting around t = 1.7 s. The spectrogram of density fluctuations as obtained from one of the channels of a (continuous-wave, not pulsed) quadrature-detection correlation reflectometer is shown in the bottom panel of fig. 2. This reflectometer is measuring near the plasma edge, but still a few cm inside the last closed flux surface. As the D_2 puff is injected and global confinement deteriorates, a clear enhancement of low-frequency turbulence is observed.

Spectrograms of pulsed radar reflectometry signals, calculated using the different methods, are shown in the third and fourth panel. For comparison with the quadrature channel at 37 GHz, the 39 GHz pulsed channel was chosen. The upper spectrogram was calculated using a sliding window FFT after linear interpolation of the missing data points. Although it shows the reduction in high frequency fluctuations starting around t = 1.7 s, the behaviour of the low frequencies is opposite to that measured by the correlation reflectometer: the low frequencies appear at a high level during RI mode, and at a much lower level afterwards in the

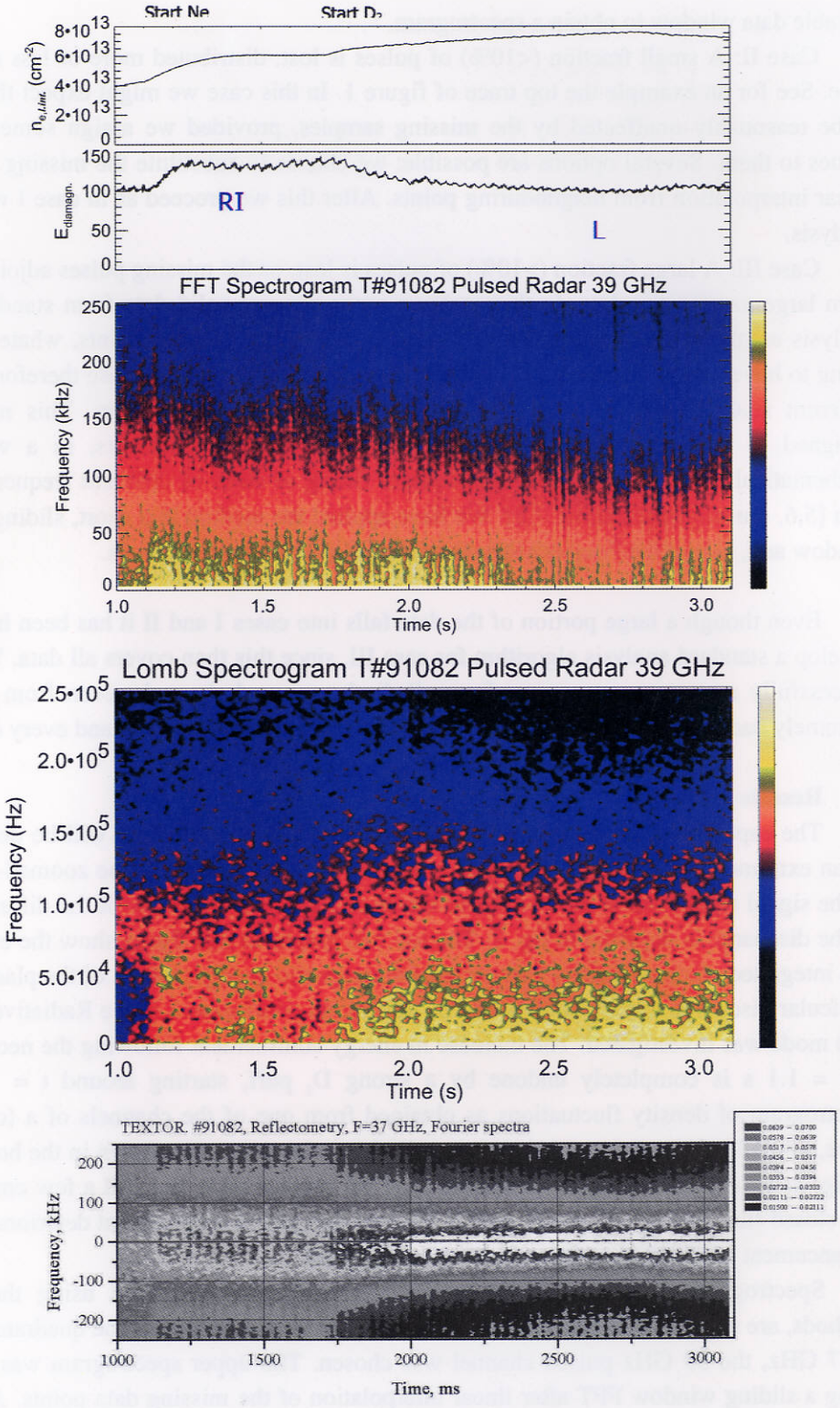

Fig. 2: Overview of Textor discharge 91082, showing (top to bottom) line integrated electron density, diamagnetic energy content, spectrogram of pulsed radar time-of-flight fluctuations calculated with FFTs after linear interpolation of missing points, the same spectrogram calculated via the Lomb-Scargle method (no interpolation needed), and, for comparison, a double-sided spectrogram from a continuous-wave, quadrature-detection reflectometer channel (courtesy of S. Soldatov).

L mode phase. The disagreement in particularly the lower frequencies is not unexpected, since the applied interpolation distorts the power spectrum mainly at frequencies with periods comparable to the gaps in the time series.

The spectrogram as calculated via the Lomb-Scargle periodogram shows good qualitative agreement with the correlation reflectometer. This agreement extends from the high frequency reduction after t = 1.7 s to the behaviour of the low frequencies: a low level in the RI mode phase, with higher levels in the following D_2 puffing phase. Note also the spread-out spectrum from 1.0 s to 1.1 s: this coincides with an asymmetric, Doppler-shifted spectrum on the quadrature channel. This spectral broadening is attributed to plasma rotation, which has been corroborated by the correlation measurement with another, poloidally separated quadrature channel.

Conclusion

Good qualitative agreement has been found between the power spectrum of fluctuations in time-of-flight (pulse group delay) as measured by pulsed radar reflectometry, and the double-sided spectrum of a continuous-wave fluctuation reflectometer. This provides a sound basis for the application of the TEXTOR-94 pulsed radar reflectometer as a standard fluctuation diagnostic.

Another important step towards the routine evaluation of pulsed radar fluctuation data from all plasma discharges has been taken with the implementation of the Lomb-Scargle normalised periodogram for power spectrum estimation. It has been shown that, using this method, spectrograms can be obtained successfully for signals with as little as 40% detected pulses.

Acknowledgements

We are grateful to S. Soldatov, V. Dreval (both from the 'Kurchatov Institute', N.F.I.) and A. Krämer-Flecken (from our TEC-partner Forschungszentrum Jülich), for providing the quadrature spectrum in figure 2 for comparison. The work presented here was performed as part of the research programme of the Stichting voor Fundamenteel Onderzoek der Materie (FOM), with financial support from the Nederlandse Organisatie voor Wetenschappelijk Onderzoek (NWO) and EURATOM.

[1] C.A.J. Hugenholtz *et al.*, Rev. Sci. Instrum. **70**, 1034 (1999).
[2] J.C. van Gorkom, M.J. van de Pol, and A.J.H. Donné, Rev. Sci. Instrum. **72**, 336 (2001).
[3] S.H. Heijnen, *Pulsed Radar Reflectometry*, Thesis University of Utrecht, Utrecht (1995).
[4] V.F. Shevchenko, A.A. Petrov, V.G. Petrov, U.A. Chaplygin, Proc. 20th Conf. on Contr. Fusion and Plasma Phys., Lisbon (1993), Europhysics Conference Abstracts, Vol. 17C, Part III, p. 1167.
[5] N.R. Lomb, Astrophysics and Space Science **39**, 447 (1976).
[6] J.D. Scargle, Astrophysical Journal **263**, 835 (1982).
[7] W.H. Press, and G.B. Rybicki, Astrophysical Journal **338**, 277 (1989).
[8] W.H. Press, S.A. Teukolsky, W.T. Vetterling, and B.P. Flannery, *Numerical recipes in C*, 2nd ed., Cambridge University Press, Cambridge (1992).

Two Channel Microwave Reflectometry and Interferometry Using PIN Switches

T. Yamada, A. Ejiri*, Y. Takase*, S. Shiraiwa*, K. Yamagishi, M. Ushigome,
N. Kasuya, Y. Nagashima, H. Nozato*, T. Mashiko, T. Akiduki*,
H.Kasahara*, H. Yamada*, H. Wada, L. M. Tozawa
School of Science, University of Tokyo, Tokyo 113-0033, Japan
*School of Frontier Sciences, University of Tokyo, Tokyo 113-0033, Japan

1. Introduction

PIN switches are waveguide switches with a quick time response. They are commonly used for generating short pulses or for switching among different frequency sources. We used PIN switches to make multi-spatial channel reflectometer and interferometer systems. In these systems, PIN switches were used to switch among several antennas to make up a multi-launching antenna system and/or a multi-receiving antenna system. In reflectometry, three-dimensional structures of fluctuations may produce complicated behaviors in the reflected wave. By using a multi-antenna system, we can determine the feasibility of reconstructing the fluctuating structures. In interferometry, a multi-antenna system is indispensable for measuring the electron density profile. This technique has a great cost advantage because we can reduce the numbers of sources, detection parts and transmission lines. For these purposes, PIN switches must have high isolation and fast switching speed. The former influences the cross talk and the latter determines the time resolution.

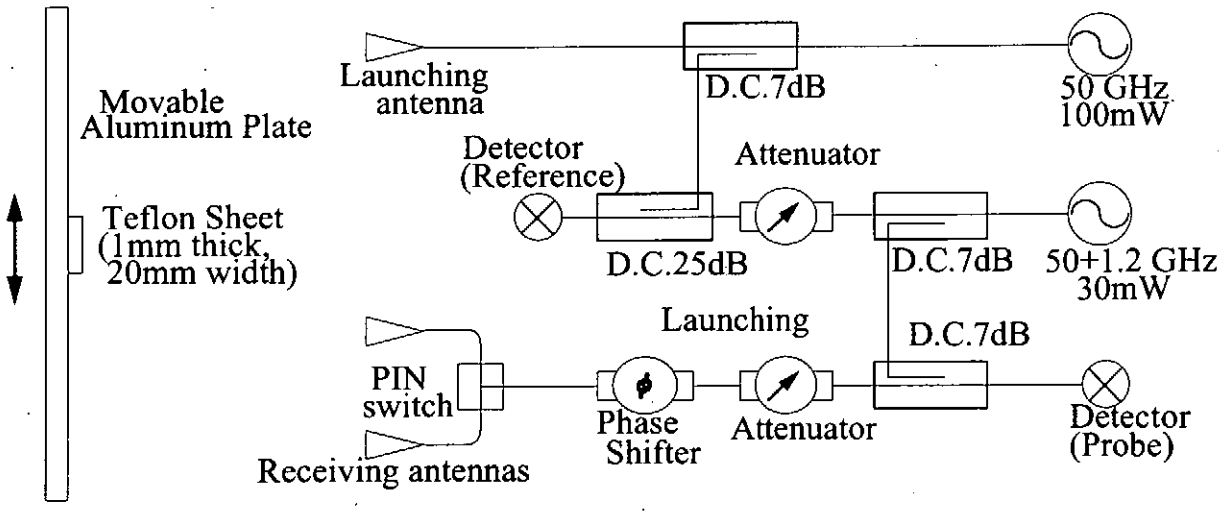

Figure 1. Schematic diagram of the reflectometer with two receiving antennas.

2. Reflectometry

A microwave reflectometer at the frequency of 50GHz was constructed. A PIN switch was used to switch between two receiving antennas, and the microwave was launched from a single antenna (Fig. 1). The intermediate frequency between the probing beam and the local oscillator was 1.2GHz, and the sine-cosine components of the wave were detected by a heterodyne receiver. An experimental test of this system was performed without a plasma. Instead of a plasma, we used Teflon sheets attached to an aluminum plate as a reflecting surface. Since Teflon has a refractive index of 1.4, we could make arbitrary perturbations by arranging the sheets on the plate. From the arrangement, we can calculate phase perturbations over the plate, so we could compare the phase and amplitude behaviors with numerical simulations using the Kirchhoff integration method.

The scalar electric field E_P at point P is given by Kirchhoff integration as

$$E_P = \frac{1}{4\pi}\int_S \left(E_S \frac{\partial}{\partial n}\frac{e^{-iks}}{s} - \frac{e^{-iks}}{s}\frac{\partial E_S}{\partial n} \right) dS,$$

where E_S is the field at the reflector surface, **k** is the wave vector, s is the range from the surface to the point P and **n** is the normal vector to the surface [1]. The Kirchhoff method approximates these values as

$$E_S = (1+R)E_I,$$

$$\frac{\partial E_S}{\partial n} = i(1-R)E_I \mathbf{k}\cdot\mathbf{n},$$

where E_I represents a wave from the launching antenna, R is the Fresnel reflection coefficient of which value is -1 and +1 for metal surface and for a plasma cutoff, respectively.

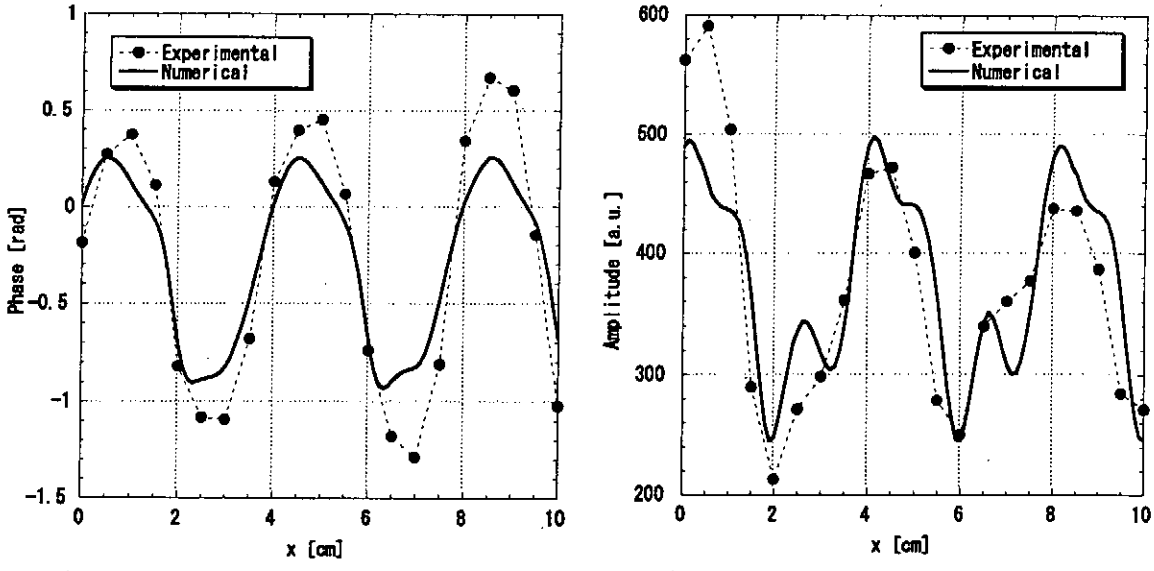

Figure 2. The phase and the amplitude of the reflected wave. The experimental result and the numerical result are plotted together.

An example of the phase and amplitude reflected by an aluminum plate with Teflon sheets is shown in Fig. 2. The left shows the comparison of the phase and the right shows the comparison of the amplitude. In this case, Teflon sheets of 2cm width were attached every 4cm. The plate was moved perpendicular to the direction of wave propagation. As shown in the figure, the experimental result and the numerical result are in a good agreement. We also tested various cases (e.g. without Teflon sheets, rotation of the plate) and found good agreement between the experiments and the calculations. These results led to the potential of the reconstruction of fluctuating structures by a multi-antenna system.

3. Interferometry

Microwave interferometry is a well-known method to measure the electron density profile and fluctuations. An interferometer at the frequency of 104GHz and the intermediate frequency of 1.2GHz is being used to measure the line-integrated density on the TST-2 spherical tokamak. TST-2 has a major radius R of 0.36m and a minor radius a of 0.23m [2]. A typical electron density is $n_e \sim 1\times10^{19}m^{-3}$. We used a PIN switch to alternate between two chords. The major radii of the two chords are 390mm, which passes near the center of the plasma, and either 435mm or 505mm (Fig. 3).

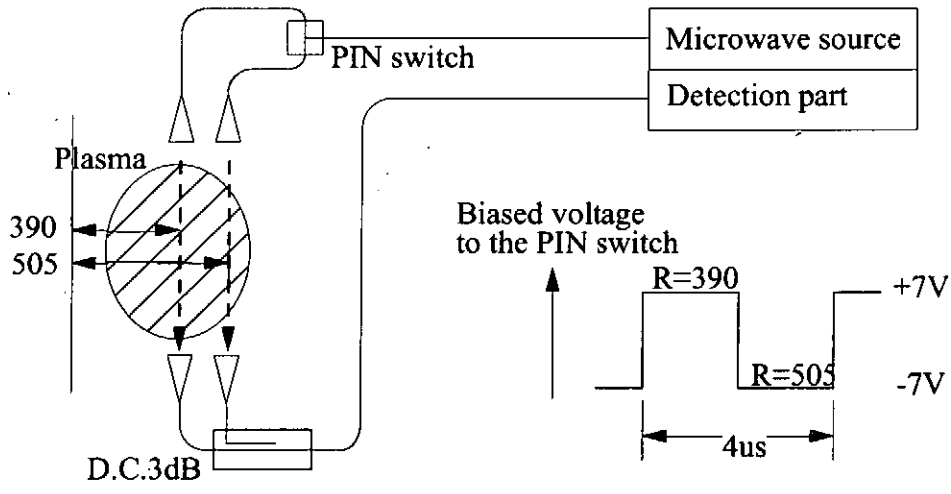

Figure 3. Schematic diagram of the interferometer which can measure two chords with a time interval of 2μs.

The refractive index of the O-mode propagation is given by

$$N = \sqrt{1-\omega_p^2/\omega^2},$$

in the cold plasma approximation, where ω_p is the electron plasma frequency. The value of the phase change is simplified to

$$\Delta\varphi = \frac{k}{2n_c}\int_{\ell} n_e d\ell ,$$

for the case of $\omega \gg \omega_p$, where n_c is a cutoff density defined by $\omega^2 = n_c e^2/\varepsilon_o m_e$.

Figure 4 shows line-integrated density of chords R=390mm, 505mm and plasma current of a typical discharge. It can be seen that the density comes to the peak at the very beginning of a discharge and then decreases slowly with sawtooth-like events. During a sawtooth-like event, the density of the central chord increases slowly and decreases suddenly with a spike in the plasma current. But the density of the outer chord stays constant or often shows an opposite behavior. Therefore, it can be explained by a slow profile peaking followed by a sudden flattening, and the particles seem to be ejected to the outer region at the crash.

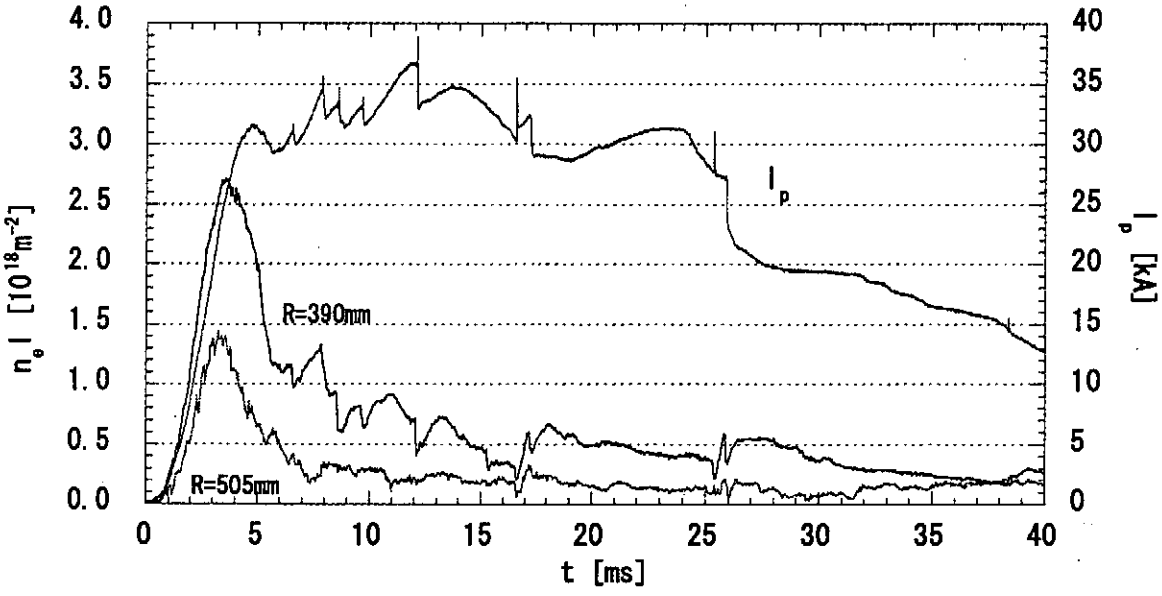

Figure 4. Line-integrated density of two chords (R=390mm, 505mm) and plasma current.

4. Summary

Two-channel microwave reflectometer and interferometer were constructed and demonstrated. The results of the reflectometer showed good agreements with the numerical simulations and the posibility of reconstructing perturbed fluctuations has been studied. Interferometer of two chords gave us a rough image of the profile of electron density in TST-2.

References

[1] G. D. Conway, Rev. Sci. Instrum. 64 (10), Oct 1993.

[2] S. Shiraiwa, et al. Proc. 27th EPS conf. Contr. Fusion and Plasma Phys. Budapest 2000.

Two-Dimensional Simulation for Ultrashort-Pulse Imaging Reflectometry

H. Hojo, K. Nakayama, G. Uruta and A. Mase[1]

Plasma Research Center, University of Tsukuba,
Tsukuba 305-8577, Japan
[1]*Advanced Science and Technology Center for Cooperative Research*
Kyushu University, Kasuga 816-8580, Japan

Abstract

The two-dimensional simulation for imaging reflectometry using ultrashort O-mode pulses is presented. The simulation model solves the full Maxwell wave equation coupled with the equation of plasma current density in a cold magnetized plasma, and can describe propagation, reflection and cross polarization scattering of O and X modes. The density profile reconstruction is performed by applying the Abel inversion to the reflected-wave signals received on an array of detectors, and is shown to work well.

1. Introduction

Microwave diagnostics such as reflectometry and cross polarization scattering method are recently receiving growing attentions in magnetic confinement researches. In order to obtain better understanding of confinement physics, more detailed measurements on the profile and fluctuations of a plasma might be required. Recently, a new type of reflectometry called as imaging reflectometry[1] has been proposed, expected as a near-coming diagnostic. As this method use an array of detectors, we can observe the multi-dimensional structure of a plasma and also visualize it. Another interesting method is to use an ultrashort pulse being subcyclic. As a subcyclic pulse is composed of many monochromatic plane waves with different frequencies, the reflectometry using ultrashort pulses has a potentiality of measuring precisely the profile and fluctuation of a plasma by only a single pulse. The ultrashort-pulse reflectometry has been already done experimentally[2,3] and theoretically[4,5].

In this paper, we present the two-dimensional simulation for imaging reflectometry in magnetically confined plasma. In the following section 2, we describe the simulation model, and in section 3 we show the simulation result of the density profile reconstruction from the reflected-wave signals received on an array of detectors.

2. Simulation Model

In this section, we describe the present two-dimensional simulation model. The basic equations to be solved are the full Maxwell wave equation for the electric field $\boldsymbol{E}$ and the equation for the current density $\boldsymbol{J}$ as follows:

$$\frac{\partial^2}{\partial t^2}\boldsymbol{E} + c^2\nabla(\nabla\cdot\boldsymbol{E}) - c^2\nabla^2\boldsymbol{E} + \frac{1}{\varepsilon_0}\frac{\partial}{\partial t}\boldsymbol{J} = 0 \quad , \tag{1}$$

$$\frac{1}{\varepsilon_0}\frac{\partial}{\partial t}\boldsymbol{J} = \omega_{pe}^2\boldsymbol{E} - \frac{e}{m_e\varepsilon_0}\boldsymbol{J}\times\boldsymbol{B}_0 \quad , \tag{2}$$

where c is the speed of light, $\omega_{pe}(=\sqrt{e^2 n/m_e\varepsilon_0})$ the electron plasma frequency, $-e$ the charge of the electron, m_e the electron mass, n the plasma density, ε_0 the permittivity of vacuum and $\boldsymbol{B}_0$ the external magnetic field. In the derivation of eq.(2), we assumed that the current density is approximated as $\boldsymbol{J} = -en\boldsymbol{v}_e$, $\boldsymbol{v}_e$ being the electron flow velocity, as we consider electromagnetic waves in GHz range. The above equations can describe both O and X modes. In the following simulation for imaging reflectometry, for simplicity, we assume $\boldsymbol{B}_0 = B_0\hat{\boldsymbol{y}}$, $\hat{y}$ being the unit vector in the y-direction.

3. Simulation Results

In this section, we perform the two-dimensional simulation for imaging reflectometry with use of an ultrashort O-mode pulse. We solve eqs.(1) and (2) in the numerical scheme which uses the Runge-Kutta method in time and finite difference in space. The snap shots of the computed two-dimensional wave profiles are shown in Figs. 1 and 2. Figure 1 shows the forward wave launched to plasma, which is assumed to have an isotropic Gaussian density profile. In the figure, the density contour is shown by solid lines. Figure 2 shows the reflected wave from the plasma. In the simulation box, the initial launched pulse being a subcyclic pulse is excited at x=−1000 in Fig.1 and the boundary condition that wave is outgoing is imposed on other three boundaries.

We show the wave signal of $E_y(t)$ at each detector (R1, R2, ..., R5) in Fig.3. The wave signal near the normalized time t=1000 shows the forward wave. From these reflected-wave signals, we estimate the time delay $\tau(\omega)$ at each detector using the zero crossing method for the density profile reconstruction. Then, we can perform the density profile reconstruction with use of the Abel inversion formula for the reflection point x_r:

$$x_r(\omega_{pe}) = \int_0^{\omega_{pe}} \mathrm{d}\,\omega \frac{c\tau(\omega)}{\pi\sqrt{\omega_{pe}^2 - \omega^2}} \quad , \tag{3}$$

The reconstructed density profile at each detector is shown in Fig.4 by open circles, where each horizontal axis corresponds to the line (shown by dashed line) connecting each detector to the center of the plasma density. We can see that the density profile reconstruction works well on each detector.

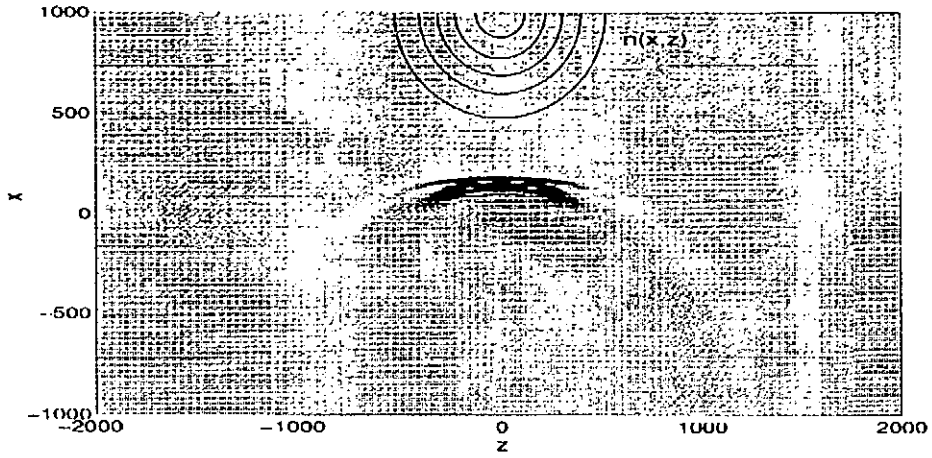

Fig.1 The wave profile $E_y(x,z,t)$ of the forward O-mode pulse. The contour of the density profile is also shown by solid lines.

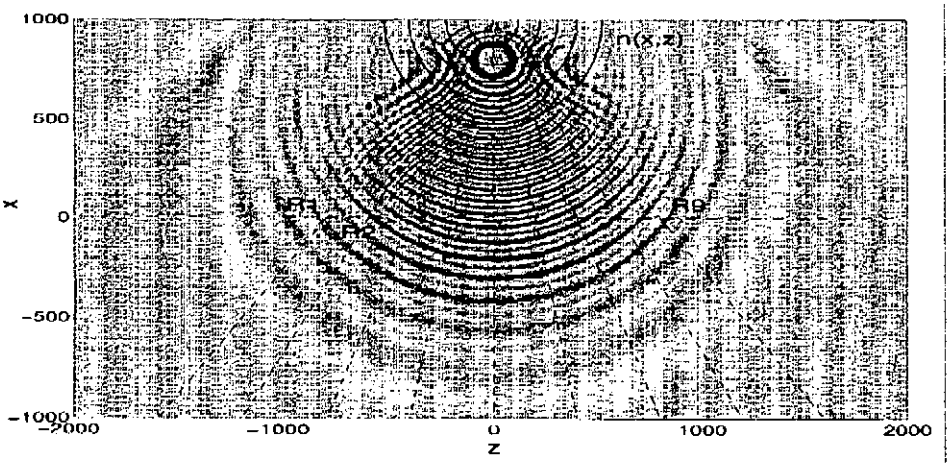

Fig.2 The wave profile $E_y(x,z,t)$ of the reflected O-mode. An array of detectors is located on the line of x=0 (R1, R2, ..., R9).

References

1. E. Mazzucato, Nuclear Fusion **41**, 203 (2001).
2. C. W. Domier, et al., Rev. Sci. Instrum. **66**, 399 (1995).
3. S. Kubota, et al., Jpn. J. Appl. Phys. **37**, L300 (1998).
4. B. I. Cohen et al., Phys. Plasmas **6**, 1732 (1999).
5. H. Hojo, R. Kurosawa and A. Mase, Rev. Sci. Instrum. **70**, 983 (1999).

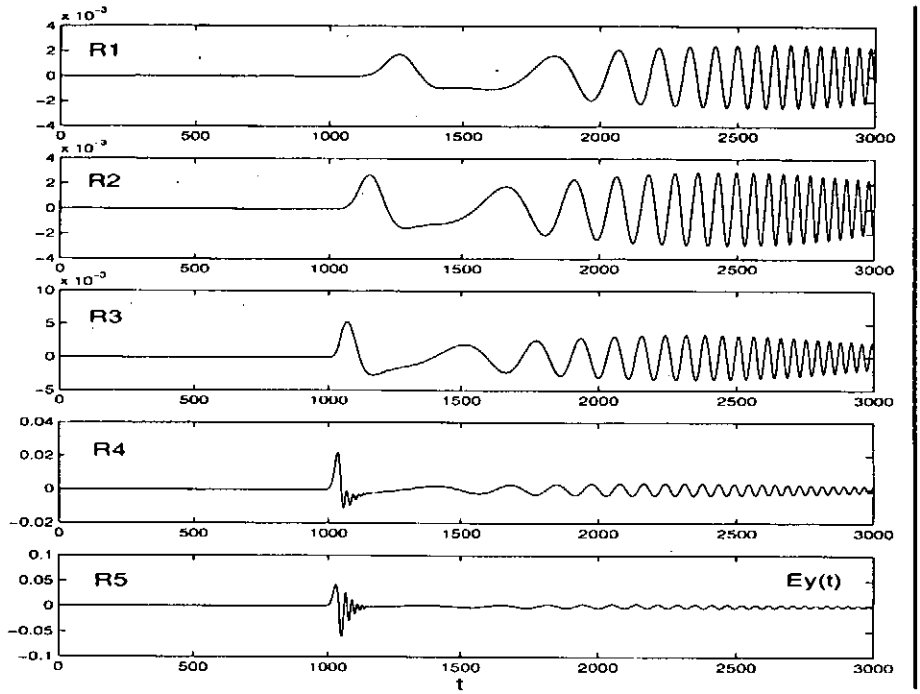

Fig.3 The wave amplitude $E_y(t)$ of the reflected O-mode received at each detector, R1, R2, ..., R5.

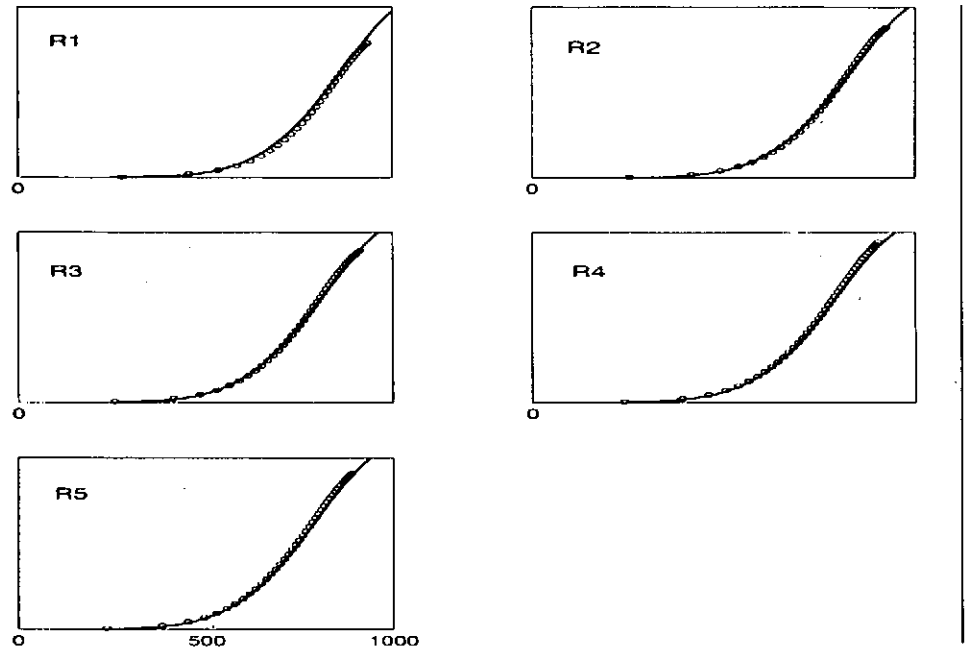

Fig.4 The reconstructed density profile (open circles) at each detector, R1, R2, ..., R5. Each horizontal axis corresponds to the line connecting each detector to the center of the plasma density.

Application of Ultrashort Pulse Reflectometry to a Steady State Plasma

A. Mase, A. Yamamoto, L. G. Bruskin, M. Ohashi, and T. Deguchi

Advanced Science and Technology Center for Cooperative Research, Kyushu University, Kasuga 816-8580, Japan

We describe here the application of an ultrashort pulse reflectometry to an inductively coupled plasma with a radio frequency source. Two types of impulse, 65 ps, 8 V and 22 ps, 3 V, are used as a source. The reflected waves are directly recorded to a digitizing scope with 50 GHz bandwidth, and analyzed by a wavelet transform based phase extraction method and a tomographic method which rely on a row signal waveform rather than on the group delay as a function of frequency. The line-integrated values of reconstructed density profiles are in good agreement with those measured by a 4 mm interferometer. The results demonstrate the potential of the current system for time resolved density profile measurements of LHD plasmas as well as low temperature processing plasmas.

1. Introduction

Reflectometry has been expected to be one of the key diagnostics to measure density profiles and density/magnetic-field fluctuations in large fusion devices. It provides good spatial and temporal resolutions, while requiring a single viewing chord and minimal vacuum access in contrast to interferometry and Thomson scattering. One of the most serious problems in density profile measurement using conventional frequency-modulation (FM) reflectometer is caused by the existence of density fluctuations in plasmas, since the multifringe phase changes produced by a reflectometer are easily masked by those due to density fluctuations. Several methods have been proposed to avoid this problem such as amplitude-modulation (AM) reflectometry or dual-frequency differential reflectometry and pulsed-radar reflectometry using moderate short pulse or ultrashort. We report here on an ultrashort pulse reflectometry applied to an inductively coupled steady state plasma (ICP) which is expected to be a source of plasma processing. The measurement of density profile is extremely important even in low temperature plasmas.

2. Ultrashort pulse reflectometer

An ultrashort pulse reflectometer uses an impulse as a source. Two types of impulse are used in this experiment: voltage amplitude A=8 V, pulse width τ_p =65 ps (PSPL-3500D) and A=3 V, τ_p =22 ps (4105C). The waveforms and its Fourier spectra are shown in Fig. 1. The characteristic frequency and the maximum frequency of an impulse are $\pi/2\tau_p$ and $2\pi/\tau_p$, respectively. In this experiment we mainly use a 22 ps impulse, since we can expect high amplitude at the frequency range of 12-18 GHz which corresponds to electron plasma frequency of ICP. The output of the impulse generator is fed through a WRD750 waveguide

that attenuates the low frequency part of the Fourier component, and stretches into a chirped pulse. The resultant waveform is radiated via a pyramidal horn into a plasma. The reflected wave picked up by an identical horn is directly fed to a sampling scope with 50 GHz bandwidth (HP-54750A). The time resolution of the scope is less than 7 ps.

3. Experimental results

Since the plasma is steady state in the present experiment, we can integrate the recorded signal which is produced at the maximum repetition rate of 1 MHz. An example of the row reflected signal is shown in Fig. 2 (upper trace). The initial peak at t<72.5 ns (dotted line) shows the reflection from a vacuum window. The second peak at t=72.7-74.5 ns (solid line) is attributed by a plasma. In order to reconstruct density profiles a filter bank followed by a detector have been used to obtain the time-of-flight (group delay) of each frequency component included in the impulse [1-3]. In the present experiment, the recorded signal can be directly analyzed by using time-frequency analysis such as wavelet transform given by [4]

$$S(\omega,t)=\int s(\tau)\varphi_{\omega}(t-\tau)d\tau$$

where we have chosen the following wavelet, known as the Gaussian or Morlet wavelet.

$$\varphi_{\omega}(t)=\sqrt{\frac{\omega}{2\pi}}\exp(i\omega t)\exp\left(-\frac{\omega^2 t^2}{8\sigma\pi^2}\right)$$

Figure 2 (lower trace) shows the wavelet spectra with and without plasma. The density profile can be reconstructed from the relation of group delay as a function of frequency. We also propose the Signal Record Analysis method of profile reconstruction which rely on a row signal waveform rather than on the group delay [5]. The method uses the analytical modeling of the impulse propagation in non-magnetized plasma. The algorithm of profile reconstruction is shown in detail in Ref. [5]. Figure 3 shows an example of reconstructed density profile by using SRA method. Since the instantaneous frequency of the recorded signal from the ultrashort pulse reflectometry is usually not well defined, the estimation of delay time appeared to be ambiguous and often failed. Comparing with the wavelet-based phase extraction method, the SRA algorithm yields plasma profiles of reasonable quality even for the data sets unacceptable for the time delay algorithm.

4. Summary

In summary, an ultrashort pulse reflectometry has been applied to an inductively coupled steady state plasma. The reflected waves are directly recorded to a digitizing scope with 50 GHz bandwidth, and analyzed by a wavelet transform based phase extraction method and a tomographic method which rely on a row signal waveform rather than on the group delay as a function of frequency. The results demonstrate the potential of the current system for time

resolved density profile measurements of LHD plasmas as well as low temperature processing plasmas.

Acknowledgements

This work was supported in part by Research Development Program of University-Industry Alliance and a Grant-in-Aid for Scientific Research from JSPS.

References

[1] C.W.Domier, N.C.Luhmann, Jr., A.E.Chou, W-M.Zhang, and A.J.Romanowsky, Rev. Sci. Instrum. **66**, 399 (1995).

[2] S.Kubota, T.Onuma, M.Kato, A.Mase, T.Tokuzawa, N.Oyama, A.Itakura, H.Hojo, L.Bruskin, T.Tamano, K.Yatsu, C.Domier, and N.Luhmann, Jr., Jpn. J. Appl. Phys. **38**, L202 (1999); A.Itakura, M.Kato, S.Kubota, A.Mase, T.Onuma, H.Hojo, and K. Yatsu, J. Plasma Fusion Res. **76**, 1198 (2000).

[3] Y.Roh, C.W.Domier, and N.C.Luhmann, Jr., Rev. Sci. Instrum. **72**, 332 (2001).

[4] L.G.Bruskin, A.Mase, T.Tokuzawa, S.Kubota, N.Oyama, A.Itakura, and T.Tamano, Rev. Sci. Instrum. **70**, 1052 (1999).

[5] L.G.Bruskin, A.Yamamoto, A.Mase, M.Ohashi, and T.Deguchi, this proceeding.

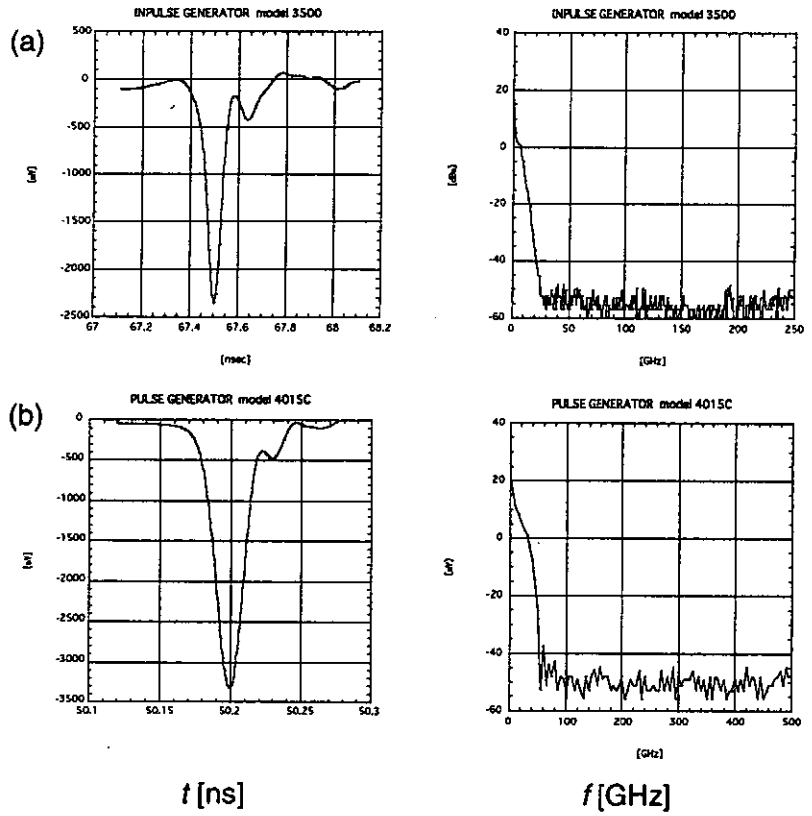

Fig. 1. Waveform and Fourier spectrum of impulse generated from (a) PSPL-3500D and (b) 4015C.

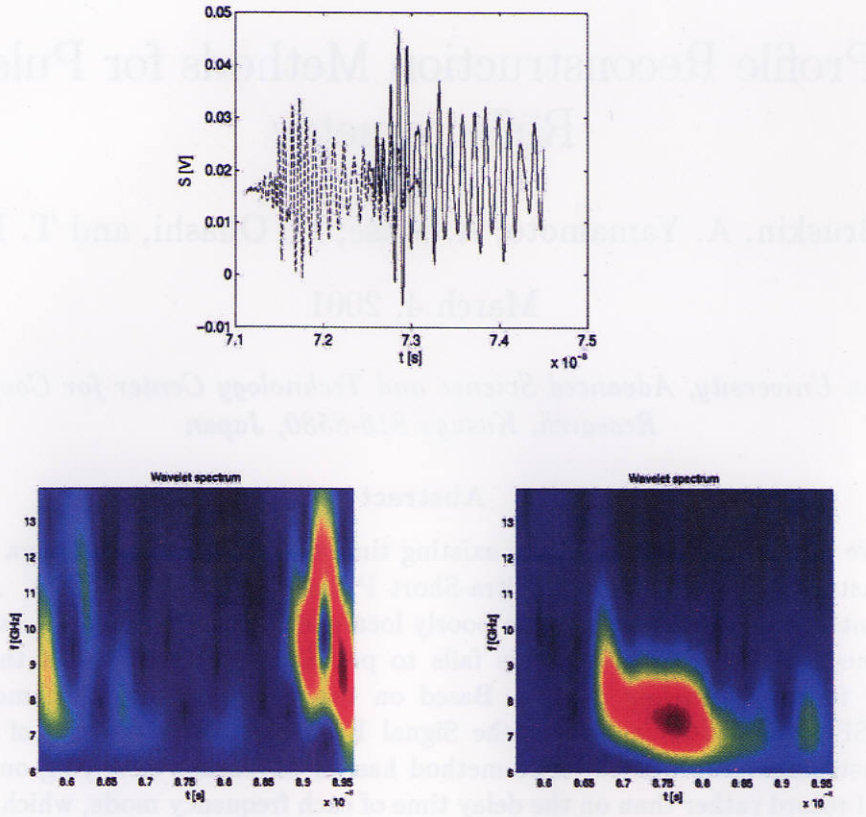

Fig. 2. Reflected wave from an inductively coupled steady state plasma, without plasma (dotted line) and with plasma (solid line). Time-frequency spectra of reflected wave using wavelet transform, without plasma (left), and with plasma (right).

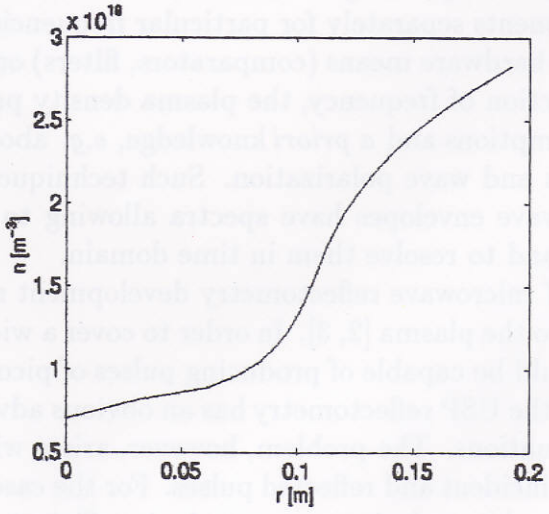

Fig. 3. Reconstructed density profile using signal record analysis method.

Profile Reconstruction Methods for Pulse Reflectometry

L.G. Bruskin, A. Yamamoto, A. Mase, M. Ohashi, and T. Deguchi

March 4, 2001

Kyushu University, Advanced Science and Technology Center for Cooperative Research, Kasuga 816-8580, Japan

Abstract

We present an analysis of the existing time delay methods of plasma profile reconstruction applied to the Ultra-Short Pulse (USP) reflectometry. As the instantaneous frequencies become poorly localized in the time domain, even the advanced time-frequency analysis fails to produce reliable values of the time delay for corresponding modes. Based on the results of analytical modeling of USP propagation in plasma the Signal Record Analysis method of profile reconstruction is proposed. The method has an advantage of relying on a row signal record rather than on the delay time of each frequency mode, which makes it more robust and reliable for the problem of density profile measurements using USP reflectometry.

Microwave reflectometry techniques have been employed over the years to measure density profiles of the plasma in fusion or plasma processing devices [1]. A typical reflectometer repeatedly launches a frequency-modulated (FM) envelope with a frequency swept within the limits, corresponding to reflection somewhere inside the plasma. By tracing the wave components separately for particular frequencies a time delay can be established using either hardware means (comparators, filters) or software tools. Given the time delay as a function of frequency, the plasma density profile can be recovered using some further assumptions and *a priori* knowledge, *e.g.* about profile initial point, ambient magnetic fields and wave polarization. Such technique implies that both input and output microwave envelopes have spectra allowing to identify uniquely the frequency components and to resolve them in time domain.

The further stage of microwave reflectometry development makes use of an ultra-shot pulses launched into the plasma [2, 3]. In order to cover a wide range of frequencies the pulse generator should be capable of producing pulses of picosecond range. Despite the technical obstacles, the USP reflectometry has an obvious advantage of being robust to the influence of fluctuations. The problem, however, arises with the time-frequency localization of the both incident and reflected pulses. For the case of USP reflectometry even the accuracy of wavelet analysis appears to be insufficient. The main obstacle in performing time delay measurements is the fact that instantaneous frequency of USP

signal in not well-defined, which means that:
1) signal components with different frequencies may exist at the same time point, and
2) signal component of a particular frequency may show up at different time points repeatedly.

We present here the results of analytical modeling of the USP propagation in non-magnetized plasma (or O-mode USP in a plasma with magnetic field). Utilizing these results, we develop a profile reconstruction technique based on a complete signal record analysis regardless of the time-localization of the signal spectrum.

In the case of the plasma density and microwave field varying in only x direction, a non-stationary full-wave equation for an O-mode microwave envelope propagating in non-homogeneous plasma reduces to

$$\frac{\partial^2 E}{\partial x^2} - \frac{1}{c^2}\frac{\partial^2 E}{\partial t^2} - \frac{\omega_0^2(x)}{c^2}E = 0 \tag{1}$$

with the boundary condition $E^{inc}(x=0) = E_0(t)$. Application of Fourier transform over t and assumption of ω_0^2 being a linear function of x allows us to represent the solution satisfying the radiation condition and the boundary condition as

$$E = \int 2\sqrt{\pi}\left|\frac{c}{\omega}\frac{d\epsilon}{dx}\right|_0^{-1/6} \tilde{E}_0(\omega)\,\exp\left(i\omega(t - \frac{1}{c}\int_0^{x_0(\omega)}\sqrt{\epsilon(x')}\,dx') + i\frac{\pi}{4}\right) \cdot A_i\left((\omega/c)^{2/3}\,|d\epsilon/dx|_0^{1/3}\,(x - x_0(\omega))\right)\,d\omega \tag{2}$$

where $\tilde{E}_0(\omega)$ is a Fourier transform of $E_0(t)$, A_i is the Airy function, $\epsilon(x,w) = 1 - \frac{\omega_0^2(x)}{\omega^2}$ is the refractive index for the ordinary wave, subscript zero marks the corresponding values in a cut-off point $x_0(\omega)$ defined by the equation $\epsilon(x_0, w) = 0$.

For a non-linear 1D plasma slab (non-linear $\omega^2(x)$ function) the solution of Eq. (1) is sought in WKB approximation as a superposition of the modes propagating with yet unknown velocity:

$$E = \int V(x,\omega)\exp\left(i\omega(t - \frac{\psi(x,\omega)}{c})\right)\,d\omega \tag{3}$$

After substituting (3) to (1) and assuming that the properties of the medium vary slowly (WKB approximation) the final expression for both incident and reflected waves can be written as

$$E = \int \frac{\tilde{E}_0(\omega)}{\epsilon^{1/4}}\,e^{\left(i\omega(t - \frac{1}{c}\int_0^{x_0}\sqrt{\epsilon(x')}\,dx') + i\frac{\pi}{4}\right)}\,2\cos\left(\frac{\omega}{c}\int_x^{x_0}\sqrt{\epsilon(x')}\,dx' - \frac{\pi}{4}\right)\,d\omega \tag{4}$$

Similar to the well-known case of monochromatic wave propagation in a non-uniform plasma [4], the WKB solution is corrected by shifting a phase of the reflected wave by additional $\pi/2$ as required by comparison of Eq.(2) and Eq. (4) rewritten for $x \to 0$. In the practical applications the signal values are recorded in the $x = 0$ point. The typical waveform calculated using Eq. (4), is shown on Fig. 1.

The results of 1D WKB modeling can be utilized as a basis for the profile reconstruction algorithm, which is further referred as Signal Record Analysis (SRA). The technical requirement for SRA implementation is availability of direct row signal record.

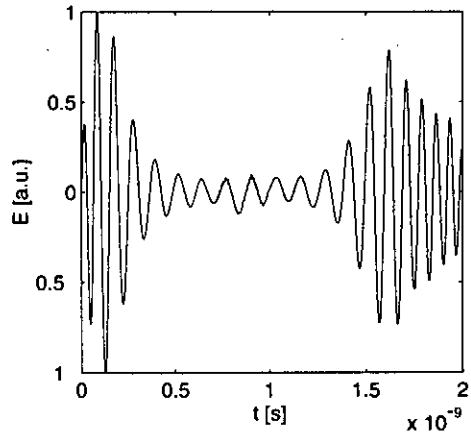

Figure 1: Signal record in the $x = 0$ point.

For the reflected modes in $x = 0$ point expression (4) can be re-written as

$$E = \int |C(\omega)| \exp\left(i\omega\left(t - \frac{2}{c}\int_0^{x_0(\omega)} \sqrt{1 - \frac{\omega_0^2}{\omega^2}}\, dx\right) + i\frac{\pi}{2} + i\arg(C(\omega))\right) d\omega \qquad (5)$$

It follows from the above equation that a signal record, represented in a form similar to Eq. (5)

$$s(t) = \int |S| e^{i\omega t - \psi(\omega)}\, d\omega \qquad (6)$$

would allow us to find out the fitting functions ψ, S, which are related to plasma parameters through Eq. (5). An important point of SRA is that the experimental estimation of delay time for corresponding modes can thus be avoided.

The SRA algorithm of profile reconstruction consists of the following stages:

1. Record the signals $s_w(t)$, $s_p(t)$ for the cases of pulse reflected from the port window and from plasma using digitization oscilloscope.
2. Represent the signals in the form (6) so that $\psi_{w,p} = -\arg(S_{w,p})$ (Fig. 2).
3. Unwrap the phase, take the phase difference $\psi_p - \psi_w$ (Fig. 3). The phase difference $\psi_p - \psi_w$, as follows from Eq. (5), is equal to

$$\psi_p - \psi_w = \frac{2\omega_0}{c}\int_0^{x_0(\omega)} \sqrt{1 - \frac{\omega_0^2}{\omega^2}}\, dx \qquad (7)$$

4. Recover the plasma profile (Fig. 4)using Eq. (7). This integral equation can be either solved numerically or reduced to Abel equation. In course of reduction it is necessary to take a derivative of $\psi_p - \psi_w$, which is not a numerically stable procedure. In the current implementation we have smoothed the $\psi_p - \psi_w$ function first as shown on (Fig. 3), but we intend to avoid smoothing and differentiation altogether by implementing an iterative gradient method of numerical solution of Eq. (7) similar to the one used in our previous paper [5].

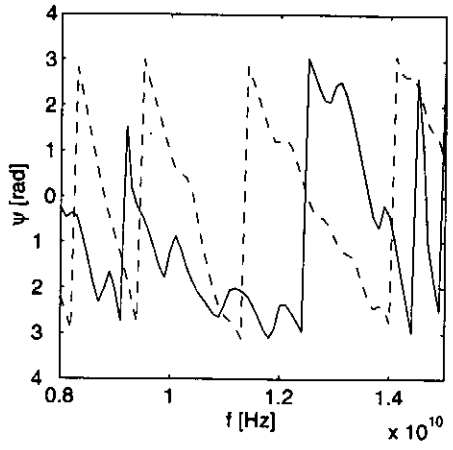

Figure 2: ψ_p (solid line) and ψ_w (broken line) phases

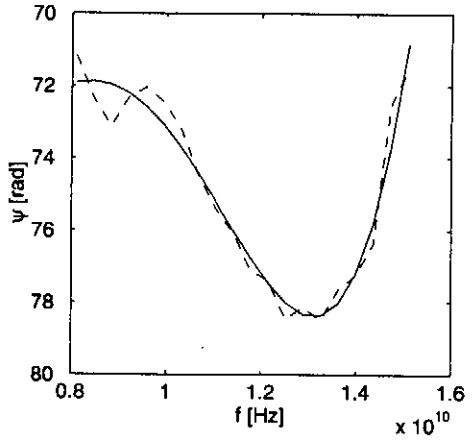

Figure 3: $(\psi_p - \psi_w)$ function (broken line) and its approximation (solid line)

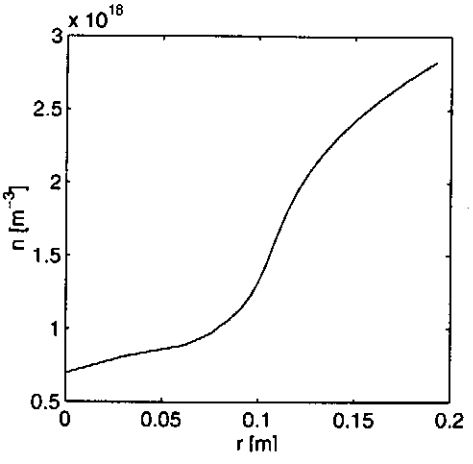

Figure 4: Plasma density profile

Although the expression (7) coincides with the main formula of FM reflectometry [1], we would like to stress that the way of defining $\psi_p - \psi_w$ has nothing in common with FM techniques that rely on measurements of the beat frequency and delay time as functions of wave frequency. Since for the case of USP the instantaneous frequency is not well defined, the estimation of delay time appears to be ambiguous and often fail-prone. The definition of $\psi_p - \psi_w$, however, is unique regardless of the time localization of the corresponding modes. Comparing the SRA algorithm with the wavelet-based time delay method, we have noticed that the former one is more robust and often yields plasma profiles of reasonable quality even for the data sets unacceptable for the time delay algorithm.

References

[1] A.C.C. Sips and G.J. Kramer, Plasma Phys. Contr. Fusion **35**, (1993), 743.

[2] C.W. Domier, N.C. Luhmann, Jr., A.E. Chou, W-M. Zhang, and A.J. Romanowsky, Rev. Sci. Instrum. **66**, (1995), 399.

[3] S. Kubota, T. Onuma, A. Mase, T. Tokuzawa, N. Oyama, A. Itakura, H. Hojo, L. Bruskin, T. Tamano, K. Yatsu, C. Domier and N.C. Luhmann, Jr., Jpn. J. Appl. Phys. **37** (1998), L300.

[4] V.L. Ginzburg, *The Propagation of Electromagnetic Waves in Plasmas*, (Pergamon Press, 1070).

[5] L.G. Bruskin, A. Mase, T. Tokuzawa, N. Oyama, A. Itakura and T. Tamano, Rev. Sci. Instrum. **69** (1998), 425.

Status of Doppler Reflectometry Investigations at the W7-AS Stellarator

M Hirsch, E Holzhauer*, J Baldzuhn, B Kurzan, B Scott

Max-Planck-Institut für Plasmaphysik, EURATOM Association, D-85748 Garching, Germany

*Institut für Plasmaforschung, Universität Stuttgart, D-70569 Stuttgart, Germany

Doppler Reflectometry is characterized by a finite tilt angle θ_{tilt} of the probing microwave beam with respect to the normal onto the cutoff layer (Fig.1). The diagnostic selects density perturbations with wave number $K_\perp = 2 \cdot k_o \cdot \sin(\theta_{tilt})$ in the reflecting layer from the -1st diffraction order. This is complementary to conventional reflectometry which probes the average distance to the reflecting layer via the 0th order of reflection. With finite θ_{tilt} the propagation velocity of the density perturbations can be calculated from the Doppler shift $\Delta\omega = \bar{v} \cdot \bar{K} = v_\perp \cdot K_\perp$. If for the density turbulence one assumes $K \perp B$ the Doppler shift results only from the velocity component of the perturbations *perpendicular to the magnetic field* (i.e. in the direction of the $E \times B$ velocity) independent of the (toroidal and/or poloidal) orientation of the antenna tilt ! However, the calculation of $v_\perp \propto K_\perp \propto \theta_{tilt}$ relies on a defined tilt angle which may vary with the discharge conditions. Therefore a differential measurement is advantageous where two antennas view the same spot with angles $\pm\theta_{tilt}$.

Doppler shifted reflectometry signals first have been considered as a perturbing effect in conventional reflectometry experiments (see refs. in Holzhauer *et al* 1998, Brañas *et al* 1999). More recently Doppler reflectometry using a deliberately tilted antenna has been proposed as a plasma diagnostic and first experimental results have been published in (Holzhauer *et al* 1998, Hirsch *et al* 1999, Zou *et al* 1999, Bulanin *et al* 2000). At the IPP Garching the potential of Doppler Reflectometry as a diagnostic for density perturbations and their (radially sheared) propagation velocity is systematically studied (Hirsch *et al* 2001).

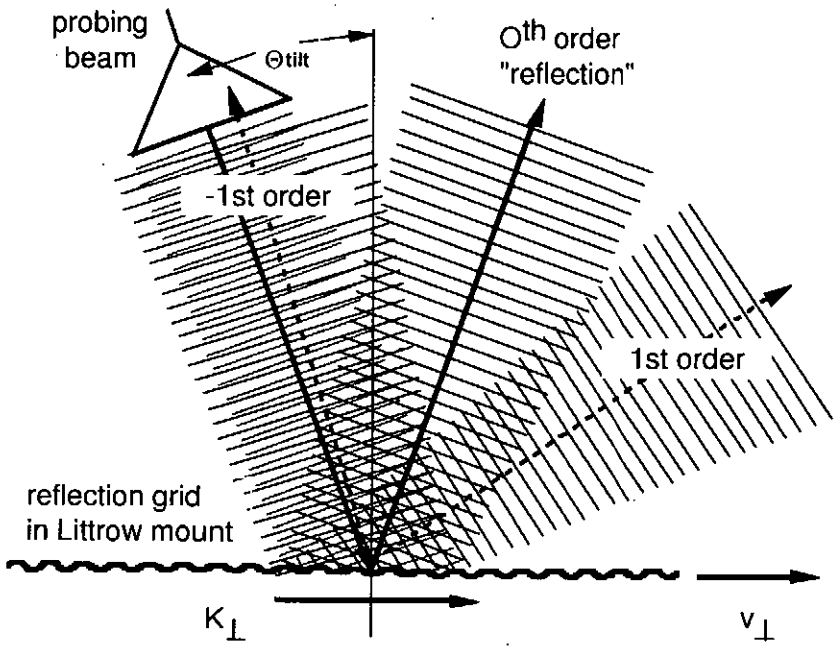

Refractive effects resulting from the background profiles and the density perturbations themselves complicate the radially localized measurement of $K_\perp$(r)-spectrum and propagation velocity $v_\perp$(r) of the density perturbations. Both complications can be studied by the so-called weighting function which describes the response of the diagnostic to a δ-function like density disturbance. As an example in Fig.2 the weighting function for a typical density profile of W7-AS (right side of Fig2) is shown probed by a microwave with $f = 85$ GHz and x-mode polarization (cutoff density $n = 3 \cdot 10^{19}\ m^{-3}$). For clarity a background profile without fluctuations is assumed.

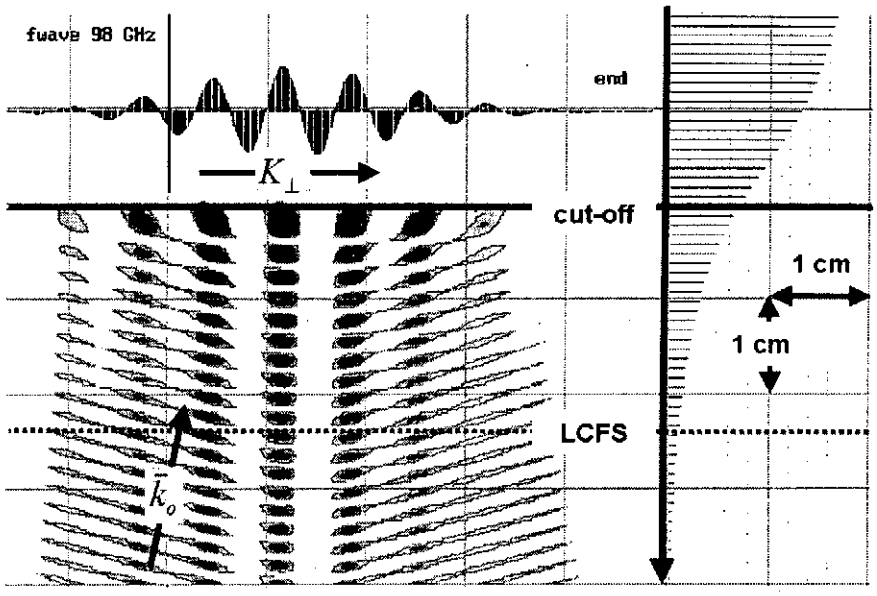

As a general result one obtains that **refractive effects due to the radial background profiles** in a 1D layered plasma do not significantly degrade the $K_\perp$-resolution of the diagnostic and the probed $K_\perp(r)$ and thus $v_\perp(r)$ can be calculated directly using the geometrical θ_{tilt} and the vacuum wavelength. The **radial localization** of the measurement results predominantly from the swelling of the electric field close to the cutoff layer in analogy to the case of conventional reflectometry. With finite θ_{tilt} this probed layer is shifted radially outward. For a plane wavefront the shift can be calculated from the 1D wave equation (Ginzburg 1964) with the result that the effective cutoff layer is shifted to a position where the index of refraction becomes $\mu = \sin(\theta_{tilt})$. For x-mode polarization the smaller wavelength of the radiation required to probe a given density results in a narrowing of the last lobe and thus a better localization compared to o-mode. In addition close to the cutoff layer the decrease of $\varepsilon_r(r) \to 0$ is more pronounced for the x-mode and thus the localization is improved. As a consequence also the radial shift of the weighting function with increasing θ_{tilt} is smaller for x-mode polarization. For W7-AS conditions and $\theta_{tilt} = 14^o$ one obtains $\delta r = 2 - 4$ mm.

The **impact of the density perturbation amplitude** is twofold: On one hand a finite turbulence level is needed for a sufficiently strong signal scattered into the -1st diffraction order. On the other hand with increasing amplitude the weighting function for the Doppler reflectometer is deformed by the very fluctuations which it is supposed to analyze. Multiple scattering or even multiple reflection occur leading to a screening of the radial layer to be investigated. Moreover an increasing amount of the microwave power is diffracted into higher orders.

Two questions must be addressed:

1. Can the absolute value of the turbulence amplitude be obtained from the amount of power

scattered into the -1st diffraction order ? - Due to screening and an unknown fraction of scattering into higher orders this task is generally difficult or impossible as it requires independent information about the turbulence characteristics. However, numerical studies show that for most cases the power scattered into the -1st diffraction order still can be used as a fast but uncalibrated monitor of the temporal evolution.

2. How does the turbulence amplitude deform the weighting function in real space and $K_\perp$-space ? This question is studied with 2D full wave code calculations. For the case of the ASDEX Upgrade Tokamak direct numerical simulations for warm ion drift Alfvén turbulence are available (Scott 2000). In W7-AS the experiments indicate that the perturbation of Doppler reflectometry by the density turbulence can be tolerated. This follows from the observation that Doppler shift and spectral width of the 0th and -1st diffraction order vary if the nominal cutoff position is changed indicating that the measurement probes a localized quantity.

Optimization of the antenna is mandatory for a satisfactory performance of Doppler reflectometry as well as for conventional reflectometry: Both diagnostic concepts are based o the separation of the 0th order of reflection from the higher diffraction orders: For Doppler reflectometry the antenna acts as a bandpass filter in K-space which suppresses the unwanted 0th order. Vice versa for conventional reflectometry the antenna acts as a low pass filter which reduces unwanted higher diffraction orders. In the ideal case of parallel wavefronts at the reflecting layer the resolution of the antenna ΔK improves with the width of the microwave beam at the illuminated spot. However, this resolution may be deteriorated by finite a curvature of the wave front and/or by a finite curvature of the reflecting layer within the beam spot. The $K_\perp$-selectivity of the antenna is insufficient to suppress the unwanted orders of diffraction completely. Additional filtering in the frequency spectrum improves the situation if the spectral features belonging to the higher diffraction orders can be separated by a sufficient Doppler shift from the 0th order. From that a further criterion for an optimized antenna follows since in the frequency spectrum 0th and higher diffraction orders are broadened due to the effective movements of the illuminated surface: A symmetric spectral width of the 0th order results from the effective radial oscillation averaged over the finite spot size. In addition the spectral width of the -1st order increases due to the modulation of the effective θ_{tilt}. With a larger spot diameter, the rms levels of both movements and thus the spectral width of the 0th and -1st order decrease.

The **antenna system in W7-AS** uses focussing Gaussian optics resulting in parallel wave fronts at the beam waist and negligible side-lobes. Side-lobes constitute a problem if the $K_\perp$-spectrum of the density fluctuations has pronounced maxima outside the selected $K_\perp$ interval or if the strong 0th order falls into a side-lobe of the receiver antenna. The distance between focussing mirror and plasma has been chosen as large as possible ($l \approx 55\,\mathrm{cm}$) within the mechanical constraints. This allows for the beam waist to lie at the probed position with nearly parallel wave fronts and negligible beam divergence even if the probing frequency is varied and the radial position of the cutoff layer changes by a few cm. The optimum spot diameter turned out to be

limited by the poloidal curvature of the reflecting layer originating from the rather small minor radius resulting in a local curvature radius of $(0.5\,\mathrm{m} < r < 0.8\,\mathrm{m})$. In view of future devices such as W7-X a systematic study on the antenna optimization criteria is under way.

Experimental results from the W7-AS stellarator (Hirsch et al 2001) obtained with an antenna where θ_{tilt} could be varied show a broad $K_\perp$-spectrum of the turbulence and a Doppler shift that varies linearly with θ_{tilt}, i.e. the density perturbations propagate with a common group velocity. During stationary phases $v_\perp(r)$ follows the profile of $v_{E\times B}(r)$ within the error bars, indicating that the intrinsic phase velocity of the perturbations riding on the background plasma must be small. Transient states of the plasma such as ELMs can be observed with a temporal resolution of $< 50\,\mu s$.

Outlook : W7-AS will start its last experimental campaign in March 2001, final shutdown is scheduled for July 2002. Four fixed frequency homodyne channels ($70\,\mathrm{GHz} \le f \le 110\,\mathrm{GHz}$) are installed sharing the bistatic tilted antenna $(\theta_{tilt} = \pm 14^o)$ with the broadband heterodyne reflectometer. This will allow for a systematic comparison between $v_\perp(r)$ of the turbulence in the density gradient region $(1\cdot 10^{19}\,\mathrm{m}^{-3} < n < 6\cdot 10^{19}\,\mathrm{m}^{-3})$ and $v_{E\times B}(r)$ measured by passive spectroscopy. Because of the large Doppler shift of up to 6 MHz and the strong variation of the reflected power data reduction by analogue techniques is preferred. For the -1st order Doppler frequency shift and power are continuously monitored with a temporal resolution of $\tau \approx 100\,\mu s$. In addition 12 fixed frequency and 7 variable bandpass filters provide a fast ($\tau \ge 20\,\mu s$) characterization of the returning signal frequency spectrum.

In conclusion Doppler reflectometry has proven to be a valuable tool for an investigation of the turbulence spectrum and the propagation velocity of the turbulence respectively its shear. Moreover, a Doppler correlation reflectometry experiment where two microwave frequencies are launched would provide a fast and simultaneous measurement of the interdependent quantities flow-shear and radial correlation length of the turbulence.

REFERENCES

Brañas B, Hirsch M, Sánchez J, Zhuravlev V 1999 *Rev. Sci. Instrum* **70**(1) 1025

Bulanin V V, Lebedev S V, Levin L S, Roytershteyn V S 2000, *Plasma Physics Reports* **26**(10) 813

Ginzburg V L 1964 *The Propagation of Electromagnetic Waves in Plasmas* (Pergamon, Oxford)

Hirsch M, Holzhauer E, Baldzuhn J, Kurzan B 2001 *Rev. Sci. Instrum* **72** (2001) 324 and *Proc. of the 4th Reflectomety Workshop, Cadarche, March 2 - 24 1999, EUR-CEA-FC-1674*

Hirsch M, Holzhauer E, Baldzuhn J, Kurzan B, Scott B 2001 submitted to *Plasma Phys. Contol Fusion*

Holzhauer E, Hirsch M, Grossmann T, Brañas B, Serra F 1998 *Plasma Phys. Control. Fusion* **40** 1869

Scott B 2000; *Phys Plasmas* 7 (2000) 1845 and *Plasma Phys. Contol Fusion* 40 (1998) 823

Zou et al 1999 *Proc. of the 4th Reflectomety Workshop, Cadarche, March 2 - 24 1999, EUR-CEA-FC-1674; Proc. 26th EPS Conf. on Controlled Fusion and Plasma Physics (Maastricht)* 1041

POLOIDAL ROTATION VELOCITY MEASUREMENT IN TOROIDAL PLASMAS VIA MICROWAVE REFLECTOMETRY

O.S.Pavlichenko, A.I.Skibenko, I.P.Fomin, I.B.Pinos, V.L.Ocheretenko, V.L.Berezhniy
Institute of Plasma Physics of NSC KhIPT, Kharkov 61108, Ukraine

Results of experiment modeling backscattering of microwaves from rotating plasma layer perturbed by fluctuations are presented. It was shown that auto- and crosscorelation of reflected power have a periodicity equal to rotation period. Such periodicity was observed by microwave reflectometry in experiments on RF plasma production on U-3M torsatron and was used for measurement of plasma poloidal rotation velocity.

I.INTRODUCTION

One of key issues of confinement studies in stellarators now is an understanding of role of the radial electric field. Heavy ion beam probe (HIBP) technic is being used (CHS) or prepared (TJ-II, LHD) for measurement of plasma potential. This technic needs special ports on device and is expensive. Indirect method of electric field measurement is observation of poloidal plasma rotation in crossed radial electric and toroidal magnetic fields. Change exchange spectroscopy (CHXS) is being used for observation of Doppler shift of ion spectral lines and calculation of poloidal rotation velocity (W7-AS, CHS). This diagnostic needs a special diagnostic neutral beam or uses plasma heating neutral beam. Therefore any new and possibly more simple diagnostics for observation of poloidal plasma rotation with a good spatial resolution are welcomed.

Microwave reflectometry is a well-known technic for measurement of electron density profiles and its fluctuations. It has a rather good spatial resolution (few mm). Microwave reflectometry is being extensively used on Uragan-3M (U-3M) torsatron for radial electron density and its fluctuation profiles measurements [1-2]. Microwave (O- and X- mode) reflectometry setup on U-3M uses 3 monostatic (launch/receive) antennas ported in one of toroidal crossections of l=3 torsatron between helical conductors (Fig.1). This setup allows to study crosscorrelation between microwave signals reflected in different poloidal locations and was used for measurement of poloidal propagation velocity of plasma fluctuations in experiments on RF plasma production/heating in U-3M torsatron [3]. It was observed that both auto (AC)- and crosscorrelation (CC) of signals had periodical structures. Closer look showed that period of modulation of both AC and CC is proportional to the time delay of CC between signals of different antennas. To understand this phenomenon we performed a model experiment on observation of microwave reflection from rotating rippled surface metallic cylinder. It was shown that the period of both AC and CC modulation is equal to the period of rotation of cylinder. This conclusion became a basis of simple measurement of poloidal rotation velocity of plasma via microwave reflectometry in U-3M torsatron.

In this paper we present results of this model experiment along with explanation (II), compare them with data obtained on U-3M torsatron (III) and conclude (IV) that modulation of AC of microwave power reflected from plasma in tilted antenna geometry can be used for measurement of poloidal rotation velocity in toroidal magnetically confined plasmas.

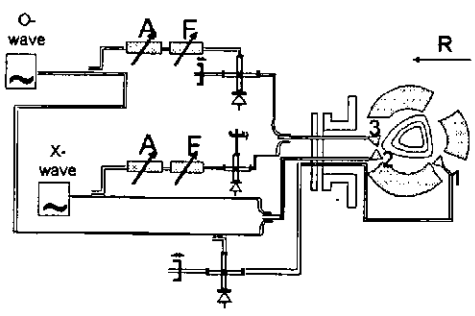

Fig.1 Reflectometry setup at U-3M

II.MODEL EXPERIMENT

The experiment was performed using the 37.5 GHz fixed frequency homodyne reflectometer similar to that one installed on U-3M torsatron. Up to 10 mW cw incident power was launched via a 20 dB standard gain horn on the rippled rotating metallic surface. The same

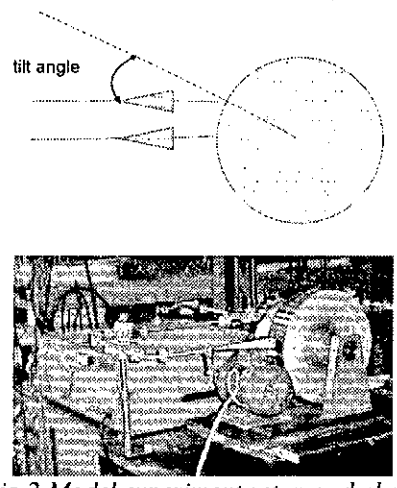

Fig.2 Model experiment setup and photo

antenna received reflected power. The reflecting rippled surface was formed from 0.2-mm-thick stainless shim mounted on the surface of grooved Al cylinder (diameter of 240 mm and height of 40 mm). This cylinder was previously used as the phase shifter of λ=337 mkm laser interferometer and had a triangular shaped grooves (period = 0.3 mm , height =0.3 mm).

The shim was pressed to form a periodical structure with triangular teeth (period = 16 mm, height=3 mm). This shim was mounted on cylinder surface without of special care about saving periodicity of teeth and could cover 90 % of cylinder circumference or total cylinder surface. The cylinder was rotating with frequency of 6 Hz.

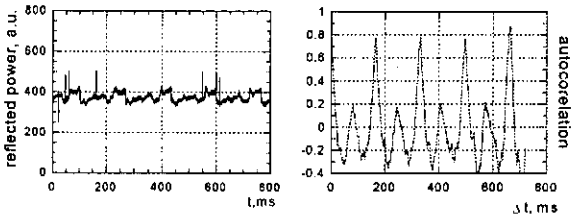

Fig.3 Reflection from grooved cylinder (left-detector signal, right- AC)

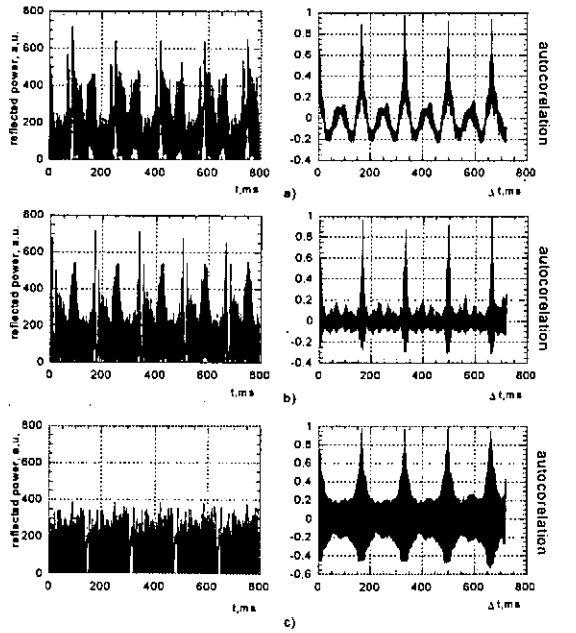

Fig.4 Reflection from 90% shim for different antenna tilt angle α [a) α=0°, b) α=6°, c) α=16°]

III.EXPERIMENT ON U-3M

Periodical structures in both auto and crosscorrelation of signals were observed previously on U-3M torsatron [1]. The typical forms of AC and CC observed at simultaneous probing of plasma by antennas 2 and 3 are shown on Fig.5. The observed periodicity can be interpreted now as result of poloidal rotation of plasma reflecting layer with frequency F ≈ 10 kHz. This rotation

The antenna was put on a distance of 30 mm from reflecting surface along a horizontal line intersecting cylinder center and could be moved vertically on a distance up to 33 mm. This movement resulted in a tilt of antenna to cylinder surface up to 16° (Fig.2).

The signal of microwave detector was digitized with ADC (τ= 4 mks) and stored. The typical signals of detector along with crosscorelation of signals are shown on Fig. 3-4.

It was observed that in all cases : no shim (Fig.3), 90 % shim (Fig.4) and 100 % shim – the signal of reflectometer exhibit periodical changes corresponding to rotation period. These changes result in a well-pronounced periodicity of crosscorrelation. As for as in the case when the reflective surface was definitely inhomogeneous (90 % shim) the periodicity of reflected signal corresponds to the cylinder rotation period, one can conclude that the period of crosscorrelation modulation is equal to the cylinder rotation period.

This observation is general. Changes in rippled surface shape and antenna tilt angle resulted only in reflected power change. For shorter periodicity of reflecting surface perturbations the modulation of reflected power was smaller. More oblique wave launch resulted in smaller backward reflection.

These observations are in a very good correspondence with data of G.D.Conway [4] and one can use all his arguments for explanation of backward reflection of microwaves from rippled reflecting surface as a result of Bragg diffraction. The novelty of our experiment is in using of a **rotating** rippled surface and showing that the periodicity in crosscorrelation of reflected power is equal to reflecting surface rotation period.

The periodic structure on autocorrelation can be understood if to take into account a fact that the frequency of microwaves reflected from moving surface is Doppler shifted. This was clearly shown in experiment on W7AS stellarator [5]. In homodyne reflectometer this results in modulation of output signal with frequency of Doppler shift. This modulation is reflected in modulation of autocorrelation of output signal.

results in a corresponding time lag in crosscorrelation between signals of 2 antennas.

Autocorrelation approach is now used in reflectometry system of U-3M torsatron for measurement of plasma poloidal rotation velocity. One of the data obtained is shown on Fig.6. This figure presents the radial distribution of poloidal rotation velocity obtained at simultaneous plasma probing with both inside and outside antennas with probing frequency change on shot-to-shot basis. The most striking feature of this observation is existence of strong poloidal velocity shear in outer plasma.

existence of strong poloidal velocity shear in outer plasma.

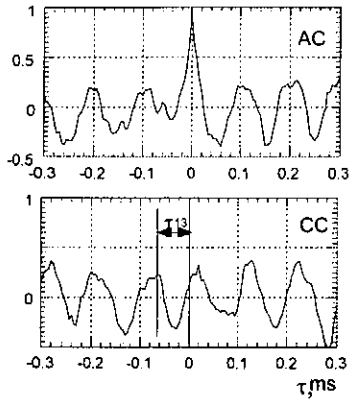

Fig.5 Typical autocorelation and crosscorelation (between antennas 1 and 3) on U-3M

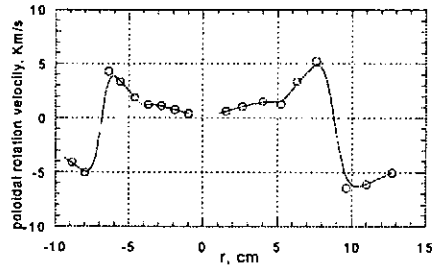

Fig.6 Radial distribution of plasma poloidal rotation velocity for RF produced plasma in U-3M torsatron measured from AC and CC

IV. CONCLUSION

It was shown that when microwaves are launched in tilted antenna geometry and are backscattered from rotating rippled plasma cut-off layer, both auto and crosscorrelations of output of homodyne reflectometer have the periodicity corresponding to rotation period. This gives a very simple and cost effective way of measurement of plasma poloidal rotation velocity. If plasma probing is being performed in one poloidal location, one can measure the value of poloidal rotation velocity only. A direction of rotation can be measured if one can port 2 antennas in different poloidal locations and use crosscorelation.

The radial distribution of poloidal rotation velocity can be measured in both tokamaks and stellarators by using multi-frequency homodyne reflectometers similar to that one used on many toroidal magnetic systems.

AKNOWLEDGEMENT

This work was partly supported by LIME Program (National Institute for Fusion Science, Japan).

REFERENCES

1. A.I.Skibenko, O.S.Pavlichenko et al., 23rd EPS Conference on Controlled Fusion and Plasma Physics, Contr.Papers., Kiev (1996), part III, p.1124
2. V.L.Berezhniy, E.D.Volkov et al., Problems of Atomic Science and Technology, Series: Plasma Physics, Kharkov (1999), issues 3-4, p.43
3. O.S.Pavlichenko, A.I.Skibenko et al., XII International Stellarator Conference, Contr.Papers, Madison (1999)
4. G.D.Conway, Rev.Sci.Instrum, 64(10) , 2782 (1993)
5. C.Christou, J.Baldzuhn et al., 25th EPS Conference on Controlled Fusion and Plasma Physics, Contr.Papers., Praha (1998), ECA Vol.22C (1998), 1466-1469

Homodyne Reflectometer For NBI Interlock On Large Helical Device

Kenji TANAKA, Akira EJIRI[1], Yasuhiko ITO, Kazuo KAWAHATA, Tokihiko TOKUZAWA
Masaki OSAKABE and Yasuhiko TAKEIRI

National Institute for Fusion Science, Toki 509-5292, Japan
[1]Graduate School of Frontier Sciences, Univ. Tokyo, Tokyo 113-0033, Japan

Abstract

Neutral Beam Injection (NBI) under low density causes serious damage on vacuum vessel wall. It is necessary to stop NBI when electron density becomes lower than $1x10^{19}m^{-3}$. This needs reliable density monitor for NBI interlock. A three-channel homodyne reflectometer was installed on Large Helical Device (LHD) and was used for NBI interlock. 28.5, 34.9 and 40.2 GHz Gunn oscillators were used with O mode injection. Their O mode cut off density correspond to $1x10^{19}$,$1.5x10^{19}$ and $2x10^{19}m^{-3}$ respectively. The simple homodyne detection is presently used. When the density reaches to the cutoff density, the reflected signals are detected. The reflected signal consists of DC signal due to local and reflected power, and AC signal due to position of cut off layer and density fluctuation. Since the change of DC signal at lower and higher than cut off density was very small, root mean square(RMS) value of AC signal were used for interlock signal. This interlock system is successfully working from the beginning of the NBI experiments campaign on LHD.

[1] Introduction

There is a big demand of the reliable NBI interlock. There is no magnetic disruption on LHD, however, the plasma terminates unexpectedly due to the radiation collapse. If NBI continues after plasma termination, neutral beam hits vessel wall and damages it significantly. More than 50% of NBI power does not deposit on plasma at lower than $1x10^{19}m^{-3}$ of electron density [1]. Therefore, when electron density decrease lower than $1x10^{19}m^{-3}$, NBI has to be stopped. A reliable NBI interlock system is required to protect vessel wall.

There are several candidates of interlock sources. One is an interferometer. This is the most accurate density monitor, but fringe jump sometimes happens at high density, so, it is not reliable. The second is polarimeter. Recently, polarimeter was used for density measurements under well known magnetic field[3,4]. This will be reasonably accurate and reliable, however, because of small phase shift of Faraday rotation, the measurements are still technically difficult. The third one is plasma emission measurements (Hα, Hβ.. etc). It is simple, but, signal intensity is not function of density but function of temperature and neutral density, so it is not accurate. Finally, we propose a microwave reflectometer. When density reaches to the cut off density, reflected signal appears. It is expected to be simple and reliable density monitor. The proof of principle experiments of reflectometer interlock system was done on CHS[4].

[2] System setup

Fig. 1 shows schematic diagram of the density interlock reflectometer. The detection is simple homodyne technique. The obtained signals are described as follows.

$$I_{homo} \propto P_R + P_L + 2\sqrt{P_R P_L}\cos(\phi_0 + \phi_n) \quad (1)$$

P_R; Reflected Power, P_L; Local Power
ϕ_0; Phase shift due to cut off position,
ϕ_n; phase shift due to fluctuation

The first and second terms are DC components and the third term is AC components. Since $P_R << P_L$, change of DC components, between at lower and at higher than cut off density, is very small. Therefore, AC components were used as an interlock signal source.

Fig.1, shows schematic view of the interlock reflectometer. RMS signal of 10~500kHz components were used for interlock signal source. The characteristic time of ϕ_0 is several tens or hundreds milliseconds, therefore, mainly RMS signals are ϕ_n components. When RMS signal decrease under the certain level, interlock signal becomes zero and stops NBI. Fig.2 shows installation on LHD. Gunn oscillators and detectors were placed 8m away from the LHD port to be free from effect of the magnetic field. Injection polarization is O mode at plasma edge. Fig.3 shows detailed schematic diagram of transmission and detection components. The system has three channels with frequencies 28.5, 34.9 and 402.GHz, which correspond to O mode cutoff at densities 1, 1.5 and $2x10^{19}m^{-3}$.respectively. Usually, 28.5 or 34.9GHz was used for interlock signal, and other channels were used for the density fluctuation measurements. Fig.4 shows cross section of the measurements. A $1/e^2$ intensity beam width is 550mm for 28.5GHz, 34.9GHz and 400mm for 40.2GHz.

Because of the large beam size, the antenna alignment is insensitive to the signal intensity.

[3] Signal characteristics

In typical NBI discharge of LHD, the plasma is produced by 82.6 or 168GHz ECRH, then is heated by NBI. Since the density of ECRH plasma sometimes does not exceed $1x10^{19}m^{-3}$, interlock system is killed until about 100 msec after the start of NBI. After NBI starts, density exceeds $1x10^{19}m^{-3}$ very quickly (in less than 100msec), therefore, the wall damage due to operation of NBI during the dead time of interlock is not problem.

Figs. 5 show an example of discharge, in which reflectometer interlock worked successfully. In this discharge, NBI pulse length was set to be t=0.4~9.4sec, but the plasma suddenly terminated at t=4sec, because of the radiation collapse. As shown in fig.5, when density starts to decrease at t=3.7sec, RMS signal of 34.9GHz O mode also starts to decrease. When RMS signal becomes lower than 0.1 A.U., which is set to be as an interlock level, interlock signal becomes zero and stopped NBI at t=3.96sec.

Figs. 6 illustrate another example of discharge, in which interlock system worked. In this discharge, plasma also terminated due to the radiation collapse. But, at t=0.7sec, 34.9GHz RMS signal increases although density decreases lower than $1.5x10^{19}m^{-3}$,(cut off density of O mode 34.9GHz). This is probably due to the increase of the forward-scattered signal. These increases are mainly lower than 50kHz components. Therefore, by using high pass filter, signals become free such increases.

Figs. 7 are example, in which reflectometer interlock did not work. In this discharge, pellets were injected at t = 0.7 and 0.8sec into the NBI heated plasma and 28.5GHz RMS signal was used for interlock signal source. As shown in fig.7 (a), after pellet injection, central density and volume-averaged density, which were derived from the multi-channel FIR interferometer [5], decrease rapidly and density profile changed from the peaked one to flat one. Two NBI stopped at t=2.2 and 2.3sec, but, as shown in fig.7 (a), interlock signal became zero at t=2.5sec. NBI stopped before interlock worked although density was already lower than $1x10^{19}m^{-3}$ (28.5GHz O mode cut off density) after t=1.1sec. 28.5GHz RMS signal is visible, even when density is lower than cut off density. This makes difficult and tricky to determine the interlock level.

Fig.8 (a) shows response of 28.5GHz RMS signal to central density. RMS signal increases almost linearly, from zero up to cut off density. This is probably due to the increase of forward scattering signal. And RMS signal becomes almost constant at higher than cutoff density. From eq. (1), homodyne signal intensity is sinusoidal function of fluctuation of cut off layer position, and its amplitude is function of local (P_L) and reflected power(P_R). Once cut off layer is formed, reflected power becomes almost constant, then if $\phi_n > 2\pi$, homodyne AC signal (the third term of eq.(1)) becomes constant. This is possible explanation of constant RMS signal at higher than cut off density.

In the discharge of fig.8, interlock level was set to be 0.5A.U. of 28.5GHz RMS signal and actual interlock density was $0.4x10^{19}m^{-3}$. Presently, interlock level is determined from try and error. As long as Gunn oscillator power does not change, the response function described in fig 8 does not change. Therefor, referring response function shown in fig.8, more precise density interlock is possible. If 28.5GHz interlock level was set to be 1.5 A.U of fig.8 (a), actual interlock density was about $0.6 x10^{19}m^{-3}$. If 28.5GHz interlock level was set to be 2.3 A.U., actual interlock density was about $1x10^{19}m^{-3}$, but system might becomes unstable.

If 34.9 or 40.2GHz RMS signal were used for the interlock, higher interlock density is possible. As shown in figs. 7 (c) and (d), when central density decreased lower than $1.5 x10^{19}m^{-3}$ (34.9GHz O mode cut off density) at t=1.1sec and $2x10^{19}m^{-3}$ (40.2GHz O mode cut off density) at t=1.0sec, RMS signals decreased like step function. This makes more reliable operation of interlock system possible. If 34.9GHz interlock level was set to be 1.7 A.U. of fig.8 (b) , actual interlock density is about $1.2 x10^{19}m^{-3}$. If 40.2GHz interlock level was set to be 0.3 A.U. of fig.8 (c) , actual interlock density is about $1.6 x10^{19}m^{-3}$.

Usually, unexpected plasma termination occurs like fig.5 or fig.6 and density decreases rapidly. Above-mentioned problem of determination of interlock level is not serious problem.

[4] Summary

A three-channel O mode homodyne interlock reflectometer was installed on LHD and is successfully working. This is the first example of use of reflectometer as a plasma heating control. Presently, the determination of interlock level is tricky and actual interlock density is lower than cut off density. However, response function will help more precise determination of interlock level

References

[1]. M.Okamato and O.Kaneko from the result of HFREYA code.

[2] Y.Kawano et al., Rev. Sci. Instrum.72,1068 (2001)

[3] T. Akiyama et al., Rev. Sci. Instrum.72,1073 (2001)

[4] K.Tanaka and A. Ejiri,J.Plasma Fusion Research, 74 supplement (1998) 186-187

[5] K.Kawahata, et al.,Rec.Sci, Instrum. **70**, 707, (1999)

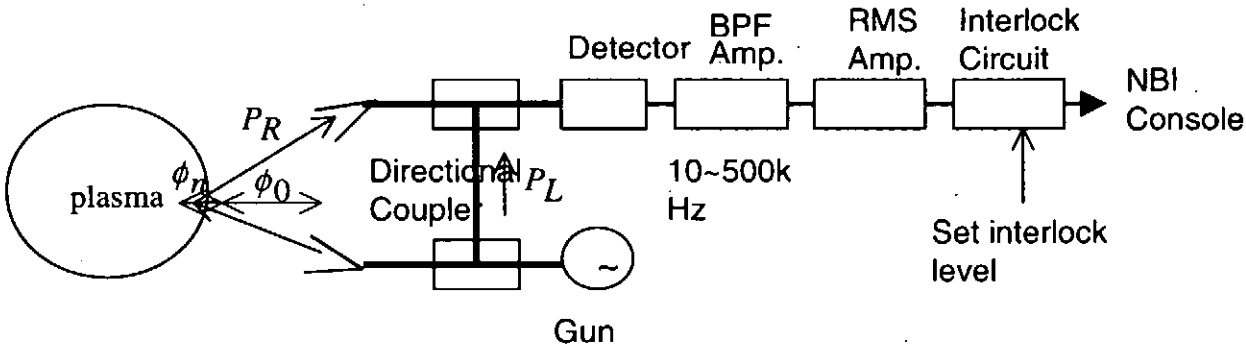

Fig.1 Schematic view of interlock reflectometer

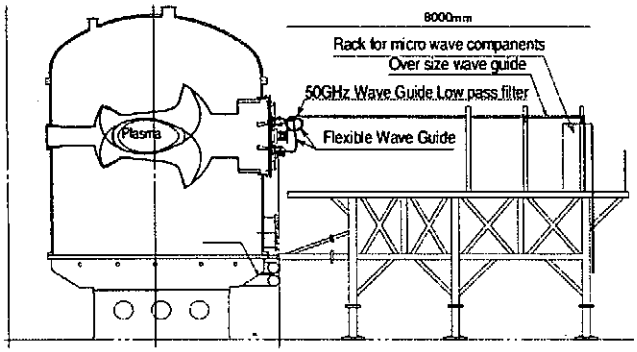

Fig.2 Layout of systems on LHD

Measured cross section is 47degree tilted to horizontal plane.

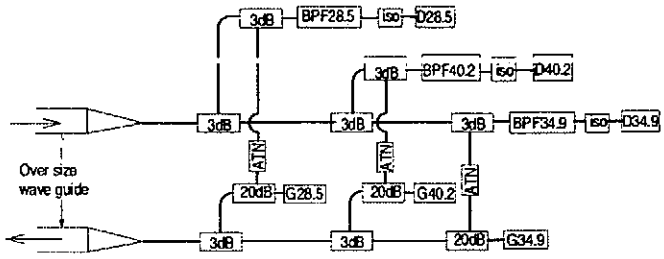

Fig.3 Detail schematic diagram

G28.5.G34.9, G40.2 indicate Gunn oscillator of 28.5,34.9,40.2GHz. D28.5.D34.9, D40.2 indicate detectors of 28.5,34.9,40.2GHz. BPF28.5. BPF 34.9, BPF 40.2 indicate waveguide band pass filter of 28.5,34.9,40.2GHz. 20dB,3dB indicate 20db and 3dB directional coupler. Iso indicates isolator.

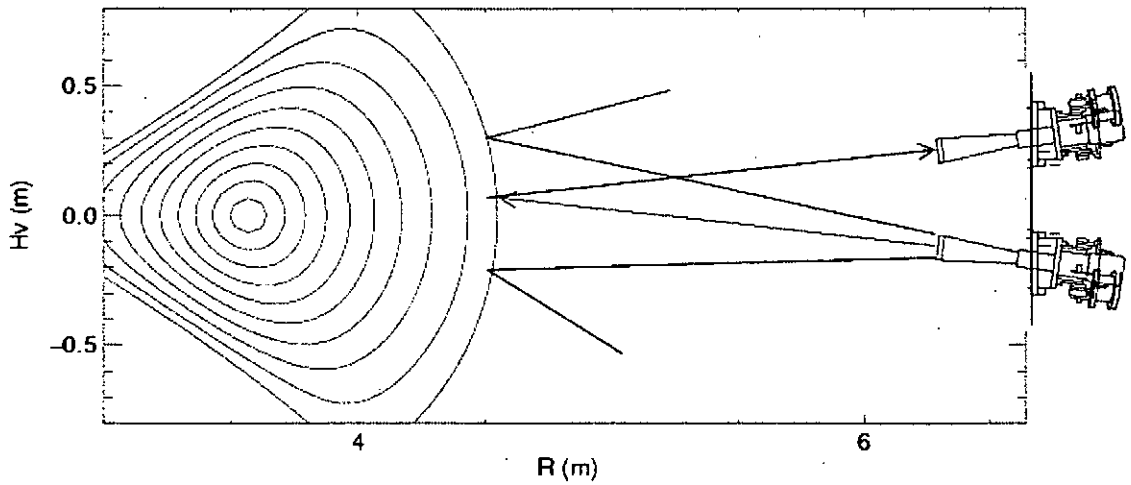

Fig.4 Cross section of the measurements. Magnetic configurations is inward shifted (magnetic axis positions are 3.6m)

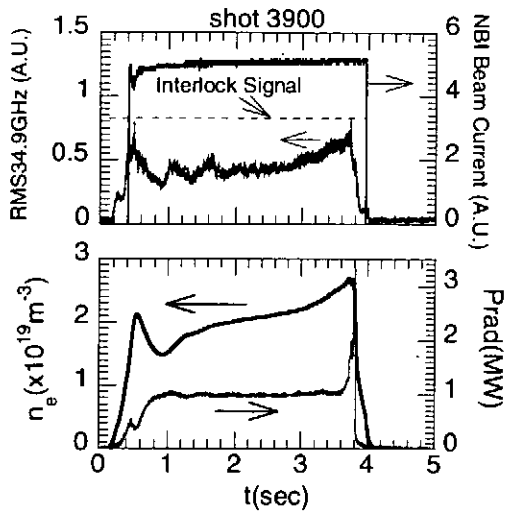

Fig.5 An example of discharge, in which interlock worked. n_e is central line averaged density.

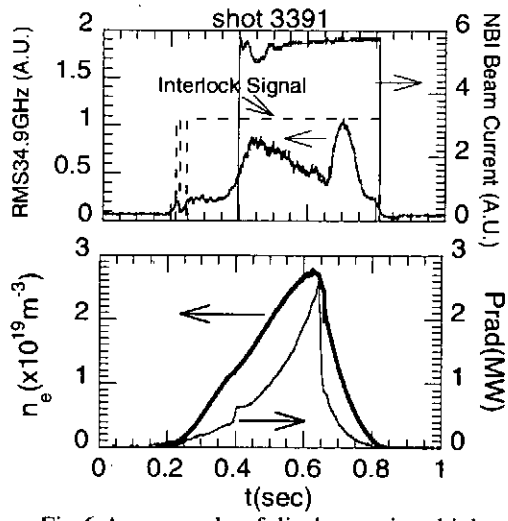

Fig.6 An example of discharge, in which interlock worked.

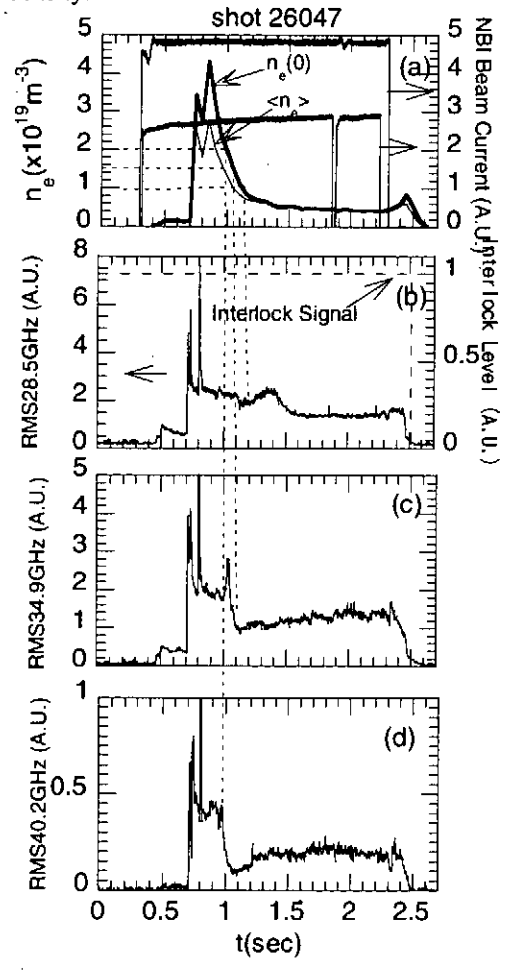

Fig.7 (a) Central and volume averaged density from FIR interferometer and NBI current (b) 28.5GHz RMS signal and interlock signal (c) 34.9GHz RMS signal and interlock signal and (d) 402.GHz RMS signal and interlock signal

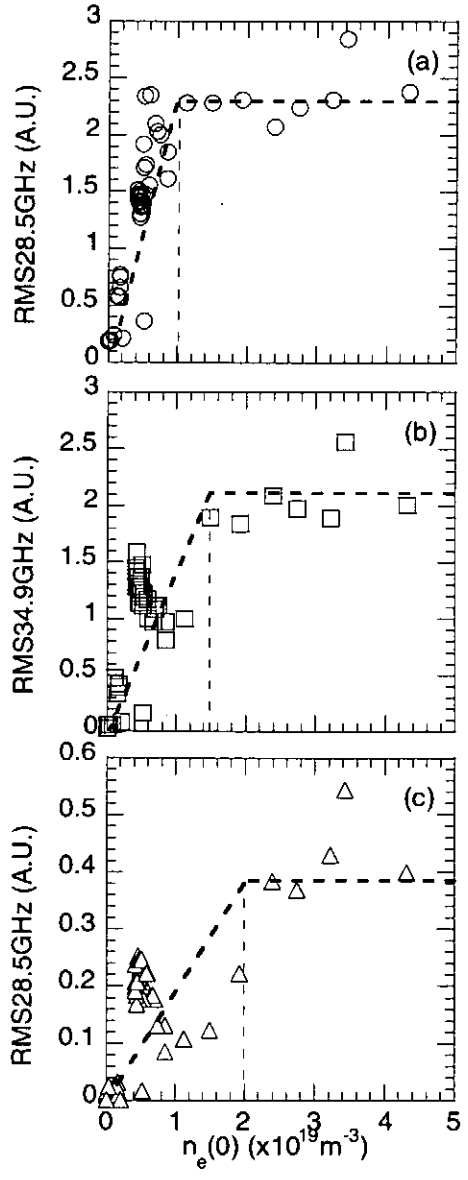

Fig.8 Response function of (a) 28.5GHz, (b)34.9GHz, and (c)40.2GHz

Recent Issues of NIFS-PROC Series

NIFS-PROC-30 研究代表者　栗下　裕明（東北大学金属材料研究所）
所内世話人　加藤　雄大
平成 8 年度核融合科学研究所共同研究「被損傷材料の微小体積強度評価法の高度化」研究会　1996年 10月　9日　於：核融合科学研究所
H. Kurishita and Y. Katoh (Eds.)
NIFS Workshop on Application of Micro-Indentation Technique to Evaluation of Mechanical Properties of Fusion Materials, Oct. 9, 1996, NIFS ; Nov. 1996 (in Japanese)

NIFS-PROC-31 岡本　正雄
講義「核融合プラズマ物理の基礎 - II」
平成 8 年度　総合研究大学院大学　数物科学研究科　核融合科学専攻　1997年 4月
M. Okamoto
"Lecture Note on the Fundamentals of Fusion Plasma Physics - II" Graduate University for Advanced Studies; Apr. 1997 (in Japanese)

NIFS-PROC-32 代表者　河合　良信
平成8年度　核融合科学研究所共同研究　研究会報告「プラズマ中のカオスとその周辺非線形現象」
Y. Kawai (Ed)
Report of the Meeting on Chaotic Phenomena in Plasmas and Beyond, 1996; Apr. 1997 (mainly in Japanese)

NIFS-PROC-33 H. Sanuki,
Studies on Wave Analysis and Electric Field in Plasmas; July 1997

NIFS-PROC-34 プラズマ対向機器・PSI・熱・粒子制御合同研究会報告
平成 9 年 6 月 27 日（金）9:00 ～16:20　核融合科学研究所・管理棟 4 F 第 1 会議室
1997年　10月
T. Yamashina (Hokkaido University)
Plasma Facing Components, PSI and Heat/Particle Control June 27, 1997, National Institute for Fusion Science T. Yamashina (Hokkaido University) ; Oct. 1997 (in Japanese)

NIFS-PROC-35 T. Watari,
Plasma Heating and Current Drive; Oct. 1997

NIFS-PROC-36 T. Miyamoto and K. Takasugi (Eds.)
Production and Physics of High Energy Density Plasma; Production and Physics of High Energy Density Plasma; Oct. 1997

NIFS-PROC-37 (Eds.)T. Fujimoto, P. Beiersdorfer,
Proceedings of the Japan-US Workshop on Plasma Polarization Spectroscopy and The International Seminar on Plasma Polarization Spectroscopy January 26-28, 1998, Kyoto; June 1998

NIFS-PROC-38 (Eds.) Y. Tomita, Y. Nakamura and T. Hayashi,
Proceedings of the Second Asian Pacific Plasma Theory Conference APPTC '97, January 26-28, 1998, Kyoto; Aug. 1998

NIFS-PROC-39 (Ed.) K. Hirano,
Production, Diagnostics and Application of High Energy Density Plasmas; Dec. 1998

NIFS-PROC-40 研究代表者　加古　孝（電気通信大学）
所内世話人　渡辺　二太
平成 10 年度核融合科学研究所共同研究 研究会「プラズマ閉じ込めに関連する数値計算手法の研究」
Ed. by T. Kako and T. Watanabe
Proceeding of 1998-Workshop on MHD Computations "Study on Numerical Methods Related to Plasma Confinement Apr. 1999

NIFS-PROC-41 (Eds.) S. Goto and S. Yoshimura,
Proceedings of The US-Japan Workshop and The Satellite Meeting of ITC-9 on Physics of High Beta Plasma Confinement in Innovative Fusion System, Dec. 14-15, 1998, NIFS, Toki; Apr. 1999

NIFS-PROC-42 (Eds.) H. Akiyama and S. Katsuki,
Physics and Applications of High Temperature and Dense Plasmas Produced by Pulsed Power; Aug. 1999

NIFS-PROC-43 (Ed.) M. Tanaka,
Structure Formation and Function of Gaseous, Biological and Strongly Coupled Plasmas; Sep. 1999

NIFS-PROC-44 (Ed.) T. Kato and I. Murakami,
Proceedings of the International Seminar on Atomic Processes in Plasmas, July 29-30, 1999, Toki, Japan; Jan. 2000

NIFS-PROC-45 (Eds.) K. Yatsui and W. Jiang,
Physics and Applications of Extreme Energy-Density State, Nov. 25-26, 1999, NIFS; Mar. 2000

NIFS-PROC-46 研究代表者　加古　孝（電気通信大学）
所内世話人　渡辺　二太
平成 11年度核融合科学研究所共同研究 研究会「プラズマ閉じ込めに関連する数値計算手法の研究」
Ed. by T. Kako and T. Watanabe
Proceeding of 1999-Workshop on MHD Computations "Study on Numerical Methods Related to Plasma Confinement June. 2000

NIFS-PROC-47 岡本正雄、村上定義、中島徳嘉、汪衛生
プラズマ物理におけるモンテカルロシミュレーション
WatanabeM. Okamoto, S. Murakami, N. Nakajima, W.X. Wang,
Monte Carlo Simulations for Plasma Physics: July 2000

NIFS-PROC-48 K. Miyamoto,
Fundamentals of Plasma Physics and Controlled Fusion: Oct. 2000

NIFS-PROC-49 (Ed.) K. Kawahata,
Proceeding of the 5th International Workshop on Reflectometry, 5-7 march, 2001; May 2001